博士論文

Development of a new continuous processing method of ramie spun yarn/PP composites and elastic modulus analysis

（ラミー紡績糸/PP 複合材料の新規連続成形法の開発と弾性率解析）

平成 27 年 3 月
（2015 年 3 月）

金　顯凡

山口大学大学院理工学研究科
システム設計工学系専攻
材料信頼性工学研究室

論文要旨

ポリマー系複合材料は、長期間に渡り人工繊維（例えば、ガラス、炭素）およびエポキシ、ポリエステル等の熱硬化性マトリックスを組み合わせることにより製造されてきた。これらの素材の多くは化石燃料から得られるものであり、環境負荷や資源の枯渇に係わる問題を顕在化させている。将来的にこれらの諸問題を乗り越えるために、代替材料として、天然繊維や生分解性樹脂のようなバイオマス材料あるいはバイオマス由来材料の開発に注目が集まっている。

天然繊維を使用する際、優先順位は、ガラス繊維系および炭素繊維系とは異なる特徴を持つ天然繊維系複合材料の製造方法の確立である。これまで、天然繊維強化複合材料を製造するためにいくつかの方法が導入されている。短繊維複合材料の場合、重要なパラメータの一つは、複合材料内部の繊維長である。繊維強化能を発揮させるため、最小の長さを意味する臨界繊維長よりも繊維を長くする必要がある。そうでなければ複合材料の引張強度およびヤング率の機械的特性を向上させることができない。過去に機械的特性を高めるために 2 段階の製造方法が提案された。大部分の繊維がその臨界繊維長よりも短かったため、機械的特性は不十分であった。一方、長繊維ペレットを製造するための製造方法が確立し、得られる短繊維複合材料は良好な機械的特性を示すことが報告された。しかし、高価な投資や複雑な技術が必要とされた。

本研究では、上述した主な問題を克服するために、代表的な植物系天然繊維糸と熱可塑性樹脂であるラミー紡績糸及びポリプロピレンを用い、新しい天然繊維強化複合材料の製造方法を開発した。

第 1 章では、まず、本研究の背景と目的を説明した。

第 2 章ではラミー紡績糸及びポリプロピレンを用い、新しい天然繊維複合材料の製造方法であるマルチピン補助含浸(M-PaRI)プロセス法を提案した。この新しい装置を使用し、複合ストランドを作製し、そしてマスタバッチであるペレットを作製した。このペレットを用い、射出成形により短繊維複合材料を作製した。得られた短繊維複合材料の引張試験から、繊維重量分率が増加するに

つれ引張強度は 30-40wt％まで増加し、その後 50wt％ではわずかに低下することが判明した。ヤング率は、繊維の重量分率の増加とともに増加した。以上から、短繊維複合材料では最適な繊維含量分率は 30-40wt％の間であると推定された。製造方法での温度の依存性を調べるため、複合ストランドの断面観察が行われた。その結果、160°C-185°C の間ではボイドが観察されたが、195°C-225°C の間ではボイドが見られなかった。これらの結果から 160°C-185°C にて作製されたペレットでは引張強度が低下したものと推測された。一方、205°C 以上では、高熱により繊維が劣化し引張強度が低下したと考えられた。短繊維複合材料から繊維を取り出し、繊維長を測定した結果、ほとんどの繊維は臨界繊維長より大きいことが認められた。

第 3 章では、M-PaRI プロセスを使用し、ラミー糸 1 本から成るストランド状長繊維複合材料、および 33 本のラミー糸からなるテープ状長繊維複合材料を作製した。後者はガラス織布複合材料の代替材として開発された。ストランド状複合材に関しては、MAPP 量による機械的性質に及ぼす影響が調査されていなかったため、MAPP の異なるシングル複合ストランドを作製した。引張試験から引張強度及び弾性率は異なる MAPP 量(0wt%-2wt%)にかかわらず、繊維重量分率の増加とともに増加した。しかし、MAPP 量による引張特性への依存性は見られなかった。テープ状複合材に関しては、M-PaRI プロセスの後、新しくロラーを取り付け作製した。テープ状複合材は寸法効果によりストランド状複合材に比べ、低い強度値に留まった。

第 4 章では弾性率の変動の原因を調査するために、糸弾性率に関する従来の理論モデルと統計的方法（最小二乗方法、一次近似二次モーメント方法）を用いて実験値を検討した。実験値と理論モデルとの比較から、長繊維複合材料の変動は、繊維配向角に主に関連付けられると考えられる。さらに、理論モデルを拡張したところ、複合材料の寸法増加にともなう弾性率の確率変動は小さくなることが明らかとなり、実験値の推移を首尾よく説明することができた。

第 5 章では、本研究の結論を要約し、今後の研究課題が述べられた。

Abstract

Polymer composite materials have been produced by combining synthetic fibers (e.g., glass and carbon) and thermoset matrix such as epoxy or polyester. These materials are obtained based on fossil fuel. The rising concerns for using fossil fuel products are environmental impact matters, exhaustion of resources, and so on. In order to overcome these problems in the future, it has been gaining much more attention to develop alternative materials using biomass-based or -derived materials such as natural fibers and biodegradable thermoplastic resins.

The first priority of using natural fibers must be the establishment of processing method since natural fibers have different characters from glass and carbon fibers. In case of a short fiber composite material, one of the critical parameters is the fiber length inside the composite material. It needs to be longer than *critical fiber length*, which means the minimum length to exhibit the original fiber strength. Otherwise the mechanical properties such as tensile strength and Young's modulus cannot be improved. Several processing methods were introduced to produce natural fiber-reinforced composite materials in the past. Two-steps production method was proposed to increase the mechanical properties. The results showed that the mechanical properties were not enough improved since most of fiber lengths were lower than its critical fiber length. The other fabrication method was actualized for producing long pellets. The results showed good mechanical properties on short fiber composite materials, but it required expensive investment and complicated technique.

In this study, thus, in order to overcome the main drawbacks explained in the above, a new method was developed to produce composite materials using ramie spun yarns and polypropylene, which are the representative plant-based natural fiber yarn and thermoplastic resin.

In Chapter 1, first, the background and purpose of this study were introduced.

In Chapter 2, a new continuous process called multi-pin assisted resin impregnation (M-PaRI) for natural fiber composite materials was explained. Using the

process, composite strands were produced, and then these were chopped to pellets called master-batch. Finally using the pellets, short fiber composite materials were produced by injection molding. From the experimental results of tensile tests on short fiber composite materials, it was confirmed that tensile strength increased with increasing fiber weight fraction until 30-40wt%, then dropped slightly at 50wt%. Young's modulus increased with increasing fiber weight fraction. It was confirmed from the experimental results that the optimal fiber content was between 30-40wt% on the short fiber composite materials. Cross-sectional areas of the resultant composite strands were studied in order to investigate dependency of temperatures during fabrication procedure. As the results, voids were observed on composite strands fabricated between 160^{o}C-185^{o}C. However, voids did not occur between 195^{o}C-205^{o}C. From these results, it was estimated that tensile strengths on short fiber composite materials fabricated between 160^{o}C-185^{o}C were low. On short fiber composite materials fabricated over 205^{o}C, over-heating caused decreased tensile strengths. According to the investigation of fiber length extracted from the short fiber composite materials, the results showed that fiber lengths were larger than its critical length.

In Chapter 3, using M-PaRI process, single yarn composite strand and composite tapes containing thirty-three ramie spun yarns were produced. The composite tapes were developed for the purpose of replacing glass woven fabric composites. Regarding single yarn composite strands, since the dependency of MAPP contents was not investigated, these materials were produced in different content of MAPP. Tensile strength and elastic modulus of the single composite strand increased with increasing fiber volume fraction irrespective of MAPP contents (0wt%-2wt%). However, the dependency of MAPP contents was not observed. With respect to composite tapes, a new process called roller system was added after M-PaRI process in order to produce the composite tapes. Tensile strengths of the composite tapes exhibited relatively lower values than composite strand due to size effect.

In order to investigate the cause of the fluctuation in elastic modulus, the experimental values were discussed with conventional theoretical models base on yarn modulus analysis and statistical methods (least squares method, first order second moment approximate method, FOSM) in Chapter 4. From the comparison between

experimental values and the theoretical models, the fluctuation on a composite yarn was mainly related to fiber orientation angles. Moreover, according the FOSM model, it is possible to reduce the fluctuation in elastic modulus of the composite materials when the composite materials were produced at bigger size.

In Chapter 5, the conclusions of this study were summarized, and future research subjects were added.

Contents

1. Introduction

1.1 Background

1.1.1 Environmental issues

Much attention has been attracting to environmental issues in many countries. The issues were early mentioned at the United Nations conference on the human environment held in Stockholm in 1972[1)]. It showed the guideline for the people how to coexist with the environment. The continuous efforts to preserve environment were discussed at the conference and published a summary of Rio declaration on environment and development in 1992[2)]. It was summarized that human beings need to develop sustainably the societies with considering environment for the future. In 1997, a famous Kyoto protocol to the United Nations framework convention on climate change was declared[3)]. It was stated that the developed nations have more responsibility not only to preserve environment, but also to cut CO2 emissions in the atmosphere. It was a critical conference for developed countries to rethink their strategies in order to meet the requirements. The world summit on sustainable development was held in Johannesburg in 2002[4)] for discussing about global warning, preserving natural resources, sustainable economic growth, etc. Recently, the basic law for the promotion of utilizing biomass was approved in a cabinet meeting by Japanese government[5)].

1.1.2 Composite materials

• Definition of composite materials

Composite materials have been used since ancient time. It can be classified in many ways depending on how and where to be used. Table 1 shows a classification of composite materials[6)]. The idea for using composite materials is to show superior properties as compare to using a single material. Composite materials can be defined as below[6)].

1) It consists of two or more physically distinct and mechanically separable materials.
2) It can be made by mixing the separable materials in such a way that the dispersion of one material in the other can be done in a controlled way to achieve optimum properties.
3) The properties are superior, and possibly unique in some specific respects, to the properties of the individual components.

Table 1 A classification of composite materials.

	Natural composite materials	Microcomposite materials	Macrocomposites
Examples	Wood, Bone, Bamboo, Muscle and other tissue	Metallic alloys (Steels), Toughend thermoplastics (Impact polystyrene, ABS), Sheet molding compounds, Reinforced thermoplastics	Galvanised steel, Reinforced concrete beams, Helicopter blades, Skis

• Advantage and disadvantage of composite materials

Composite materials have advantage and disadvantage properties when the composite materials are used for structural materials. Advantage and disadvantage of composite materials are given as below[6)-7)].

Advantages

1) A higher performance for a given weight leads to fuel and energy savings, when the strength per unit weight and modulus per unit weight are considered. Those are called specific strength and specific modulus of composite materials.
2) Laminate patterns and ply buildup in a part can be tailored to give the required mechanical properties in various directions.
3) It is easy to produce complex parts of the composite materials in one manufacturing method.
4) It gives high temperatures and weathering resistance, corrosion, high chemical stability, low smoke density, low flammability, low toxicity of decomposition products, huge selection of possible component size and shape, good design practice, low assembly costs.

Disadvantages

1) High cost of raw materials and fabrication.
2) Composite materials show reversible and irreversible changes in property which occur owing to contact with humid environments and to temperature fluctuations.
3) Week transverse properties.
4) Repairing process of composite materials is complex and requires refrigerated transport and storage.

1.1.3 Natural fiber composite materials

Natural fiber composite materials have been gaining attention in the field of composite materials because of environmental problems, oil crisis, rising demand in automobile industry, etc.[8)-9)]. The main purpose of natural fiber composite materials is to replace glass fiber composite materials[10)].

Advantages and disadvantages of natural fiber composite materials are given as below[11)-13)].

Advantages

1) Cost effective
2) Renewable
3) Recyclable and biodegradable
4) Lower environmental impact as compared to glass fiber composites
5) Fuel efficiency and reduction of emissions in automobile application

Disadvantages

1) Relatively high moisture absorption
2) Lower operating life
3) Poor impact strength
4) Poor adhesion between fiber and matrix
5) Variation in mechanical properties
6) Lower processing temperature
7) Variation in price of natural fibers

1.1.4 Natural fibers and thermoplastic matrices

Natural fibers can be classified by plant/lignocellulosic and animal fibers[14)]. Plant/ lignocellulosic fibers can also be divided by wood, stem/bast, leaf, seed/fruit, and grass. Fibers such as ramie, jute, hemp, and flax belong to the group of stem/bast. Photographs of natural fibers are shown in Figure 1[15)].

Table 2 shows properties of glass and natural fibers[16)-17)]. Natural fibers have advantages of biodegradable, compatible specific strength, low density. However, it has also disadvantages of hydrophilic nature, relative low temperature during fabrication process.

Thermoplastic polymers have been used as alternative materials for thermoset polymers because of their various applications such as plastic bag, disposable containers. The mechanical properties of thermoplastic polymers are listed in Table 3[18)].

Ramie

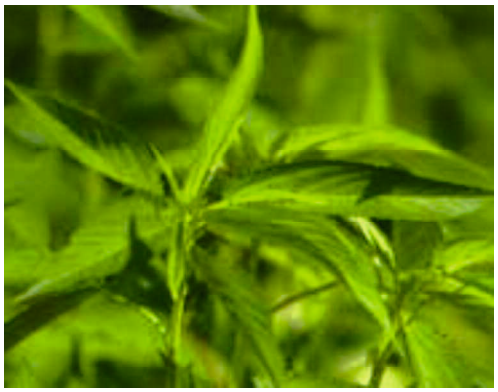

Jute

Hemp

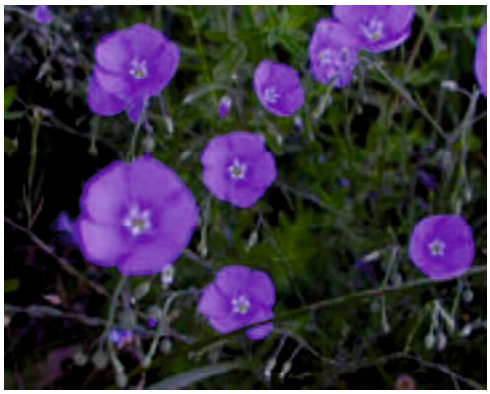

Flax

Figure 1 Photographs of natural fiber, e.g., Ramie, Jute, Hemp, and Flax[15)]

Table 2 Properties of glass and natural fibers

Fibers	Tensile strength [MPa]	Young's modulus [GPa]	Microfibrill angle [°]	Cellulose content [wt%]	Lignin content [wt%]	Mean fiber length [mm]	Mean cross section [μm2]
E-Glass	1400-2500	76	—	—	—	—	—
Ramie	560	24.5	7.5	68.6-76.2	0.6-0.7	150	815
Jute	393-773	13-26.5	8	61-71.5	25-30	1.5-5	161
Hemp	690	—	6.2	70.2-74.4	3.7-5.7	5-55	297
Flax	345-1100	27.6	10	71	2.2	25-30	184

Table 3 Properties of thermoplastic polymers.

	Tensile strength [MPa]	Young's modulus [MPa]	Fracture strain [%]	Specific gravity [g/cm^3]
PE	21-38	414-1245	15-100	0.94-0.97
PVC	41-52	2410-4136	40-80	1.30-1.58

1.1.5 Adhesion

Natural fibers and thermoplastic polymers are hydrophilic and hydrophobic materials, respectively. Thus, adhesion between two materials is important factor to improve mechanical properties on the composite materials.

Maleic anhydride grafted polypropylene (MAPP) called coupling agent was commonly used in wood/PP composite materials. Figure 2 shows the mechanism of interaction of cellulose fibers with MAPP[19]. The reaction between cellulose and MAPP can be divided into two main steps as shown in Figure 2. The copolymer is converted into the more reactive anhydride form; esterification of the cellulose fibers takes place in the second place.

Hristove et al. investigated wood flour/PP composite materials with different contents of MAPP[20]. The results showed that tensile properties such as strength, elongation were improved as compared to MAPP-free composite materials. Danyadi et al. also studied interfacial interaction between wood flour and PP on the composite materials[21]. It was confirmed that composite materials containing MAPP showed much better tensile strength than MAPP-free composite materials. The results also showed that the amount of MAPP has optimal contents

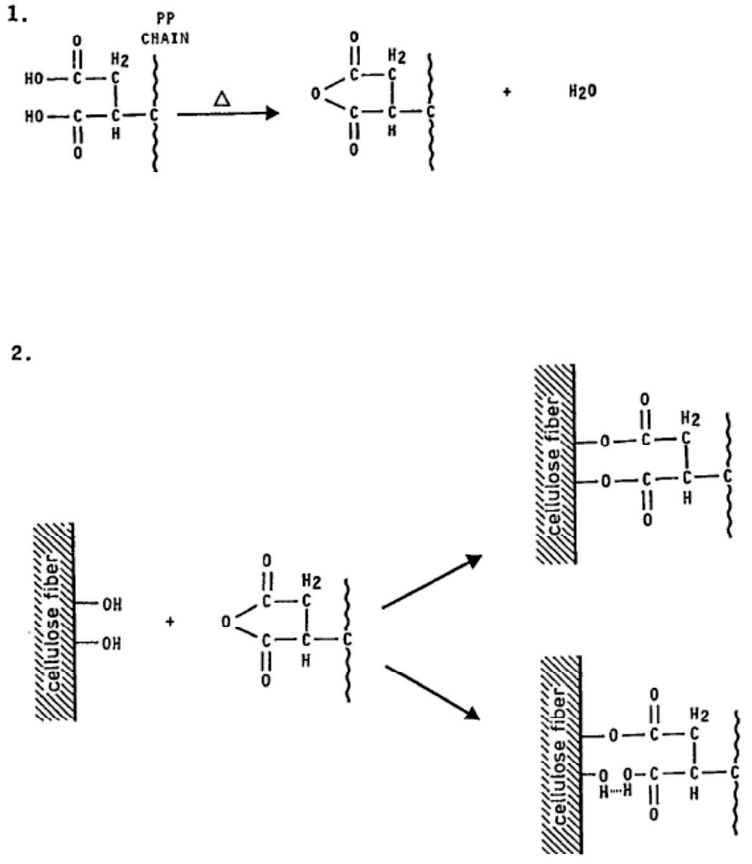

Figure 2 Mechanism of interaction between cellulose fibers and MAPP[19].

around 0.05-0.1 MAPP/wood ratio. Keledi et al. investigated tensile and impact properties on PP/wood/elastomer composite materials[22]. Adding MAPP also increased mechanical properties because of good adhesion.

Thomason investigated jute fiber/PP composite materials[23]. In his study, the injection molding process was carried out to compound fibers and matrix. The results showed that mechanical properties increased adding 2wt% of MAPP. Yan et al. published a research paper dealing with hemp fibers/PP composite materials[24]. It was confirmed that tensile, flexural, and impact strength increased with increasing the content of MAPP.

1.2 Motivations

Fabrication methods of producing composite materials have been studied in many countries. Tanaka et al. developed a continuous process method using jute yarns, polypropylene (PP), and MAPP of 5wt%[25]. In their study, jute yarns were fed into a die of twin-screw extruder. The yarn twisted reversely in order to infiltrate matrix among fibers. The obtained composite materials were chopped into pellets of 4mm and 12mm length for injection molding. The results showed that tensile strength and initial modulus were 52.1MPa and 6.18GPa, respectively, with fiber volume fraction of 50wt%. It can be stated that the results showed the improved mechanical properties on short fiber composite materials. However, it needs complicated techniques during untwisting process.

Fung et al. introduced a fabrication method with sisal fiber yarn, PP, and MAPP[26]. Sisal fiber yarn passes through a die assembly connected with a single screw extruder. In this process, sisal yarns were impregnated with MAPP. The results showed that MAPP was welled infiltrated between sisal fiber yarns. The obtained composite materials were chopped into pellets of 5mm for injection molding. The results showed that tensile strength and Young's modulus with fiber volume fraction of 10wt% were 35.51MPa and 3.07GPa in case of low temperature for injection molding. It was confirmed the reduction of temperature during injection molding.

Cichocki et al. invented moldable pellet with natural fibers and thermoplastic polymers[27]. The fabrication method is very similar with the process suggested by Fung et al. The obtained pellets can be used for injection molding, extrusion compression molding, and compression molding.

Angelov et al. carried out experimental tests adopting pultrusion process[28]. The pultrusion process has been used in early stage of composite industries. In their study, flax yarn and PP were used as reinforcement and matrix, respectively. It was confirmed that composite materials

were obtainable by uisng natural fiber yarn from their processing method. They also pointed out that thermal degradation was occurred during the pultrusion process.

Bledzki et al. suggested two-step processing method before injection molding was conducted[29]. Abaca fiber yarns and man-made cellulose were used as reinforcements. PLA and PP were also used as matrices. At the first stage, fiber yarns were coated at a die attached a twin-screw extruder. Then, the obtained composite materials were chopped into pellets. The pellets were inserted into a single-screw extruder at the second stage. The resultant composite materials were repeatedly chopped into pellets for injection molding. It was confirmed that the dispersion of fibers in the composite materials was excellent, but the fiber length of the resultant composite materials was short due to the effect of the process of second stage.

The main drawbacks for producing natural fiber composite materials studied in the past are high cost, complexity, not enough impregnation between fibers, huge energy consumption.

1.3 Purposes

◆ Development of a new fabrication method using biomass.

As pointed out in section 1.2, a new approach for producing natural fiber composite materials needs to be considered in order to overcome the disadvantages. The fabrication should be simple, low cost, less energy consumption, but the results of mechanical properties on composite materials need to show promising outcomes.

◆ Evaluation of the resultant composite materials.

In the past study, Doi et al. investigated long fiber composite materials using ramie yarns[30]. Cyclic loading was conducted in order to improve the mechanical properties of the resultant composite materials. Recently, Nakamura et al. discussed about elastic properties of green composites using ramie twisted yarns[31]. It was confirmed that elastic modulus of the yarn composite materials decreased with decreasing fiber orientation angle. Few studies for the effects of MAPP on natural fiber yarn/PP composites have been done in previous studies as also explained in section of 1.1.3.

In this study, thus, the effect of MAPP was investigated on a ramie spun yarn/PP composite strand. In addition, a ramie/PP composite tape was also produced to discuss about the possible application for woven fabric composite materials. Moreover, elastic modulus of a ramie spun yarn/PP strand was compare with conventional theoretical models.

1.4 References

1)http://www.unep.org/Documents.Multilingual/Default.asp?documentid=97&articleid=1503

2)http://www.jus.uio.no/lm/environmental.development.rio.declaration.1992/portrait.a4.pdf

3) http://unfccc.int/kyoto_protocol/items/2830.php

4) https://www.un.org/jsummit/html/basic_info/basicinfo.html

5) http://www.maff.go.jp/j/shokusan/biomass/b_kihonho/

6) Hull, Derek, An introduction to composite materials, Cambridge University Press, 1981.

7) Keith B. Armstrong, L., Graham Bevan, William F. Cole II, Care and repair of advanced composites, second edition, SAE International, 2005.

8) Omar Faruk, Andrzej K. Bledzki, Hans-Peter Fink, Mohini Sain, Boicomposites reinforced with natural fibers: 2000-2010, Progress in Polymer Science, 37, 1552-1596, 2012.

9) Chandramohan, D. and J. Bharanichandar, Natural fiber reinforced polymer composites for automobile accessories. American Journal of Environmental Science, 9 (6), 494-504, 2013.

10) A. Ticoalu, T. Aravinthan & F. Cardona, A review of current development in natural fiber composites for structural and infrastructure applications, Southern Region Engineering Conference, 2010.

11) U.S. Bongarde, V.D. Shinde, Review on natural fiber reinforcement polymer composites, International Journal of Engineering Science and Innovative Technology, Vol. 3, Issue 2, 2014.

12) S.V. Joshi, L.T. Drzal, A.K. Monhanty, S. Arora, Are natural fiber composites environmentally superior to glass fiber reinforced composites?, Composites: Part A, 35, 371-376, 2004.

13) M.S. Huda and L.T. Drzal, A.K. Mohanty, M. Mishra, Natural-fiber composites in the automotive sector, Woodhead Publishing Limited, 2008.

14) D. Chandramohan, and K. Marimuthu, A REVIEW ON NATURAL FIBER, Vol. 8, Issue 2. IJRRAS_8_2_09.pdf, 2011.

15) http://www.naturalfibres2009.org/en/fibres/ramie.html

16) C. Baley. Composites Part A: Applied Science and Manufacturing, 2002.

17) Toru Fujii, Takashi Nishino, Koichi Goda, Tadashi Okamoto supervision, "Development and application of environmentally friendly composite materials", CMC Publishing, Chapter 4, Section 1, "Biodegradable Polymer Blends ", p.122-137, 2005.

18) Silva.F.A, Chawla.N, Filho.R.D.T, Tensile behavior of high performance natural (sisal) fibers, Composites Science and Technology, Vol.68, 2008.

19) Johan M. Felix and Paul Gatenholm, The Nature of Adhesion in Composites of Modified Cellulose Fibers and Polypropylene, Jnournal of Applied Polymer Science, Vol. 42, 609-620, 1991.

20) V. N. Hristov, M. Krumova, St. Vasileva, G. H. Michler, Modified Polypropylene Wood Flour Composites. Ⅱ. Fracture, Deformation, and Mechanical Properties, Journal of Applied Polymer Science, Vol. 92, 1286-1292, 2004.

21) Livia Danyyadi, Tunde Janecska, Zoltan Szabo, Gabor Nagy, Janos Moczo, Bela Pukanszky, Wood flour filled PP composites: Compatibilization and adhesion, Composite Secinec and Technology, 67, 2838-2846, 2007.

22) G. Keledi, A. Sudar, Ch. Burgstaller, K. Benner, J. Moczo, and B. Pukanszky, Tensile and impact properties of three-component PP/wood/elastomer composite, EXPRESS polymer letter, Vol. 6, No.3, 224-236, 2012.

23) J.L. Thomason, Dependence of Interfacial Strength on the Anisotropic Fiber Properties of Jute Reinforced Composites, Polymer Composites, Vol. 31, Issue 9. 1525-1534, 2010.

24) Z.L. Yan, H. Wang, K.T. Lau, S. Pather, J.C. Zhang, G. Lin, Y. Ding, Reinforcement of polypropylene with hemp fibres, Composite: Part B, 46, 221-226, 2013.

25) Tatusya Tadaka, Yasuo Hirano, Long Fiber Pellet Production Plants and their Application to Natural Fiber Composites (Eco-Composites), Advanced Processing Technologies for Environmental Protection, Vol. 51, No. 2, 2001.

26) K.L. Fung, X.S. Xing, R.K.Y. Li, S.C. Tjong, Y.-W. Mai, An investigation on the processing of sisal fibre reinforced polypropylene composites, Composites Science and Technology, 63, 1255-1258, 2003.

27) Frank R. Cichocki, James L. Thomason, Terry L. Cheney, Moldable pellet based on the combination of synthetic cellulose fibers and thermoplastic polymers, Patent publication number: US6756114 B2, 2004.

28) I. Angelov, S. Wiedmer, M. Evstatiev, K. Friedrich, G. Mennig. Pultrusion of a flax/polypropylene yarn, Composite: Part A, 1431-1438, 2007.

29) Andrzej K. Bledzki, Adam Jaszkiewicz, Dietrich Scherzer, Mechanical properties of PLA composites with man-mad cellulose and abaca fibres, Composites: Part A 40, 404-412, 2009.

30) Takafumi DOI, Masahiro ITO, Takeshi KAJI, Rie NAKAMURA, Koichi GODA, and Junji OHGI, Improvement in Strength Properties of Ramie Fibers and Ramie Yarn Green Composites through Cyclic Tensile Loading, Journal of the Japan Society for Composite Materials, 35, 2, 56-63, 2009.

31) R. Nakamura, K. Goda, J. Noda and A. Netravali, 'Elastic properties of green composites reinforced with ramie twisted yarn', Vol. 4, 1605-1614, 2010.

2. Yarn composite pellet production by M-PaRI process

2.1 Introduction

As mentioned in Chapter 1, the challenges for producing natural fiber composite materials are how to utilize the characters of natural fibers and thermoplastic polymers. Natural fibers are usually formed in a yarn during roving process. Thus, it will be convenient to develop a technique by using a yarn as reinforcement. The technique can be applied to any natural fiber yarns. The critical point using a natural fiber yarns is that the yarn needs to be impregnated with thermoplastic polymers as pointed out in section 1.2. It means that good impregnation of thermoplastic polymers between fibers is the key points to improving mechanical properties of short fiber composite materials. Furthermore, when the composite pellets were obtained by chopping yarn composite materials, it can be used as additive masterbatch for mass-production of interior parts in the field of transport industries such as automobile, railroad, and airplane.

2.2 Experimental methods

2.2.1 Materials

Continuous ramie single yarns, having fineness of 95 tex, Type no. 16 (Tosco Co., Ltd., Japan) and polypropylene (Prime Polymer Co. Ltd., Japan) were used as reinforcement and matrix material, respectively. Physical and chemical properties of ramie fibers and mechanical properties of polypropylene are listed in Table 2.1[1)-2)], and Table 2.2[3)]. According to 1) and 2), although cellulose contents vary widely from 65% to 85%, both data are in an agreement in terms of low lignin contents. The cross-sectional area of ramie fibers is not circular, but rather elliptical as shown later. The major axis is approximately 30μm. The degree of microfibrillar angle of ramie fibers is one of the smallest classes among plant-based natural fibers.

As mentioned in Chapter 1, high adhesion between hydrophilic fibers and hydrophobic resin by chemical bonding is known to be induced by available OH groups on the fiber surface. The resin adheres to the fiber surface through molecular chain entanglement. During this reaction, maleic anhydride grafted polypropylene (MAPP) functions as a coupling agent to realize chemical bonding. In this study also, MAPP (Kayaku Akzo Co. Ltd., Japan) was used to promote chemical interaction between the fiber and matrix, of which the aspect used in this study is shown in Figure 2.3

(a) (b)

Figure 2.1(a) Aspect of ramie spun yarn on a textile bobbin. (b) Magnified observation of a ramie spun yarn

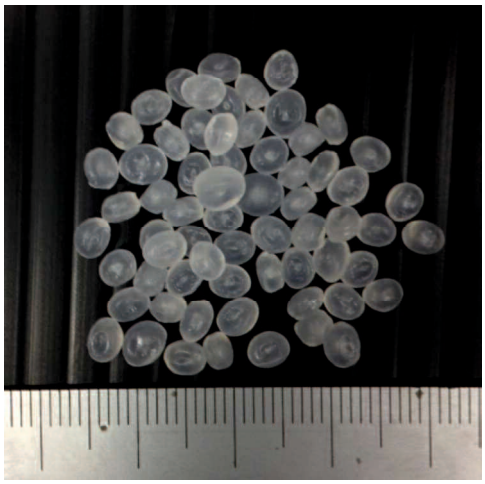

Figure 2.2 Polypropylene pellets.

Table 2.1 Physical and chemical properties of ramie fibers[1)-2)].

Density	Cell diameter	Cell length	Microfibril angle	Moisture content	Chemical composition (wt%)					
(g/cm^3)	(mm)	(mm)	(°)	(wt%)	Cellulose	Lignin	Hemicellulose	Pectin	Wax	Ref.
1.5	-	-	7.5	8	68.6-76.2	0.6-0.7	13.1-16.7	1.9	0.3	1)
	40-50	154	7.5-1.2	-	80-85	0.5	3-4	-	-	2)

Table 2.2 Mechanical properties of polypropylene[3)].

	Tensile strength [MPa]	Young's modulus [MPa]	Fracture strain [%]	Specific gravity [g/cm^3]
PP	32-42	689-1176	200-700	0.89-0.91

Figure 2.3 Granular maleic anhydride grafted polypropylene (MAPP).

2.2.2 Yarn composite pellet production

Figure 2.4 shows a schematic of the present fabrication system. Continuous ramie single yarn/PP composites were produced through a new combined technique proposed in this study, which consists of resin coating and multi-pin-assisted resin impregnation (M-PaRI) processes, as shown in Processes A and B of Figure 2.4. Six ramie spun yarns were first delivered via preheating process into a cross-head die attached to a ϕ 15mm single screw extruder (MusashinoKikai Co., Ltd., Japan), into which PP pellets and MAPP powders were fed at the same time. The mixed resin was coated onto the ramie yarns in the die at Process A (resin-coating process). Subsequently, it was impregnated into interfibers through the multi-pin system, as shown in Process B (M-PaRI) of Figure 2.4. The number and diameter of pins used here were 22 and 5 mm, respectively. M-PaRI is a new processing method proposed in this study, which is added to the conventional production procedure. Temperatures of the single screw extruder were all set at 190◦C with a screw speed of 7.0 rpm. Following this process, a motor was set to draw the composite strand with a screw speed of 45.0rpm. The continuous composite strands containing six ramie yarns were chopped to pellets of 2mm length for injection molding, as shown in Figure 2.6. The set temperature(s) was 190◦C at Process A, and was changed in the 160-225◦C range for Process B.

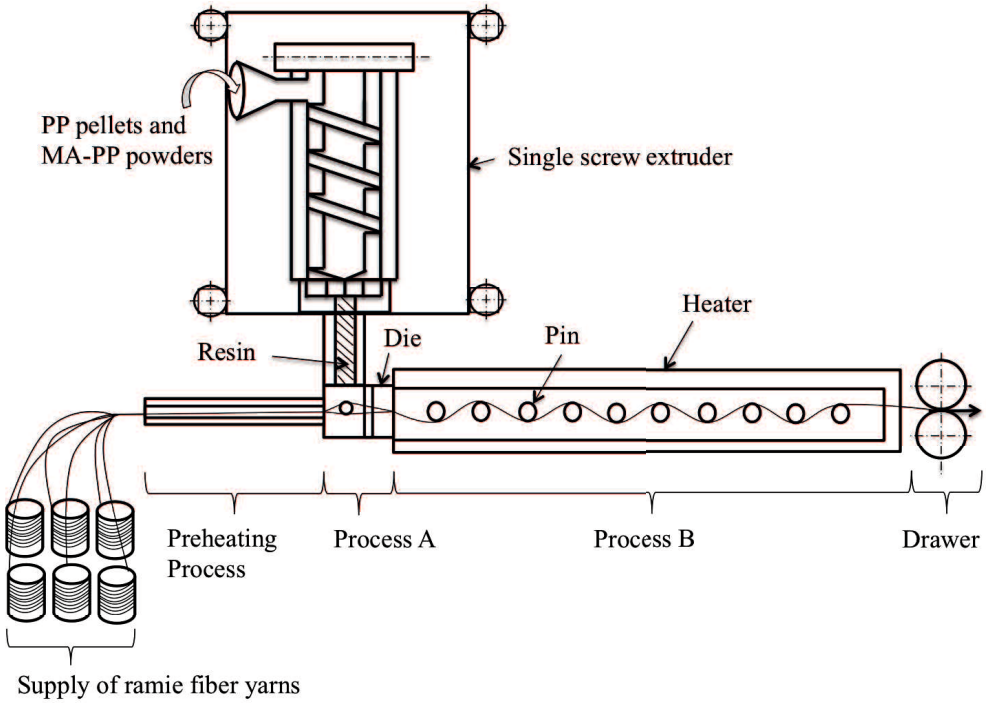

Figure 2.4 Schematic view of the present fabrication system. Process A: resin-coating process, Process B: multi-pin-assisted resin impregnation (M-PaRI) process.

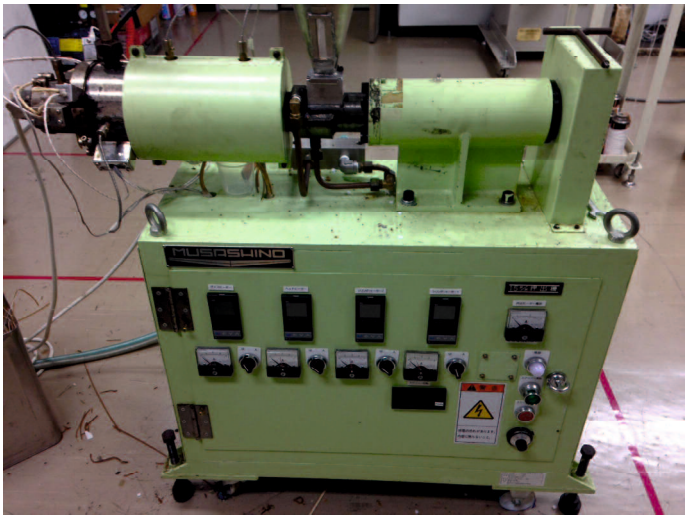

Figure 2.5 A photograph of a single screw extruder.

2.2.3 Injection molding

PP pellets containing granular MAPP were again mixed with the chopped pellets in order to obtain different fiber contents before conducting injection molding process. The resultant pellets

Figure 2.6 A chopped pellet containing six ramie single yarns by M-PaRI included process.

were molded into specimen dies of two types on an injection molding machine (Shinko Sellbic Co., Ltd.), as shown in Figure 2.7. Temperatures of cylinder, lock, and nozzle were set at 180°C, 180°C, and 185°C, respectively. Fiber contents of injection-molded tensile specimens were adjusted to 30 wt% and 10-50wt%, respectively.

Figure 2.7 A photograph of injection molding machine.

2.2.4 Tensile tests

Tensile tests of injection-molded ramie short fiber composite materials were carried out using a universal testing machine (Desktop type universal testing machine, LSC-1/30, JT Toshi Co. Ltd.). Shape and dimensions of small-sized (Japanese Industrial Standards, JIS K 7162, Type 5B) and medium sized (JIS K 7162, Type 1BA) specimens are shown in Figure 2.8. Tensile speeds for small and medium sized specimens were set at 10 mm/min and 17 mm/min,

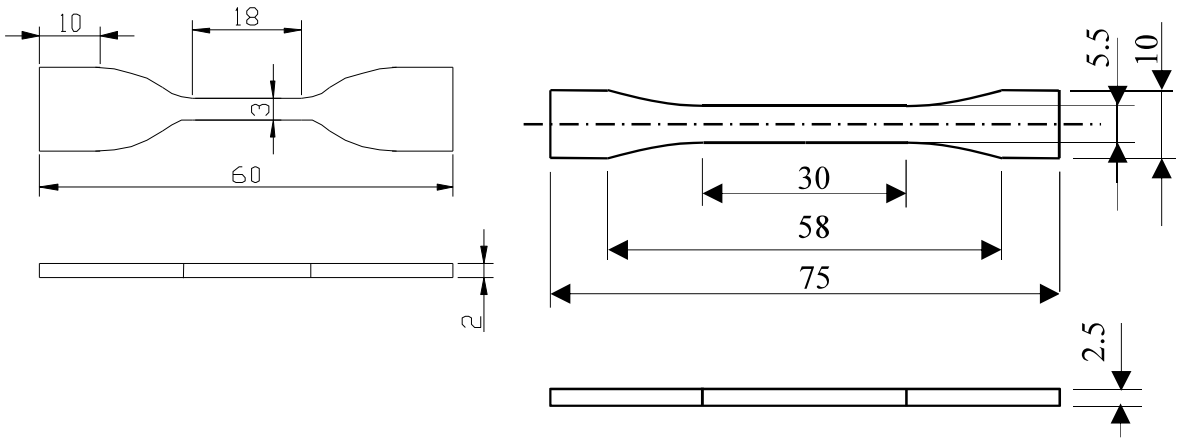

(a) Small sized (b) Medium size

Figure 2.8 Shape and dimension of tensile specimens.

respectively, that is equivalent to 10 mm/min at the same strain rate. The mean cross-section areas of small and medium sized specimens were determined by micrometer-measuring three locations along the longitudinal direction, and then taking an average. Five specimens were evaluated to reduce variation in mechanical properties. Tensile strength was obtained by dividing the measured maximum load by the mean cross-sectional area, and Young's modulus was evaluated in a linear region between 0.05 and 0.25% strains on a stress–strain curve for each test.

2.3 Results and discussion

2.3.1 Degree of impregnation of the resultant composite strands

In order to investigate infiltration of matrix among fibers, the obtained composite strands were filled with EP4901 and cured by addition of Jeffamine at the oven of 25^{o}C for 24 hours. Then, the harden materials were polished to examine the cross-section of the resultant composite strands. Microscopic cross-section images of ramie/PP composite strands are shown in Figure 2.9, in which the temperature of Process B was set at 195^{o}C. The strand was taken out of the fabrication system after it was stopped intentionally. Its several cross-sections before or inside Process B were observed. It is apparent from Figure 2.9(a) that many voids exist among fibers before Process B, although resin is locally infiltrated. Bledzki et al.[4)] carried out a

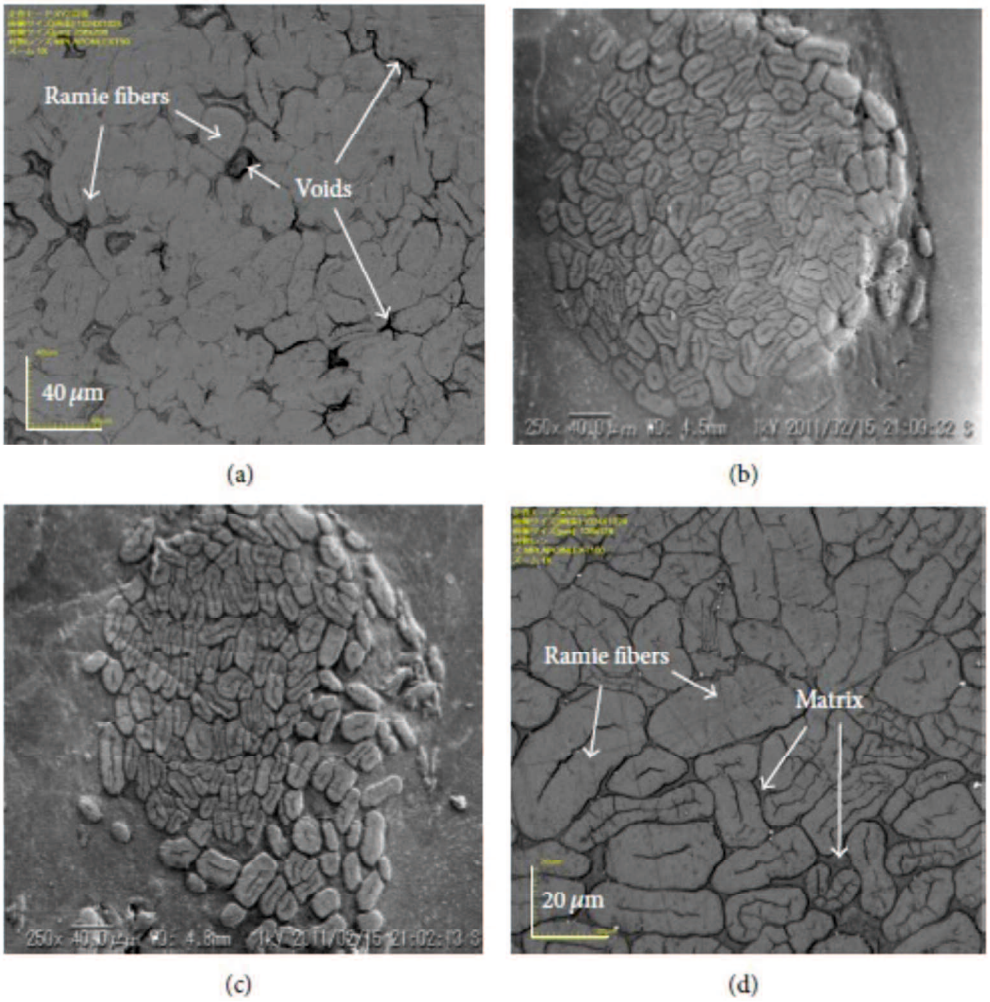

Figure 2.9 Cross-sectional images of ramie/PP composite strands—(a) before M-PaRI process, (b) after 11th pin, (c) after 15th pin, and (d) final product. Images in (a) and (d) are obtained using 3D laser measuring microscopy. Images in (b) and (c) were obtained using scanning electron microscopy.

two-step extrusion process, in which abaca/PLA strands obtained firstly by yarn coating process were pelletized and secondly inserted into a single extruder. It is guessed that the second process was conducted because such voids might not be removed in the first-step process. Figures 2.9(b) and 2.9(c) show images after the 11th and 15th pins, respectively. They show almost no void. The final product in Figure 2.9(d) shows that the cross-section contains the resin completely infiltrated among fibers with no void. It is well verified that the attached multi-pin system assists in impregnating the resin into interfibers. This system does not need any additional extrusion process. The mechanism of this impregnation is estimated such that continuous contact and rubbing between resin-coating yarns and pins flattens the yarns and widens the interfiber spaces. Consequently, the resin can be impregnated easily among fibers.

Tanaka and Hirano[5] achieved complete resin impregnation for jute-twisted yarn, as mentioned in Chapter 1. They also widened the interfiber spaces through an untwisted yarn process. Although this process can control the magnitude of the spaces by changing the number of untwists, it has to be prepared for each yarn. It demands complicated and expensive facilities. On the other hand, the composite process proposed herein can be widened among fibers by a simple process, as mentioned previously. It is concluded that, thereby, the composite strands can be produced successfully and more easily through such a combined technique: a conventional resin-coating process (Process A) followed by M-PaRI process (Process B).

2.3.2 Tensile properties

2.3.2.1 *Stress-Strain Behavior*

Figure 2.10 shows the effect of temperature during Process B on the tensile stress-strain behavior of the composites specimens containing 30 wt% fibers. The size of specimen was a small type in Figure 2.8(a). All of the stress-strain curves shown on linearity at around 2-3%, but the stress levels during deformation of composite specimens are much higher than that of PP. The level of composite stress also depends on the temperature at Process B. Composite specimens produced at low temperatures during Process B, that is, 160°C and 185°C, exhibit less stress, while composite specimens produced at 195°C, 205°C, and 225°C show higher stress and almost identical stress-strain behavior, especially at the initial stage. However, composite specimens produced at 160°C, 185°C, and 195°C exhibit a similar strain at break, whereas those produced at 205°C and 225°C show less fracture strain. In other words, less fracture energy is

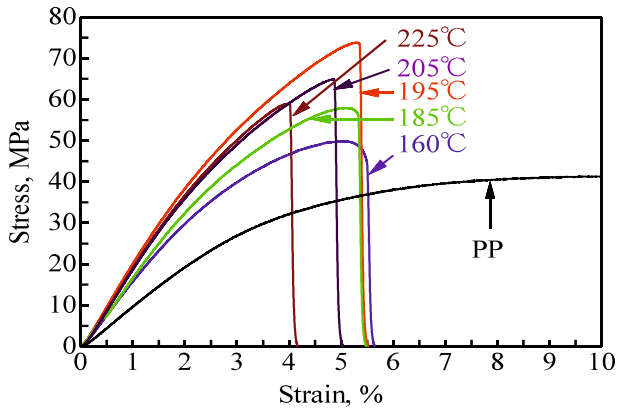

Figure 2.10 Typical stress-strain curves of short ramie/PP reinforced composites produced at different temperatures during Process B.

Table 2.2 Tensile properties of short ramie/PP composites

Material	T_{rip} °C	Young's modulus (GPa)	Tensile strength (MPa)	Fracture strain (%)
PP (0wt%)	-	1.04 (0.071)	42.4 (0.027)	>200
Composites	160	1.45 (0.11)	50.6 (0.053)	5.65 (0.083)
	185	1.64 (0.080)	55.1 (0.066)	5.32 (0.077)
	195	1.94 (0.072)	69.2 (0.046)	5.37 (0.040)
	205	1.72 (0.12)	67.7 (0.032)	5.26 (0.039)
	225	1.72 (0.086)	53.1 (0.086)	4.04 (0.093)

T_{rip}: Temperature at Multi-pin-assisted resin impregnation (M-PaRI) process
Numbers in parentheses denote coefficients of variation

brought from thermal exposure higher than 195°C during Process B.

2.3.2.2 *Tensile Strength and Young's Modulus*

Table 2.2 shows averages and coefficients of variation of the tensile properties of the small-sized PP and composite specimens. It can be seen that tensile strength and Young's modulus increase with increasing temperature over the whole 160–195°C range. Eventually, in the composites specimens of 195°C, not only did tensile strength improved 1.63 times higher than that of PP specimens, but also Young's modulus increased 1.87 times. However, a slight decrease in tensile strength in the specimens of 205◦C is found with a subsequent dramatic decrease of 225◦C. From the above, the maximum properties of composites could be obtained at 195-205◦C in the present fabrication system. It was observed that voids did not disappear, similar to Figure 2.9(a), when the composite strands were produced at 160◦C and 185◦C as shown in Figure 2.11. That is to say, the resin was not impregnated completely into interfibers even after Process B. The remaining voids decreased tensile strength and Young's modulus, as well as the whole stress level. It is inferred that, for the composite specimens of 205◦C and 225 ◦C, overheating causes degradation of ramie fibers during Process B. It is considered that such a thermal degradation of fibers induces premature fracture of the composite specimens.

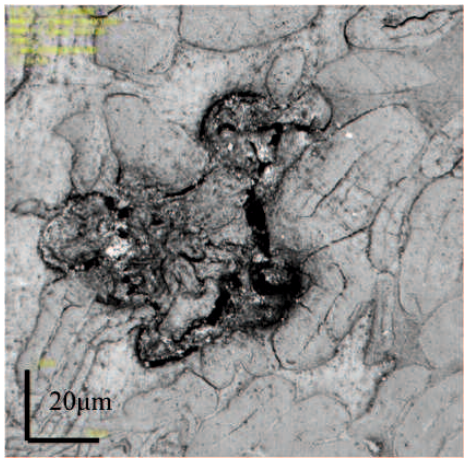

160°C

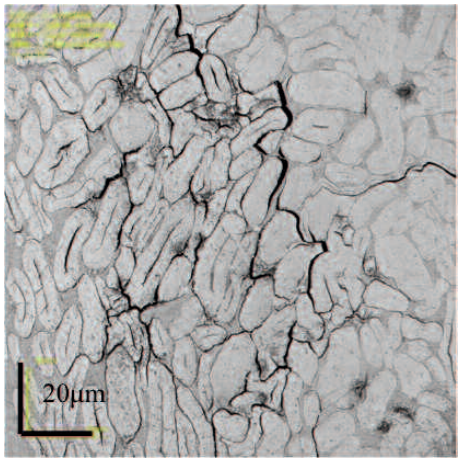

185°C

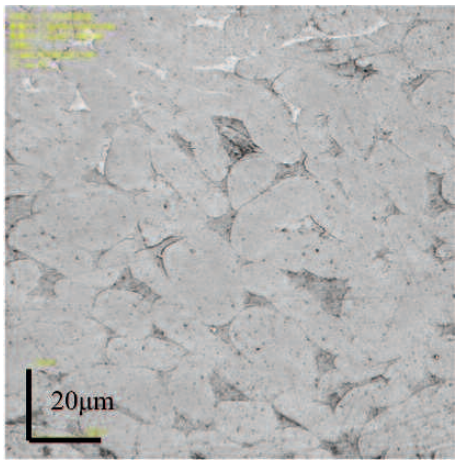

195°C

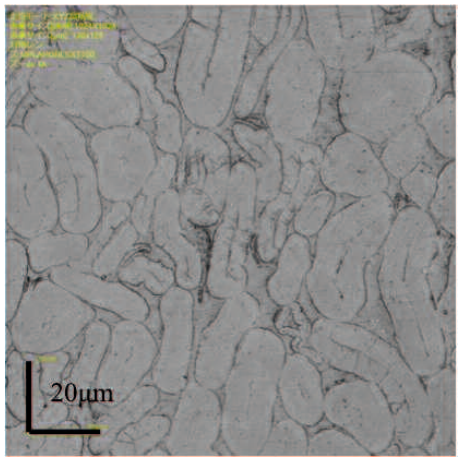

205°C

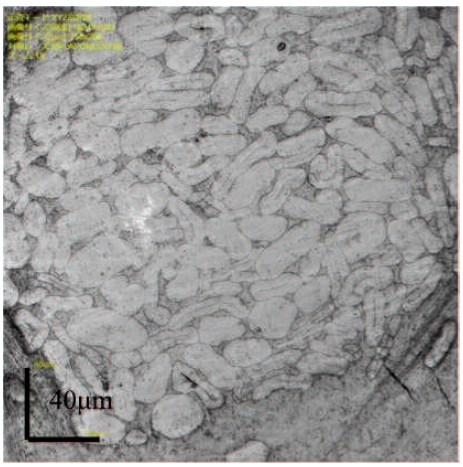

225°C

Figure 2.11 Cross-section images of the resultant composite strands. The Temperatures were set in the range 160°C -225°C during M-PaRI process.

2.3.2.3 *Effects of Fiber Content*

Figure 2.12 presents effects of fiber content on tensile properties of composite specimens. The size of the specimens was medium size of a type in Figure 2.8. For the specimens, the pellets produced at 195◦C during Process B were used. It is apparent in Figure 2.12(a) that the tensile strength increases with increasing fiber content. This trend reaches a maximum level at 40wt%. Tensile strength of 40wt% increased 1.73 times higher than PP specimens. Above this level of fiber content, the tensile strength starts to decrease. As can be seen in Figure 2.12(b), a continuous increase in Young's modulus occurs as the fiber content increases. That of 50 wt% specimens increased 2.17 times higher than the PP specimen. Results for fracture strain are shown in Figure 2.12(c). It is seen that fracture strain is decreased almost linearly between 4.0 and 7.0%. Consequently, although it exists between 30-50wt%, it can be said that the weight fraction of fiber content giving the best tensile properties is about 40wt%.

2.4 Fiber Dispersion and Fiber Length Distribution

Figure 2.13 shows a polished view of transverse section in a small-sized specimen produced at 195◦C during Process B. The fiber content in Figure 2.13 is 30 wt%. The black bar-like areas show marks of ramie fibers separated from matrix during the polishing process. White dots denote cross-sectional area of ramie fibers. As presented from Figure 2.13, a higher proportion of white dots is visible. Such a phenomenon can also be observed on glass fiber-reinforced composite specimens[6)-7)]. This means that short ramie/PP reinforced composites have a high degree of fiber orientation to the flow direction.

Figure 2.14 shows a magnified view of Figure 2.13. Results show that individual fibers after injection molding are well dispersed, despite the fact that high-density fiber bundles were obtained after M-PaRI process, as shown in Figure 9(d). When being strongly bonded, it is known that the bundles act as a reinforcing unit, which means that pull-out of bundles occurs at much lower stresses[7)]. Consequently, it should be noted that much higher interfacial stress can be yielded on the surface of the fibers. To confirm the change in fiber length after the applied fabrication processes, small-sized composite specimens produced at 195◦C during Process B were dissolved in boiling xylene for 24 hr to remove PP resin. Then, extracted ramie fibers were dried at 100◦C for 2hr. Figure 2.15 shows an SEM micrograph of ramie fibers. Although partial microfibril detachment is observed, the single fibers maintain their original structure even after Processes A and B with subsequent injection molding processing applied. Fiber length distribution of the specimens dissolved above is presented in Figure 2.16. The total

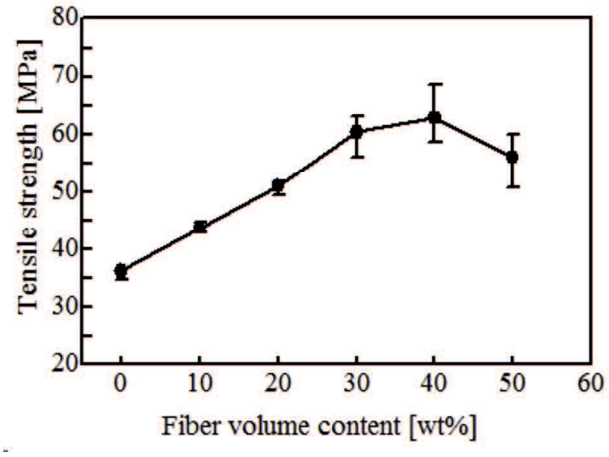

(a) Tensile strength versus fiber volume fraction.

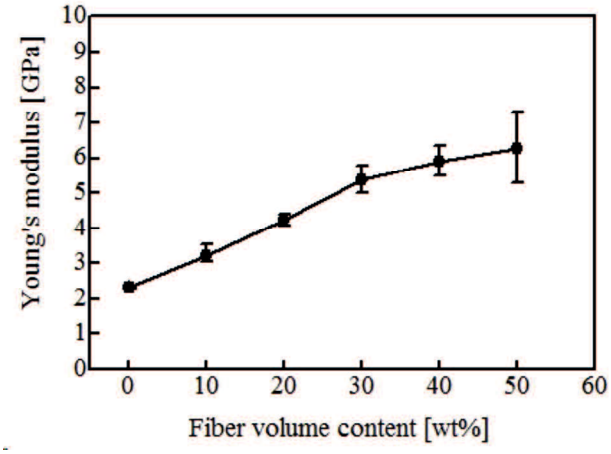

(b) Young's modulus versus fiber volume fraction.

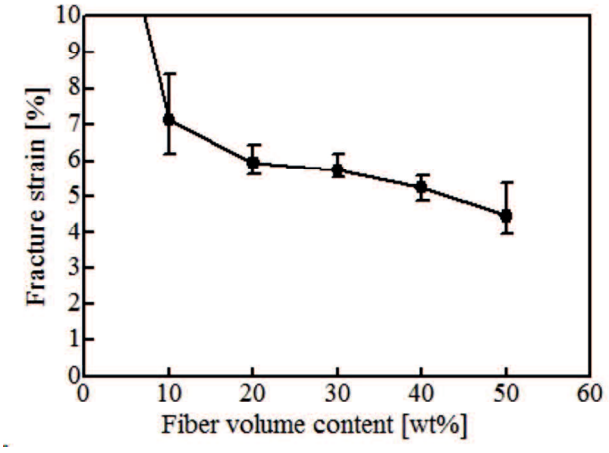

(c) Fracture strain versus fiber volume fraction.

Figure 2.12 Effect of fiber content on tensile properties of short ramie/PP reinforced composites produced at 195°C during Process B

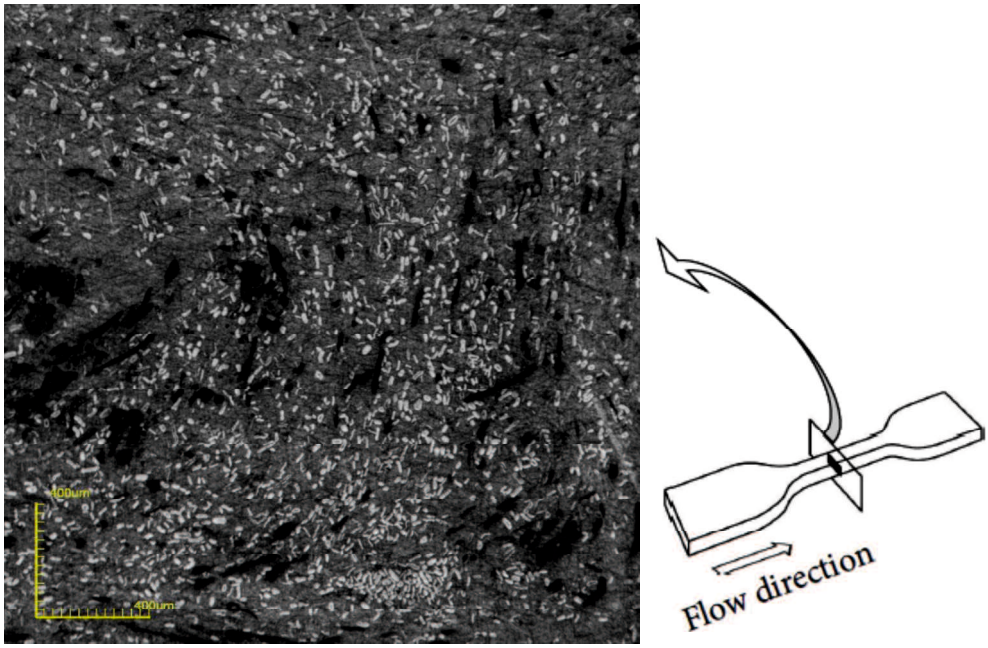

Figure 2.13 Laser micrograph of transverse section of short ramie/PP reinforced composites produced at 195◦C during Process B.

number of measured fibers was 780. Average fiber length was 1.56mm and the standard deviation was 0.61mm. It is necessary for short fiber-reinforced composites to be longer than the critical fiber length. According to an earlier report[8], the critical fiber length of ramie fiber is 0.47 mm. It can be clearly seen that over 98% of ramie fibers are longer than the critical length in this study. This brings sufficiently high stress to composite

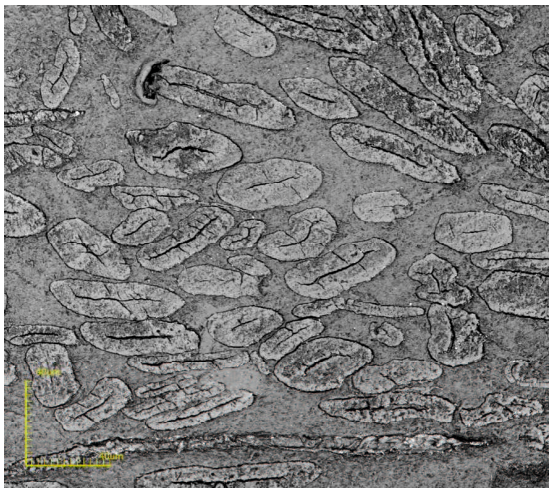

Figure 2.14 Laser micrograph of transverse section of short ramie/PP reinforced composites produced at 195°C during Process B.

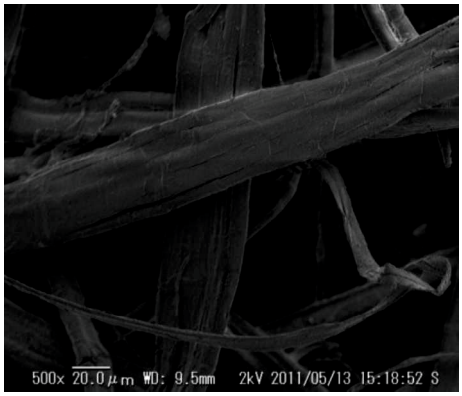

Figure 2.15 SEM micrograph of extracted fibers from short ramie/PP reinforced composites produced at 195°C during Process B.

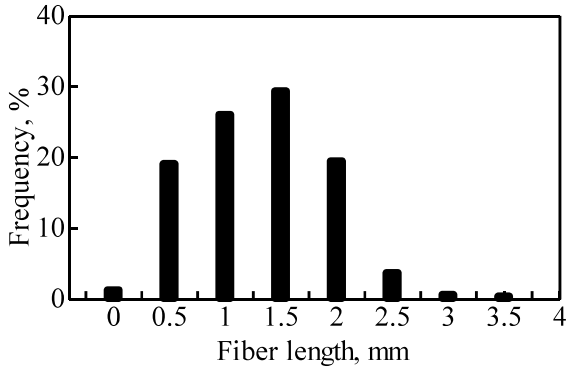

Figure 2.16 Fiber length distribution of extracted fibers from short ramie/PP reinforced composites produced at 195°C during Process B.

2.5 Conclusion

A new combination technique of resin-coating and multi pin-assisted resin impregnation (M-PaRI) processes was introduced to produce a continuous ramie single yarn/polypropylene (PP) reinforced composite strand. By addition of M-PaRI process, we found that the resin can be impregnated completely into the yarn interfibers. Furthermore, tensile tests of injection-molded composites were conducted using strands produced at different temperatures of M-PaRI process. Results show that the maximum mechanical properties of composites could be obtained between 195 and 205^{o}C.The fiber content giving the best tensile properties was about 40wt%. The new process presented in this study demonstrates marked improvements of mechanical properties on composites in comparison with conventional methods, in which fibers are inserted directly during the extrusion process. A fascinating point is the simplification of production for long natural fiber-reinforced composites. The composite strands obtained here are expected for use as a semi-finished material for injection and compression molding products.

2.6 References

1) Koichi Goda, M. S. Sreekala, Alexandre Gomes, Takeshi Kaji, Junji Ohgi, Improvement of plant based natural fibers for toughening green composites – Effect of load application during mercerization of ramie fibers, Composites, Part A 37, pp 2213-2220, 2006.

2) K.G. Satyanarayana, J.L. Guimarães, F. Wypych, Studies on lignocellulosic fibers of Brazil. Part Ⅰ: Source, production, morphology, properties and applications, Composites, Part A 38, pp 1694-1709, 2007.

3) Silva.F.A, Chawla.N, Filho.R.D.T, Tensile behavior of high performance natural (sisal) fibers, Composites Science and Technology, Vol.68, 2008.

4) A.K. Bledzki, A. Jaszkiewicz and D. Scherzer, Mechanical properties on PLA composites with man-made cellulose and abaca fibres, Composites, Part A 40, pp 404-412, 2009.

5) T. Tanaka and Y. Hirano, Kobe steel engineering reports, Vol. 51, No. 2, pp 62-66, 2001

6) Bowyer, W. H. & Bader, M., On the re-inforcement of thermoplastics by imperfectly aligned discontinuous fibres, Journal of Materials Science 7, pp 1315-1321. 1972.

7) Hull D, An introduction to composite materials, 1st ed., Cambridge: Cambridge University Press, pp 208-210, 1981.

8) L. Angelini, A. Lazzeri, G. Levita, D. Fontanelli and C. Bozzi, Industrial Crops and Products, Vol. 11, pp 145-161, 2000.

3. Single yarn composite strand and tape productions by M-PaRI process

3.1 Introduction

In Chapter 2, a new method of producing a ramie yarn/PP composite strand was developed and the mechanical properties of short ramie/PP composite materials were also discussed for application to mass-production using the pellets of long ramie/PP composite strands. On the other hand, composite tapes were also developed as the application of high strength composites in the past.

In the early stage, Burns invented a process using metal to create a composite tape[1)]. Eaton invented a fabrication method for composite tape[1)]. Truckner et al. also invented a fiber reinforced composite tape made by casting a mixture comprising high temperature metal or continuous ceramic fibers and a polymeric binder[2)]. Kim et al.[3)] and Hauber et al.[4)] discussed about computer programed lay-up process. However, few studies have been done using natural fibers.

In this section, thus, the tensile properties of a continuous ramie spun yarn/PP composite strand were discussed in different contents of MAPP using M-PaRI process. Furthermore, by adding a die and a roller system after M-PaRI process, a ramie/PP composite tape was also produced. The aim of producing a composite tape is application to plain woven fabric reinforced composite materials like glass roving clothes.

3.2 Experimental methods

3.2.1 Materials

Materials used in Chapter 3 were single ramie spun yarns, polypropylene pellets, and granular MAPP, which were the same as the materials used in Chapter 2. To investigate the effect of MAPP content on mechanical properties, MAPP-0.5 wt%, 1.0 wt%, and 2.0 wt% were added to PP neat resin. In addition, MAPP-free resin was prepared as a matrix constituent.

3.2.2 Productions of single yarn composite strand and yarn composite tape

Figure 3.1 shows a schematic illustration of continuous fabrication method for single ramie yarn /PP composite strand. The production procedure is the same as that in Chapter 2, but the number of the ramie spun yarn is just one. Figure 3.2 shows a schematic illustration of continuous fabrication method for ramie/PP composite tapes. Thirty-three ramie spun yarns pass through Process B all together. A 7×1 mm rectangular die with 2mm length was additionally attached to control its shape at the end of M-PaRI process, as shown by 'Die' in Figure 3.2. A new process was also added after Process D. In this process, two rollers were placed at different heights to produce a flatter ramie/PP composite tape as shown in Process E. One was placed at 110mm height (Type I), and another was at 270mm (Type II). The composite tape was

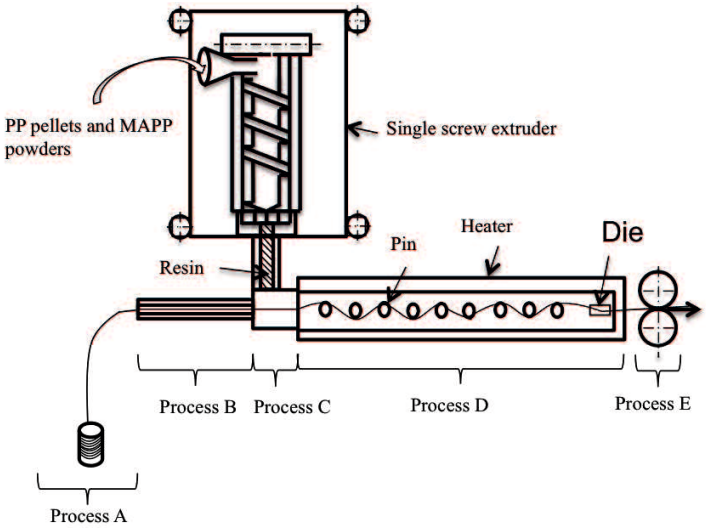

Figure 3.1 A schematic representation of continuous fabrication method for a ramie/PP composite strand. Process A: Raw material supply, Process B: Pre-heating, Process C: Resin coating, Process D: Multi-pin-assisted resin impregnation (M-PaRI), Process E: Pull out. (Processes C and D in this figure are equivalent to Processes A and B in Figure 2.4.)

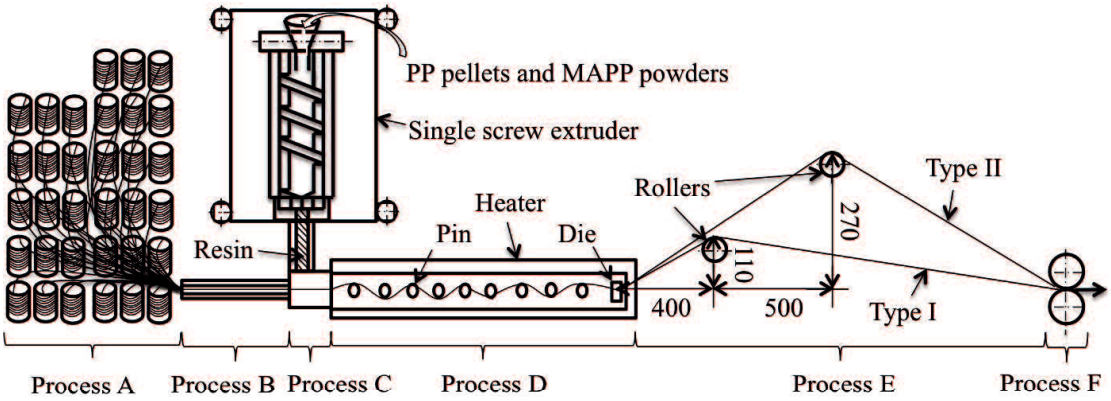

Figure 3.2 A schematic representation of continuous production of ramie/PP compoiste tapes. Proess A: Raw matrial supply, Process B: Pre-heating, Process C: Resin coating, Process D: M-PaRI, Process E: Flattening, Process F: Pull out.

continuously pulled out, as shown in Process F. The temperatures of Process C and Process D were set at 190°C and 200°C, respectively. The motor rotation speed at Process F was 45.0 rpm. The tapes were prepared only for MAPP-free or MAPP-2wt% contained matrix.

3.2.3 Tensile specimens

Figure 3.3 shows shape and dimension of tensile specimens for a yarn and tape composite materials. Tensile tests for a yarn and tape specimen were conducted using a universal testing machine (Desktop type universal testing machine, LSC-1/30, JT Toshi Co. Ltd., Japan) and Instrong (Shimadzu Corporation, Japan) at a crosshead speed of 1 mm/min. Each specimen was taken using a digital microscope (Digital microscope KH-1300; Hirox Co. Ltd., Japan). To obtain an average cross-section area of the specimen, diameters of 50 locations along the strand axis of each specimen were measured using software of SimpleDigitizer. Each diameter was measured with 1 mm interval along the axial direction. The Average cross-section area of a tape specimen was measured two locations along the axial direction. The gauge length of a yarn and

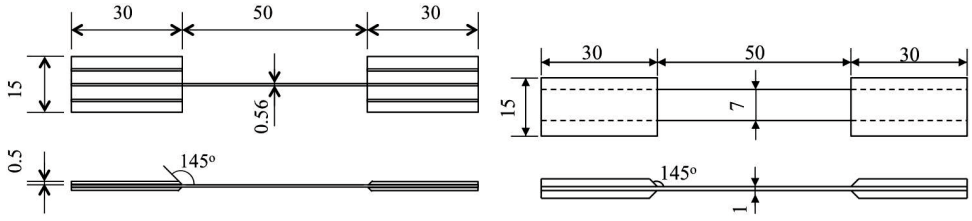

(a) Single yarn composite strand (b) Yarn composite tape

Figure 3.3 Tensile specimens of ramie spun yarn/PP composites.

tape specimen was 50 mm. Tensile strength was determined from the resultant stress–strain diagram. The elastic modulus was measured through linear approximation between 0.1–0.25% strains on the diagram. The meaning of 'elastic modulus' described here is the same as Young's modulus in the field of mechanical engineering. Strain gauge was used to measure the elastic modulus of tape specimens. However, in case of yarn specimens, strain gauge did not used since its thin width.

3.2.4 Measurement of fiber volume fraction and surface orientation angle

The ramie spun yarn and its composite strands and tapes were weighed using a semi-micro analytical balance (AUW220D; Shimadzu Corp., Japan). The fiber volume fraction on a composite strand was calculated using the following equation.

$$V_f = \frac{\frac{W_f}{\rho_f}}{\frac{W_f}{\rho_f} + \frac{W_m}{\rho_m}} \tag{1}$$

where V_f is the fiber volume fraction of the composite strand. W_f and W_m respectively denote the weight fractions of ramie spun yarn and matrix. In addition, ρ_f and ρ_m respectively denote the densities of ramie fiber and matrix: 1.16 g/cm^3 and 0.9 g/cm^3.

To obtain a statistical property of surface fiber orientation angle, many ~~fiber orientation~~ angles on the strand surface were measured through microphotographs by the above-mentioned digital microscope. Figure 3.4 shows the side-view of a strand and measurement method. The angles were finally obtained through image analysis.

3.3 Results and discussion

3.3.1 Single spun yarn composite strand

3.3.1.1 Surface morphology

Ramie spun yarn/PP composite materials were produced in different contents of MAPP. Surface morphology of the resultant strands was investigated by using scanning electron microscope before it was conducted tensile tests.

Figure 3.5 shows surface morphologies of a ramie yarn/PP composite material taken by a scanning electron microscope. Figure 3.5(a), (b), (c), and (d) were contained MAPP-free, 0.5wt%, 1wt%, and 2wt%, respectively. Magnified views of the composite strands were also shown in Figure 3.6.

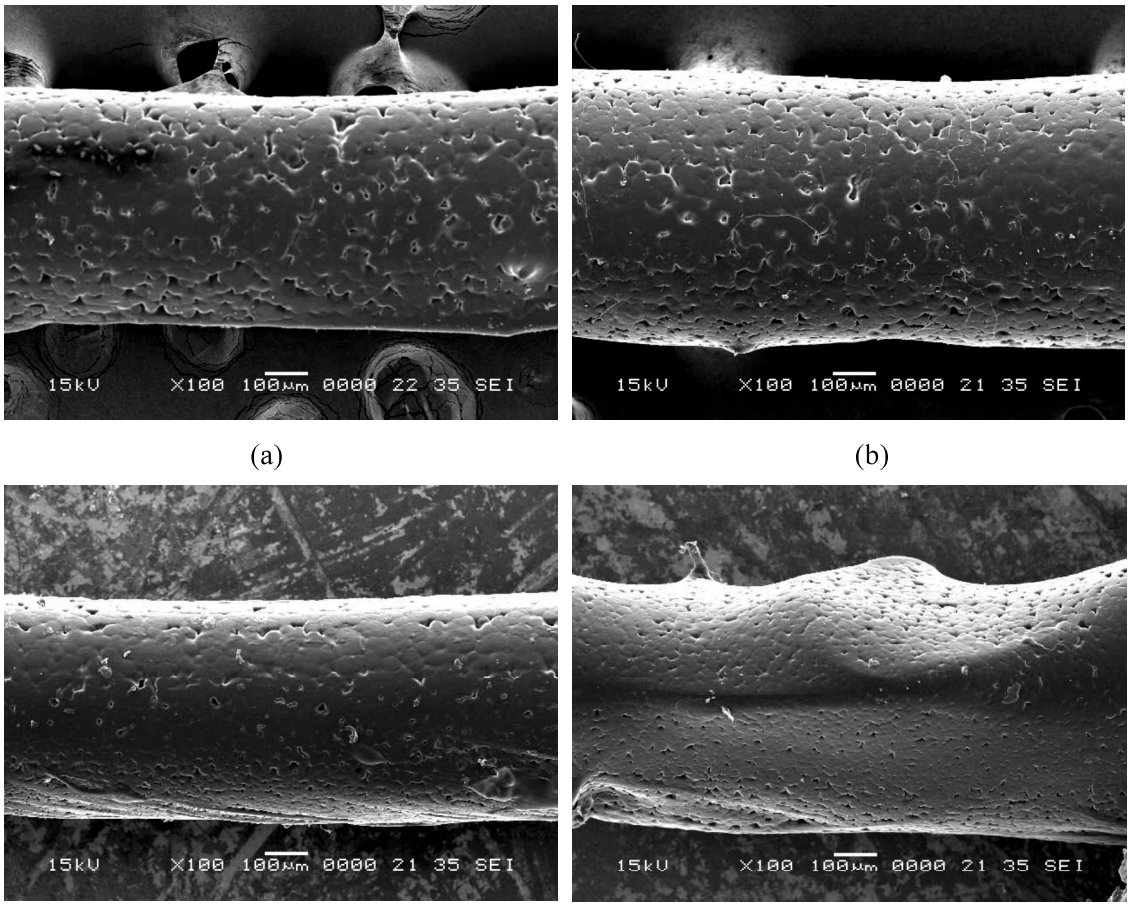

Figure 3.5 Surface morphologies of a ramie yarn/PP composite material. MAPP-free: (a), MAPP-0.5wt%: (b), MAPP-1wt%: (c), and MAPP-2wt%: (c).

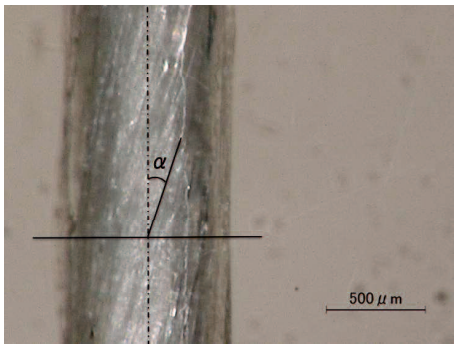

Figure 3.4 Measurement of a surface fiber orientation angle of the ramie spun yarn/PP composite strand.

It was observed that the diameters of the resultant composite strands were not uniform as shown in Figure 3.5. The diameter distribution is shown in Figure 3.7. The diameter varied in the range of 0.3 to 0.9mm. The mean and coefficient of variation (C.V.) were measured as 0.53mm and 0.187, respectively.

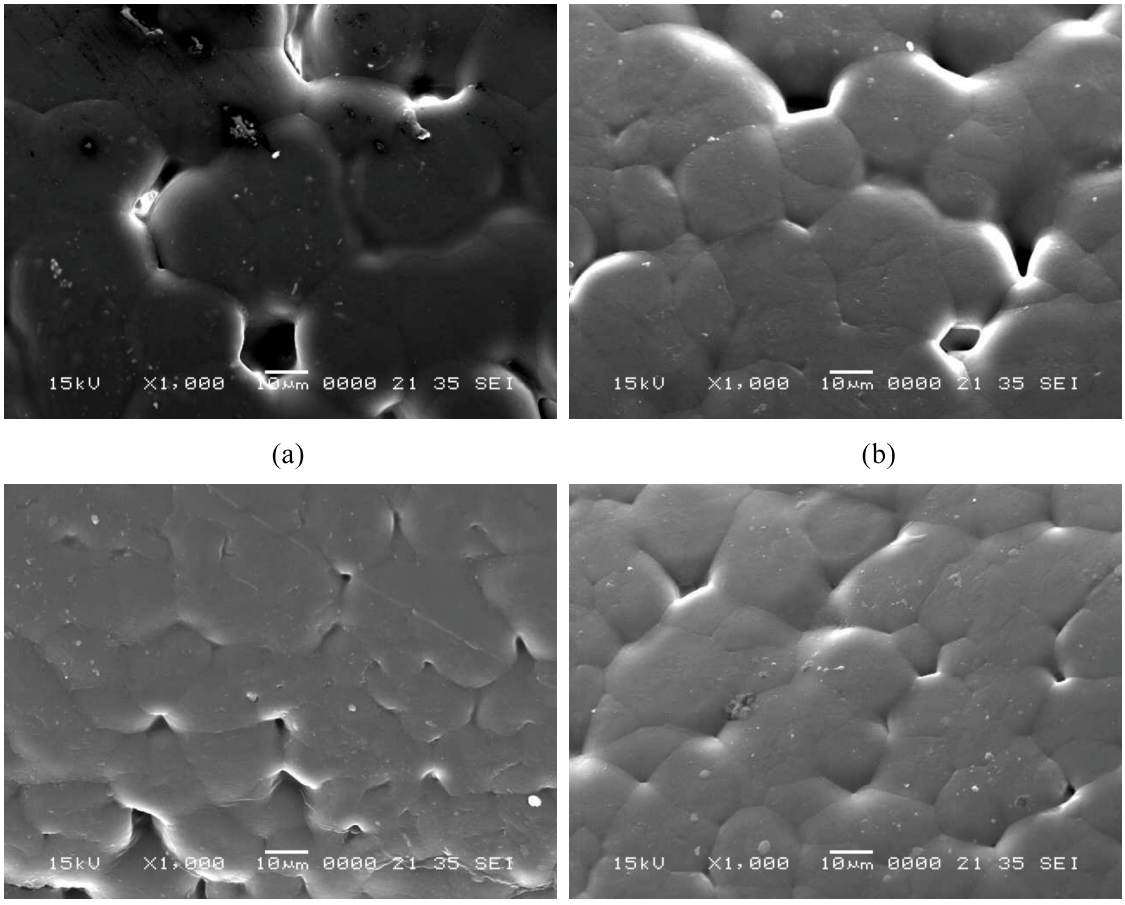

(a) (b)

(c) (d)

Figure 3.6 Magnified views of composite strands. MAPP-free: (a), MAPP-0.5wt%: (b), MAPP-1wt%: (c), MAPP-2wt%: (d).

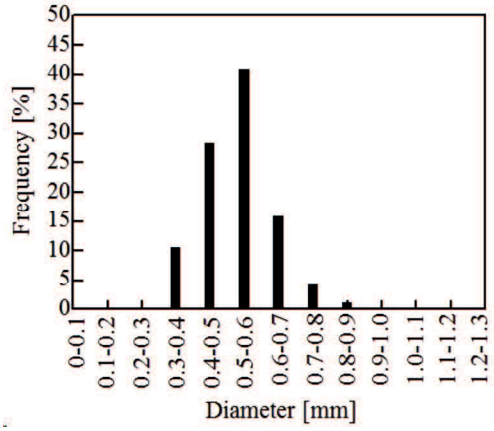

Figure 3.7 Diameter distribution of ramie spun yarn/PP composite specimens.

3.3.1.2 *Tensile properties*

Table 3.1 lists the tensile properties of ramie spun yarn/PP composite strands. Considering MAPP contents, tensile strength and elastic modulus decreased with in creasing MAPP contents. However, fiber volume fraction increased with increasing MAPP contents. Thus, it can be stated that MAPP brings more neat-PP on the composite surface as compared to MAPP-free.

Table 3.1 Tensile properties of ramie spun yarn/PP composite strands

MAPP content [wt%]	Number of specimens	Fiber volume fraction		Tensile strength		Elastic modulus	
		Mean V_f	C.V.	Mean [MPa]	C.V.	Mean [GPa]	C.V.
0	33	0.507	0.323	205	0.273	15.3	0.249
0.5	24	0.335	0.095	143	0.225	10.5	0.149
1	23	0.392	0.210	155	0.217	11.9	0.166
2	12	0.340	0.111	160	0.112	11.4	0.102

C.V.: Coefficient of variation

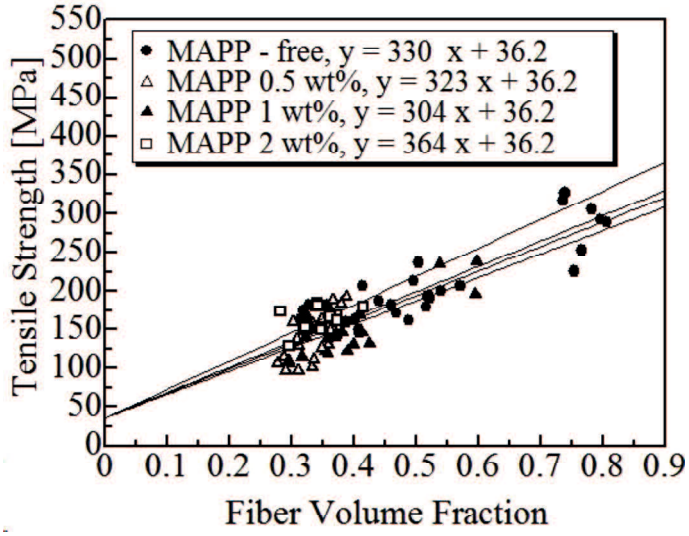

Figure 3.8 Relation between tensile strength and fiber volume fraction with different MAPP contents.

Tensile strengths of the resultant composite strands were plotted all together as shown in Figure 3.8. It was confirmed that tensile strengths increased with increasing fiber volume fraction. It was also confirmed that the slopes of tensile strength were not significantly changed with increasing MAPP contents. Thus, the regression lines were measured for each MAPP condition, as shown in Figures 3.8 and 11. By giving tensile strength and Young's modulus of neat PP as 36.2 MPa and 2.33 GPa, respectively, all regression lines were drawn to be in

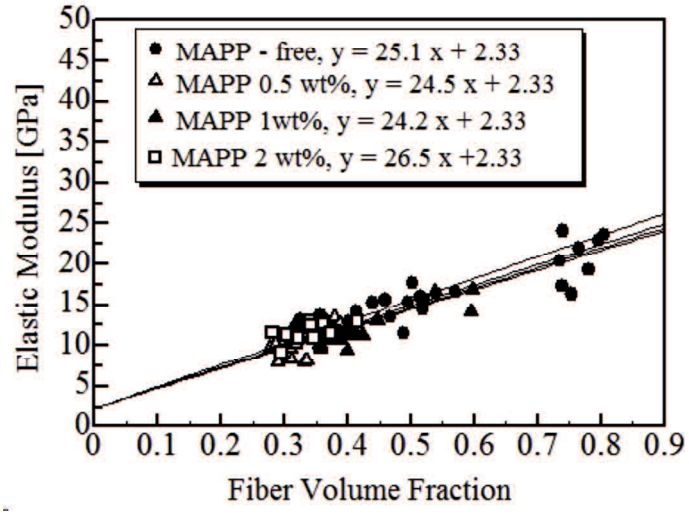

Figure 3.9 Elastic modulus versus fiber volume fraction with different MAPP contents.

agreement at their intercepts. It is evaluated from the equations of regression lines shown in Figure 3.8 that strands contained MAPP of 2wt% are relatively high in tensile strength as compared to other strands, while the equations of elastic moduli in Figure 3.9 are almost the same. This is because elastic modulus is measured in a linear stress-strain range before occurrence of interfacial debondings, affected by interfacial strength. The slopes of tensile strength and elastic modulus in total were 326 MPa and 24.9 GPa, respectively. The most difference from the total slope is 12% in tensile strength of MAPP-2wt% strands in Figure 3.8, but other strands are much closer to the total slope, i.e. 326 MPa. However, the fiber volume fractions of MAPP-2wt% strands are mainly in the range of 0.3 to 0.4, and therefore we cannot say that such a difference continues to be kept in a longer range. From the viewpoint of optimal MAPP contents, thus, we conclude that tensile strength and elastic modulus did not change so greatly in different MAPP contents.

3.2.1.3 *Fractography*

Photographs of fracture surface of ramie spun yarn/PP composite strand were shown in Figure 3.10. Figures 3.10(a), (b), (c), and (d) were MAPP-free, MAPP-0.5wt%, MAPP-1wt%, and MAPP-2wt%, respectively. Interface failure and frictional forces determined fracture surfaces. Large amounts of fiber pullout among fibers and matrices were observed in Figure 3.10(a). Relatively strong interfacial strength between fibers and matrices resulted that matrices were still adhered to a yarn as shown in Figure 3.10(b), (c), and (d) as compared to Figure 3.10(a). In addition, shear failures were also observed in Figures 3.10(b), (c), and (d).

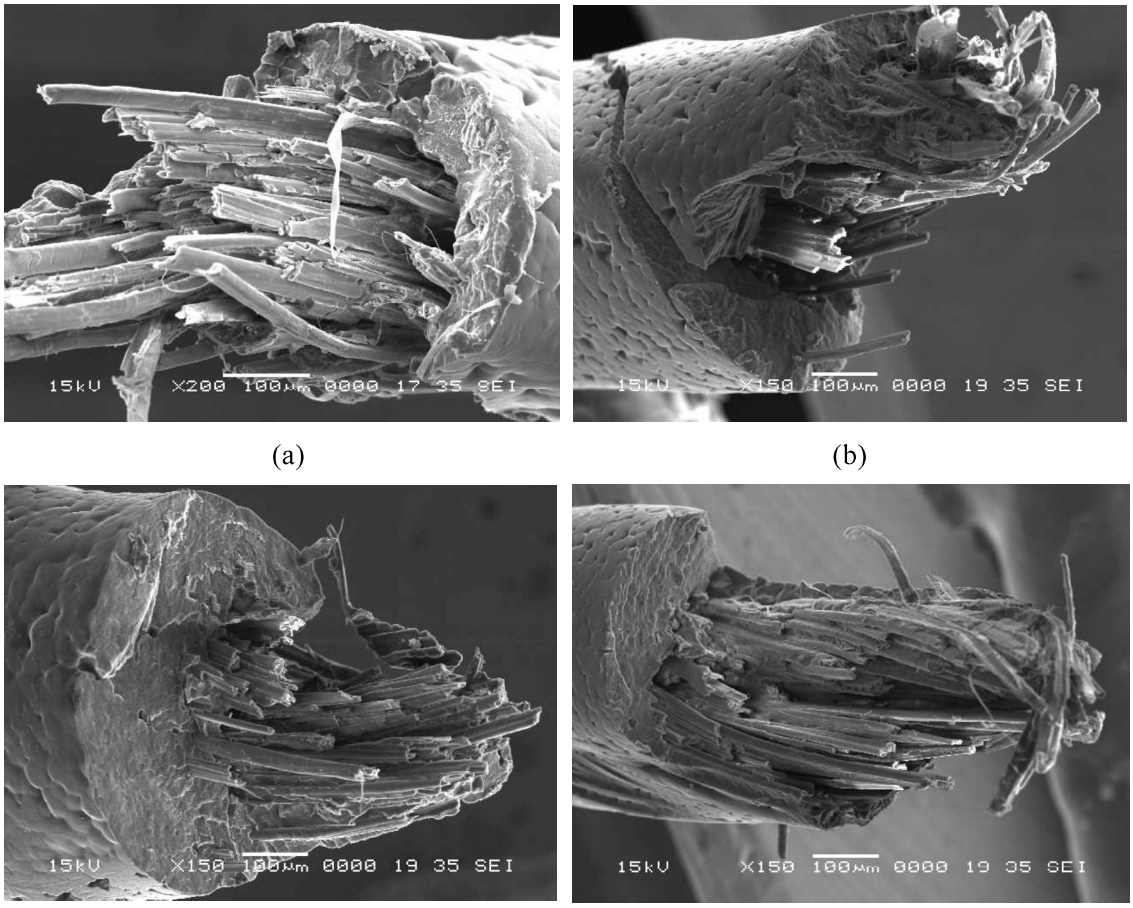

(a) (b)

(c) (d)

Figure 3.10 Photographs of fracture surface of ramie spun yarn/PP composite strands. MAPP-free: (a), MAPP-0.5wt%: (b), MAPP-1wt%, and MAPP-2wt%: (d).

3.3.2 Yarn composite tape

3.3.2.1 *Cross-section of the tape and fracture mode*

Figure 3.11 shows the typical cross-sectional micrographs of a yarn composite tape. Figure 3.11 (a), (b), and (c) were obtained by without Process E, Tpye I, and Tpye II in Figure 3.2, respectively. The resultant composite tape obtained without Process E was waved and curved as shown in Figure 3.11 (a). However, by applying Process E, a flat and rectangular shape of cross-section was obtainable as shown in Figure 3.11 (b). It means that, by using a roller placed at higher location than M-PaRI process, tension capable to the flat shape was actualized.

The effect of MAPP on the tensile fracture mode was investigated. The macroscopic fracture modes were shown in Figure 3.12. Large scale debonding occurs in the MAPP-free PP matrix specimen, as shown in Figure 3.12(a), while no macroscopic debonding occurs in the MAPP-2wt% contained PP matrix specimen of Figure 3.12(b). In other words, MAPP addition contributes to achieve strong fiber-matrix interfacial bonding. On the other hand, the large-scale longitudinal separation seen in Figure 3.12(a) is quite disadvantage in adopting the tape as a semi-finished material which is again used toward final products. Thus, mechanical properties of MAPP-free PP matrix specimens had not been examined.

(a)

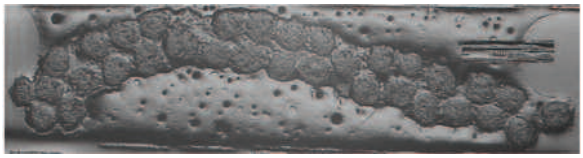

(b)

(c)

Figure 3.11 Cross-section images of a composite tape. (a), (b), and (c) were obtained by without Process E, Tpye I, and Type II in Figure 3.2, respectively.

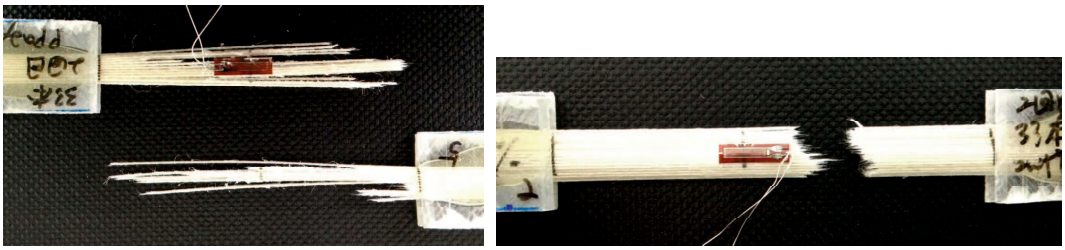

(a) MAPP-free PP matrix (b) MAPP-2wt% contained PP matrix

Figure 3.12 Fractured specimens after tensile test.

3.3.2.2 *Tensile properties*

Table 3.2 lists tensile properties of ramie yarn/PP composite tapes containing MAPP of 2wt%. Tensile strengths of the resultant composite tapes were plotted all together with the tensile strengths obtained by the composite strands in order to compare the differences as shown in Figure 3.13. It was confirmed that the slopes of the tensile strengths from the composite Type I and Type II were 22% and 27% lower as compared to the total mean slope, 326MPa, of the composite strands. These differences were brought from size effect of the composite tapes since the composite tapes contained thirty-three ramie spun yarns. Figure 3.14 shows elastic moduli of the composite strands and tapes. The slopes measured by composite tapes were slightly higher than the slopes of the composite strands since elastic moduli of the composite tapes were measured by strain gauge.

Table 3.2 Tensile properties of ramie spun yarn/PP composite tapes

Type of specimens	MAPP content [wt%]	Number of specimens	Fiber volume fraction		Tensile strength		Elastic modulus	
			Mean [V_f]	C.V.	Mean [MPa]	C.V.	Mean [GPa]	C.V.
I	2	5	0.561	0.023	179	0.090	17.7	0.041
II	2	5	0.605	0.025	181	0.020	20.6	0.040

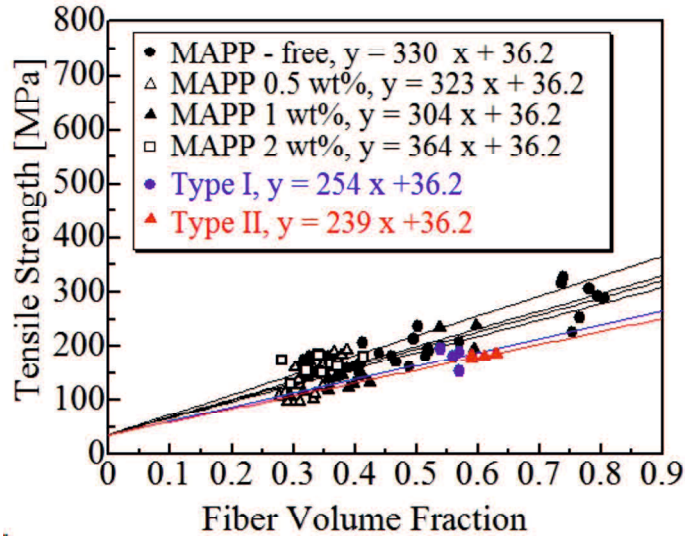

Figure 3.13 Tensile strengths of composite strands and tapes.

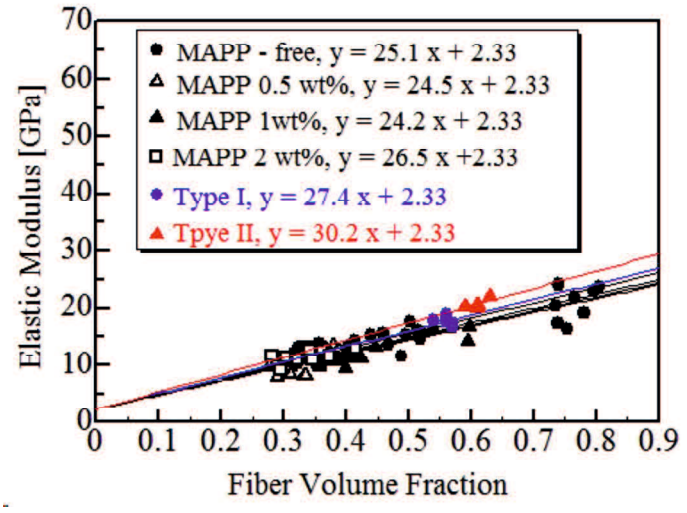

Figure 3.14 Elastic moduli of composite strands and tapes.

3.4 Conclusion

A single ramie spun yarn/PP composite strand and a yarn composite tape were produced using M-PaRI included process. To produce the yarn composite tape, the production system was improved by attaching a tape flattering roller system. The resultant composite specimens were tensile-tested to ascertain their mechanical properties such as tensile strength and elastic modulus. Results of the strand tensile tests and estimated regression lines showed that the tensile strength and elastic modulus did not change so greatly in different MAPP contents. The tensile properties increased concomitantly with increasing fiber volume fractions. The mean elastic modulus and coefficient of variation (C.V.) were 12.7 GPa and 0.260, respectively. The strength level of the composite tapes was less than that of the composite strands because of size effect.

3.5 References

1) Carmen D. Burns, Apparatus and process for laminating composite tape, US4296912 A, 1981.

2) William G. Truckner, Jon F. Edd, Casting a mixture consisting of high temperature metal or intermetallic particles, ceramic fibers and polymeric binders, stacking to form multilayer stack, pyrolysis to remove binder, hot isostatic pressing, US5405571 A, 1995.

3) Hee June Kim, Sun Kyung Kim, and Woo Il Lee, A Study on Heat Transfer During Thermoplastic Composite Tape Lay-up Process, Experimental Thermal and Fluid Science, 13, 408-418, 1996.

4) David E. Hauber, Rob J. Langone, James P. Martin, Scott F. Miller, Michael J. Pasanen, Composite tape laying apparatus and method, US7063118 B2, 2006.

4. Analysis of elastic modulus on composite stands and tapes

4.1 Introduction

In section 3, a ramie spun yarn/PP composite strand was produced using M-PaRI process. The resultant mechanical properties such as tensile strength and elastic modulus were also discussed along with those of the composite tapes. Meanwhile, it is necessary to explain the experimental values of elastic modulus on the composite yarns by comparing with theoretical models.

Theoretical models regarding mechanical properties of fiber reinforced composite materials have been developing by many researchers. Most of them developed their own strength models of the composite materials, because it is estimated that the composites tend to have a large variation in strength. Sinclair et al. published their research for graphite fibers/epoxy composite materials in 1981[1)]. In their study, it was clear that elastic modulus of the composite materials showed very little fluctuation with increasing off-axial angle.

In this study, however, elastic modulus on twisted yarn composite materials showed large fluctuation[2)-3)]. Despite of such results, few researches have been carried out regarding reliability models of elastic modulus on twisted yarn composite materials.

Firstly, in this section, the experimental values of elastic modulus obtained by the composite strands were compared with conventional theoretical models, i.e., Hearle et al., Rao-Farris, and Thwaites[2)-4)]. Next, the cause of fluctuation of elastic modulus on composite strands was explained using the three theories with the help of residual standard deviation (R.S.D.).

Lastly, the fluctuations of elastic modulus on composite strands were evaluated by using first order second moment (F.O.S.M.) approximation method, and furthermore this method was extended to reliability model of yarn composites' elastic modulus with different size.

4.2 Conventional theoretical models of elastic modulus

Theoretical models of a twisted yarn have extensively been discussed in the field of textile engineering from the early 1900's. Table 4.1 shows a summary of theories of twisted continuous yarns[2]. Most of theories were developed to calculate elastic modulus of the twisted yarns. It is considered that such extensive studies about elastic modulus of twisted yarns were conducted due to a large variation in experimental elastic modulus of the twisted yarns. Such variability also induced many researchers to propose different approaches for the theories in order to predict elastic modulus of twisted yarns.

When a twisted yarn is subject to tension, the simplest equation for a yarn modulus is expressed as $E_y=E_f\cos^2\alpha$, in which E_y, E_f, and α are yarn modulus, elastic modulus of fiber, and surface fiber orientation angle on a twisted yarn, respectively. In order to measure precisely elastic modulus of twisted yarns, additional theories were applied to the previous theory.

In this study, three prominent theories having different approach to elastic modulus of twisted yarns were selected to compare with experimental values of the present composite strands.

Hearle et al.[2] introduced geometric character of a yarn in 1960's. Hooke's law was used as the basis of the theory. This theoretical model cannot be explained without an assumption of ideal twisted geometry of $R/\tan\alpha=r/\tan\theta$, where R and α are outer radius and surface fiber orientation angle, respectively, which are given as constants. r and θ are inner radius and its fiber orientation angle, respectively, which are given as variables. It was taken the effect of lateral compression into account. After considering the complicated mathematical formulae, relatively simple expression for elastic modulus (E_y) of a yarn in case of constant volume fraction was derived as below. More detailed mathematical formulae are written in Appendix A.

$$E_y = E_3\left(\frac{3\cos^2\alpha}{1-\cos^2\alpha}\ln\cos^2\alpha+\frac{9}{4}\cos^2\alpha+\frac{1}{4}\right) \quad (1)$$

Using transformed reduced compliances, a complex equation for elastic modulus of a yarn was derived by Rao-Farris[3]. The stress-strain relation was formed on plane-stress state in classical lamination theory. The derived elastic modulus $\hat{E}(\alpha)$ is given as follows. Additional explanations are written in Appendix B.

Table 4.1 A summery of theories of twisted continuous filament yarns[1)]

Name and data	Nature of theoretical treatment
Gegauff (1907)	Theory of spun yarns, but includes basic equations of simplest treatment of filament yarns
Platt (1950)	Tensile forces only: Includes effects of lateral contraction, large extensions, and deviations from Hooke's Law
Hearle (1958)	Tensile and transverse forces: Small strains, Hook's Law, no lateral contraction
Hearle, El-Behery, and Thakur (1961)	(i) Tensile and transverse forces, small strains Hooke's Law, with lateral contraction
	(ii) Tensile forces only: large strains, lateral contraction, deviations from Hooke's Law
Treloar and Hearle (1962)	Corrects an error in previous two papers
Treloar (1962)	Continuum rubber filament model
Wilson and Treloar (1961)	Two-filament rubber model
Wilson (1962)	7 and 19 filament rubber models
Treloar and Riding (1963)	Energy method-includes effects of transverse forces, constant volume deformation, large strains, deviation from Hooke's Law
Symes (1959)	Cord properties, with approximations
Kilby (1964)	Develops theory to consider effect of equalization or nonequalization of tension in migrating filaments and effect of bending strains
Treloar (1965)	Applies energy method to yarn with migrating filaments
Treloar (1965)	Applies energy method to multi-ply cords
Wilson (1965)	Model yarns with five filaments in regular pattern around a core filament

$$\hat{E}(\alpha)=\frac{1}{\tan^2\alpha}\left[\begin{array}{l}\dfrac{b}{2c^2}\ln\dfrac{(a+b+c)T_0^2}{\left(aT_0^2+bT_0+c\right)}-\dfrac{T_0-1}{cT_0}\\ +\left(\dfrac{\left(b^2-2ac\right)}{2c^2\sqrt{b^2-4ac}}\right.\\ \left.\ln\dfrac{\left(2a+b-\sqrt{b^2-4ac}\right)\times\left(2T_0+b+\sqrt{b^2-4ac}\right)}{\left(2aT_0+b-\sqrt{b^2-4ac}\right)\times\left(2a+b+\sqrt{b^2-4ac}\right)}\right)\end{array}\right] \tag{2}$$

$$T_0=\cos^2\alpha,\ a=\frac{1}{E_z}+\frac{1}{E_y}+\frac{1}{E_s}+\frac{2v_{yz}}{E_z},\ b=\frac{1}{E_s}-\frac{2}{E_y}-\frac{2v_{yz}}{E_z},\ c=\frac{1}{E_y}$$

E_z and E_y respectively denote elastic moduli along the fiber and transverse axes. E_s is a shear modulus. v_{yz} is a Poisson's ratio.

Thwaites[4] added the effect of shear stresses to Hearle et al.'s model. Hooke's law and ideal twisted geometry were also adopted. The theory was based on laminate theory in cylindrical coordinates. Elastic modulus (a_{11}) in tension was expressed as below. Detailed mathematical formulae are written in Appendix C.

$$a_{11}=E_3\left\{-2+\left[\frac{6(\upsilon_{12}-2)}{1+\upsilon_{12}}+\frac{18G}{E_3}\right]\cot^2\alpha\ln\sec\alpha-\frac{9G}{E_3}\cos^2\alpha+\left(1-\frac{\sin^2\alpha}{2}\right)\frac{9}{1+\upsilon_{12}}\right\} \tag{3}$$

where E_3, υ_{12}, G, and α are elastic modulus of transverse axis, Poison's ratio, shear modulus, and surface fiber orientation angle, respectively. υ_{12} = 1-E_1/2E_3, in which E_1 is transverse elastic modulus of fiber.

4.2.1 Differences among the theoretical elastic moduli

In order to clarify differences of the conventional elastic moduli between Thwaites and Rao-Farris, transverse modulus (E_1) in equation (3) was given to 0. Figure 4.1 shows the results obtained from the elastic modulus of Thwaites (Equation (3)) and Ro-Rarris (Equation (2)). Two black lines were the results obtained from the theory of Thwaites. When given to E_1 = 0, it was confirmed that elastic modulus was decreased. In this case, almost similar results were obtained from the Rao-Farris as shown in blue line. From this result, the values obtained from Thwaites were slightly higher due to the effect of E_1.

To compare the two theories suggested by Thwaites and Hearle et al., shear modulus (G) in equation (3) was given to 0. Figure 4.2 shows the results. Two black lines were the results obtained from the theory of Thwaites. When given to G = 0, it was confirmed that elastic modulus was decreased. In this case, almost identical results were obtained from the Hearle et al. as shown in red line. From this result, it is considered that the differences between two theories

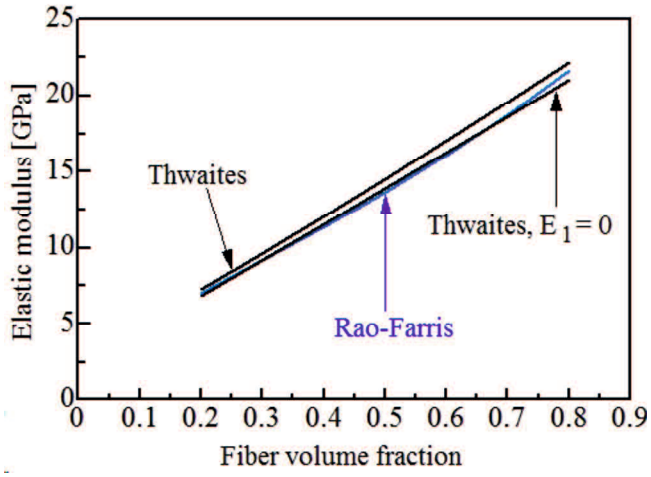

Figure 4.1 Comparison of elastic moduli between Thwaites and Rao-Rarris. In case of Thwaites's theory, transverse elastic modulus (E_1) was given to 0.

were caused by the influence of the shear modulus (G).

Table 4.2 summarizes the differences of three elastic moduli. Figure 4.3 shows an idealized geometry of a yarn used in theoretical models, in which a multi-layer structure is assumed. In the theory suggested by Thwaites, it was confirmed from the above mention that transverse elastic modulus (E_1) between layers and shear modulus (G) in a layer are considered. Although G is taken into account in the Rao-Farris's theory, E_1 is not considered. In the Hearle et al.

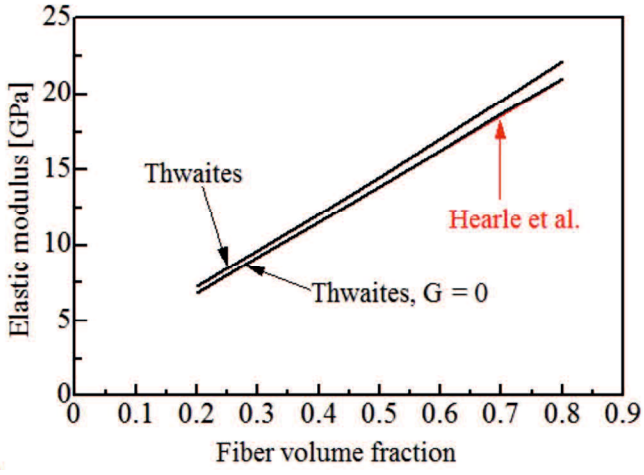

Figure 4.2 Comparison of elastic moduli between Thwaites and Hearle et al. Shear modulus (G) was given to 0 in the theory of Thwaites.

Table 4.2 Summery of differences among conventional elastic moduli of a twisted yarn material.

	G	E_1
Thwaites	○ (Between the elements)	○
Rao-Farris	○ (Within a layer)	×
Hearle et al.	×	○

theory, on the contrary, G is not considered.

It can be also noted that transverse elastic modulus (E_1) between layers and shear modulus (G) in a layer are considered in the theory suggested by Thwaites. Although, E_1 is taken into account in Hearle et al.'s theory, G is not considered.

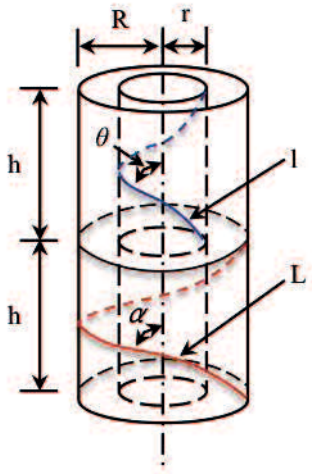

Figure 4.3 Schematic representation of an idealized geometry of a yarn[2)].

4.3 Comparison experimental values with theories of elastic modulus

Since it was confirmed that elastic moduli measured in this study were not affected by MAPP contents, as described in Chapter 3, these modulus data are treated all together in the below. Mean elastic modulus and C.V. of the total data were, respectively, 12.7 GPa and 0.260. Surface fiber orientation angles of the strands were measured as shown in Figure 3.4 of Section 3.2.4. Figure 4.4 shows the relative frequency of measured fiber orientation angles, on the ramie spun yarn/PP composite strands. Hereinafter, fiber orientation is denoted as α. The total number of data was 800, and the mean value and C.V. of α were, respectively, 14.4° and 0.218. It is noteworthy that C.V. of the elastic modulus shows a comparable level to that of fiber orientation angles.

Elastic moduli of fiber's longitudinal axis and transverse axis were respectively determined by the rule of mixture and Reuss models[5]. Moduli of ramie fiber and PP were given as 28.3GPa and 2.33GPa, respectively. Shear modulus in the theory of Rao-Farris was estimated as half of transverse elastic modulus E_y, because shear modulus E_s is often given as 0.5 to 0.8 times of E_y [6]. Poison's ratio v_{zy} was given 0.5. α was assigned as 14.4°, the mean fiber orientation angle on the actual yarn surface, as described above. Glossary list of notations for the theories is listed in Table 4.3.

Figure 4.5 shows the results of comparison between experimental values and theoretical models. Open circles represent experimental values of elastic modulus for composite strands. Red, blue, and black lines indicate the results from Hearle et al., Rao-Farris, and Thwaites models, respectively. It was observed that the values obtained by Hearle et al. were almost identical with those of Rao-Farris. The theoretical values of Thwaites had slightly higher values as compared to Hearle et al. and Rao-Farris.

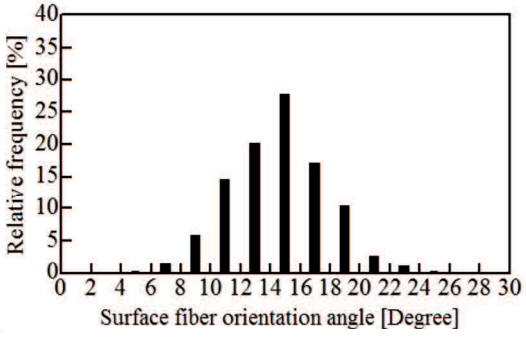

Figure 4.4 Distribution of surface fiber orientation angle on the ramie spun yarn/PP composite strands.

Table 4.3 Glossary list of notations for the theories.

	Elastic modulus		Shear modulus	Poison's ratio
	Fiber axis	Transverse axis		
Hearle et al.	E_3	-	-	v
Thwaites	E_3	E_1	G	v_{12}
Rao-Farris	E_z	E_y	E_s	v_{zy}

Figure 4.6 represents a schematic representation of an ideal yarn composite. The fibers are uniformly aligned to the same direction, which is the common concept between the theoretical models. However, as explained above, fiber orientation angles vary statistically in real yarn composite strands as illustrated in Figure 4.7. In this study, thus, the structure of a composite strand was assumed such that the strand comprises of n-segments with a small distance Δx and each segment has a different α.

Elastic moduli of theoretical models were obtained from equations (1), (2), and (3) by substituting measured α into each segment. Figures 4.8(a), (b), and (c) show comparison between experimental results and the values obtained by Hearle et al., Rao-Farris, and Thwaites. Any theoretical elastic modulus decreased with increasing fiber volume fraction in the fluctuation range of 5GPa to 10GPa, and fit well within the range of the experimental data. It was also confirmed that elastic modulus increased with decreasing surface fiber orientation

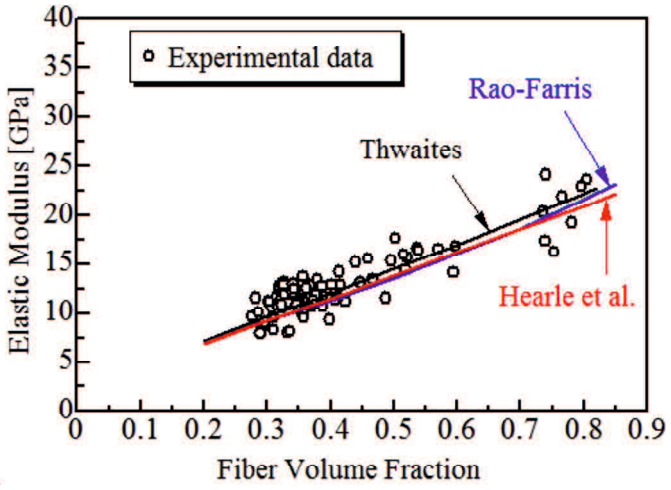

Figure 4.5 Comparison of experimental values with theoretical models. Using mean surface fiber orientation angle, theoretical values were obtained.

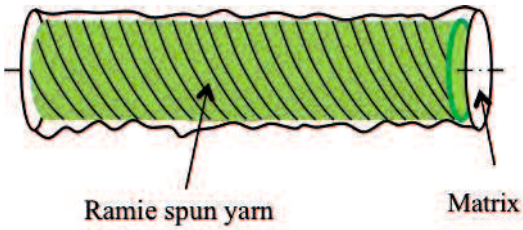

Figure 4.6 A schematic representation of an ideal yarn composite strand. Fiber ~~angles~~ are uniformly aligned.

angles. Regarding the magnitude of theoretical elastic modulus range, Thwaites model showed the smallest one.

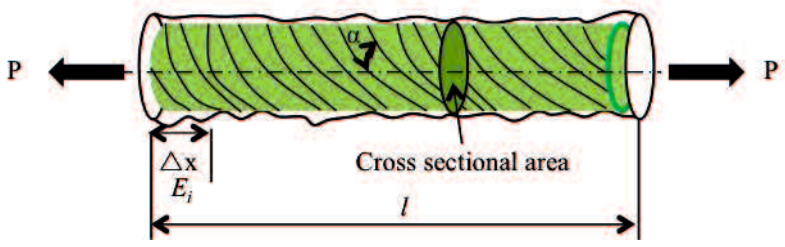

Figure 4.7 A schematic representation of a real yarn composite strand.

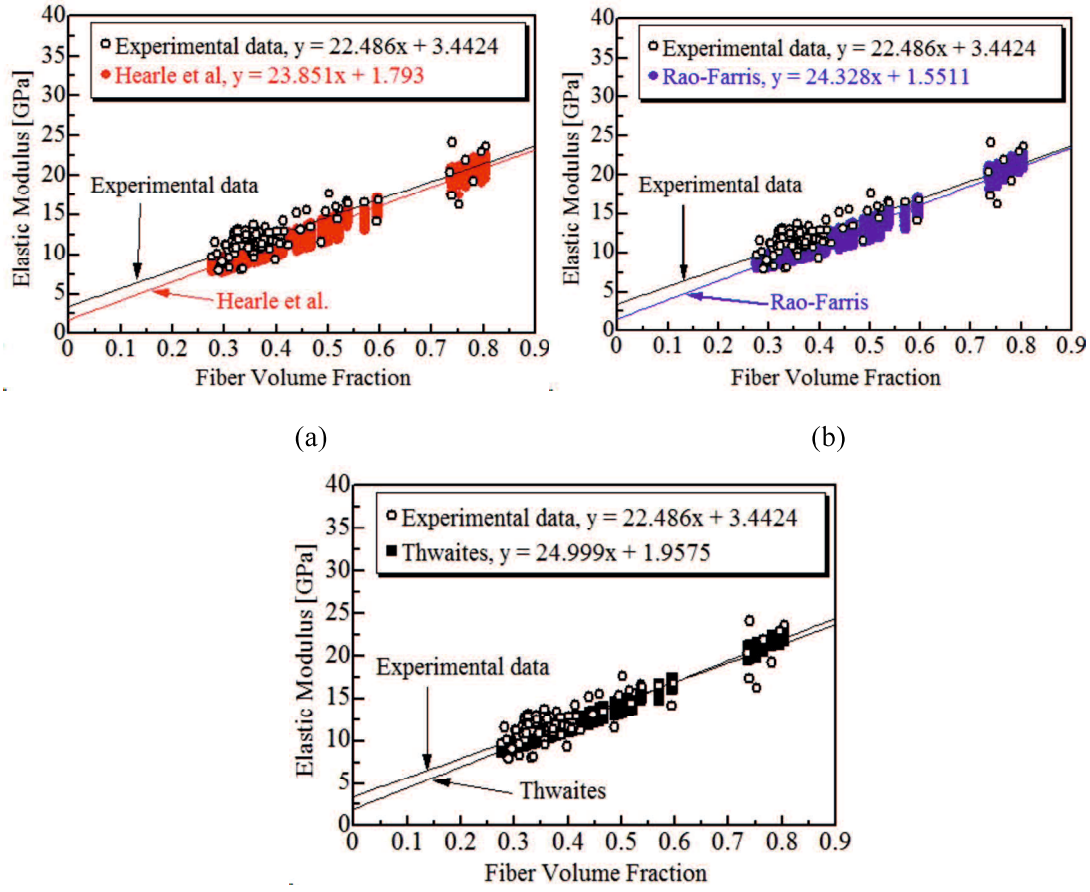

Figure 4.8 Comparison experimental values with theoretical models. (a): Hearle et al., (b): Rao-Farris, (c): Thwaites.

4.4 Reliability of elastic modulus on composite strands and tapes evaluated by first order second moment approximate method

Composite materials have different mechanical properties with different fiber directions. The variations of strength on the composite materials are caused by uncertainty in internal structure such as distributions of fiber orientation and length, and structural geometry[7]. Statistical analysis was developed in order to calculate the strengths of fibrous composite materials[8]. Finite element models (FEM)[9)-11)], Monte Carlo simulation[12)-14)], and first order second moment (F.O.S.M.) approximate method[15] are among the well-known methods to estimate the strength reliability of the composite materials. In this section, F.O.S.M. approximate method is introduced for statistical analysis of elastic modulus of twisted yarn composites.

4.4.1. Single random variables

A general function Y of a single random variable X in F.O.S.M. approximate method can be expressed as[16]

$$Y = f(X) \quad (4)$$

The mean [$E(Y)$] and variance [$Var(Y)$] of Y can be also obtained as below.

$$E(Y) = \int_{-\infty}^{\infty} f(X) f_x(x) dx \quad (5)$$

and

$$Var(Y) = \int_{-\infty}^{\infty} [f(x) - \mu_X]^2 f_x(x) dx \quad (6)$$

μ_X is the mean of X.

In order to calculate the mean and variance of a function of Y, it is necessary to know probability distribution function of $f_x(x)$. On the other hand, by using a Taylor series, the function of $f(X)$ can be obtained. The mean value of a Taylor series is expressed as

$$f(X) = f(\mu_X) + \frac{(X-\mu_X)}{1!}\frac{df}{dX} + \frac{(X-\mu_X)^2}{2!}\frac{d^2f}{dX^2} + \cdots + \frac{(X-\mu_X)^n}{2!}\frac{d^nf}{dX^n} \quad (7)$$

in which the derivatives are evaluated at μ_X.

The linear terms in the Taylor series is expressed as

$$E(Y) \simeq f(\mu_X) + \frac{(X-\mu_X)}{1!}\frac{df}{dX} \quad (8)$$

The mean value of a function of Y in F.O.S.M. approximation method is expressed as

$$E(Y) \simeq f(\mu_X) \quad (9)$$

and variance of a function of Y is

$$Var(Y) \simeq Var(X-\mu_X)\left(\frac{df}{dX}\right)^2 = Var(X)\left(\frac{df}{dX}\right)^2 \quad 10$$

The standard deviation $[S_T(Y)]$ of a function of X is expressed as

$$S_T(Y) = \sqrt{Var(Y)} \quad 11$$

Firstly, using equation of elastic modulus proposed by Hearle et al., The standard deviation (S_T) in F.O.S.M. approximation method using equation 10 can be obtained as

$$S_T = S_d(-2cos\alpha sin\alpha E_f V_f) \quad 12$$

Secondly, by using equation of elastic modulus derived by Rao-Farris, The standard deviation (S_T) can be also obtained as

$$S_T = S_d\left\{-\frac{\delta}{2\zeta^2}\left\{2cot\alpha csc^2\alpha\left[\ln\cos^4\alpha - \ln\left(\frac{\beta\cos^4\alpha+\delta\cos^2\alpha+\zeta}{\beta+\delta+\zeta}\right)\right] + 4\cot\alpha + \cot^2\alpha\left(\frac{-4\beta\cos^3\alpha\sin\alpha-2\delta\cos\alpha\sin\alpha}{\beta\cos^4\alpha+\delta\cos^2\alpha+\zeta}\right)\right\} + \right.$$

$$\left.\frac{\delta^2-2\beta\zeta}{2\zeta^2\sqrt{\delta^2-4\beta\zeta}}\frac{1}{\sin^3\alpha}\left[2cos\alpha\ln\frac{\left(2\beta\cos^2\alpha+\delta-\sqrt{\delta^2-4\beta\zeta}\right)\left(2\beta+\delta+\sqrt{\delta^2-4\beta\zeta}\right)}{\left(2\beta\cos^2\alpha+\delta+\sqrt{\delta^2-4\beta\zeta}\right)\left(2\beta+\delta-\sqrt{\delta^2-4\beta\zeta}\right)} + \frac{\cos^3\alpha\sin^2\alpha}{\left(2\beta\cos^2\alpha+\delta-\sqrt{\delta^2-4\beta\zeta}\right)}\frac{8\beta\sqrt{\delta^2-4\beta\zeta}}{\left(2\beta\cos^2\alpha+\delta+\sqrt{\delta^2-4\beta\zeta}\right)}\right]\right\} \quad 13$$

where $\beta = \frac{1}{E_p} + \frac{1}{E_q} - \frac{1}{G_{pq}} + \frac{2\nu_{pq}}{E_p}$, $\delta = \frac{1}{G_{pq}} - \frac{2}{E_q} - \frac{2\nu_{pq}}{E_p}$, and $\zeta = \frac{1}{E_q}$.

Lastly, using equation of elastic modulus derived by Thwaites, the standard deviation (S_T) is expressed as

$$S_T = S_d E_3\left\{\left[\frac{6(\upsilon_{12}-2)}{1+\upsilon_{12}} + \frac{18G}{E_3}\right]\left(\frac{-2cos\alpha ln\frac{1}{cos\alpha}}{\sin^3\alpha} + \frac{cos\,\alpha}{sin\,\alpha}\right) + \frac{18G}{E_3}cos\alpha sin\alpha - \frac{9}{1+\upsilon_{12}}sin\alpha cos\alpha\right\} \quad 14$$

where $\upsilon_{12} = 1 - \frac{E_1}{2E_3}$, $E_1 = \frac{1}{\frac{V_f}{E_f}+\frac{1-V_f}{E_m}}$, and $E_3 = V_f E_f + E_m(1-V_f)$.

The mean (μ_X) and standard deviation (S_d) of measured surface fiber orientation angle on composite strands were 14.4 [Deg] and 3.14 [Deg], respectively. The mean fiber volume fraction on composite strands was 0.41.

Table 4.2 Residual standard deviation (R.S.D.) of experimental elastic modulus of composite strands, and comparison with theoretical R.S.D. and first order second moment (F.O.S.M.).

Experimental R.S.D. [GPa]	Theoretical R.S.D. [GPa]			F.O.S.M. [GPa]		
	Hearle et al.	Rao-Farris	Thwaites	Hearle et al.	Rao-Farris	Thwaites
1.49	0.545	0.557	0.317	0.453	0.477	0.288

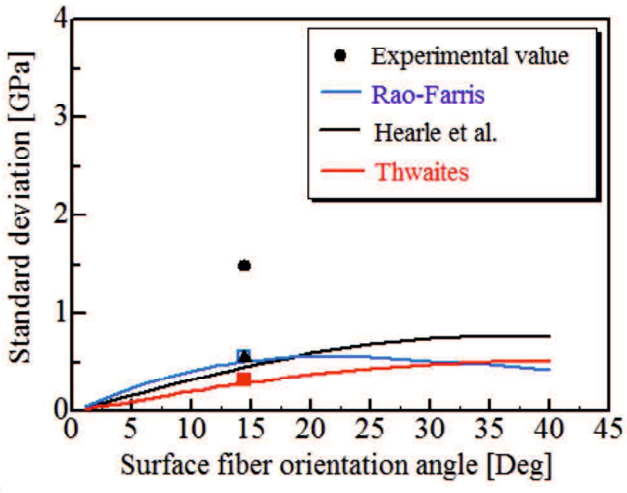

Figure 4.6 Standard deviation of elastic modulus versus surface fiber orientation angle. Symbols (●, □, ▲, ■) show experimental R.S.D., and theoretical R.S.D. of Rao-Farris, Hearle, et al. and Thwaites, respectively. Lines were obtained by F.O.S.M. approximate method.

By using F.O.S.M. approximate method, the S.D. of elastic modulus can be estimated in terms of surface fiber orientation angle. Table 4.2 lists residual standard deviation (R.S.D.) of experimental elastic modulus, theoretical R.S.D. obtained from Fig. 4.5, and standard deviations by F.O.S.M. approximate method. It was confirmed that experimental values showed higher than both theoretical values. Regarding the comparison between F.O.S.M. and R.S.D., on the other hand, the two theoretical S.D. showed similar values.

Figure 4.6 shows the S.D. of elastic modulus versus surface fiber orientation angle. Black closed circle was obtained by experimental value. Blue line, black line, and red line were calculated by F.O.SM. approximate method of Rao-Farris, Hearle et al., and Thwaites, respectively. Using R.S.D., blue rectangle, black closed triangle, and red closed rectangle were obtained by Rao-Farris, Hearle et al., and Thwaites, respectively. It can be observed that the S.D. estimated by F.O.S.M. in case of Hearle et al. and Thwaites increased with increasing surface fiber orientation angle. However, the S.D. obtained by Rao-Farris increased with increasing surface fiber orientation angle until 21 degree. After this maximum point, the S.D. gradually started to decrease. From the viewpoint of coefficient of variation, however, the statistical variation in elastic modulus would increase in any model, because the mean of elastic modulus decreases largely with increasing surface fiber orientation angle. As shown in Fig. 4.6, it is

proved in any case that F.O.S.M. approximate model based on a single variable described here cannot predict well the S.D. of experimental elastic modulus.

4.4.2 Multi random variables

Regarding the cause of variation in elastic modulus, in this subsection, fiber volume fraction is also taken into account, in addition to surface fiber orientation angle. A general function of multi random variables X_1, X_2 ... X_n in F.O.S.M. approximate method can be expressed as

$$Y = f(X_1, X_2, \dots X_n) \quad (15)$$

By using a Taylor series as same way of single random variables, the mean value of multi random variables in F.O.S.M. approximate method are expressed as

$$E(Y) \simeq f\left(\mu_{X_1}, \mu_{X_2}, \dots \mu_{X_n}\right) \quad (16)$$

and variance of multi random variables of a function of X is expressed as

$$Var(Y) \simeq \sum_{i=1}^{n} {S_d}_{X_1}{}^2 \left(\frac{\partial f}{\partial X_1}\right)^2 \quad (17)$$

The standard deviation $[S_d(Y)]$ of a function of X is expressed as

$$S_d(Y) = \sqrt{Var(Y)} \quad (18)$$

In case of using equation of elastic modulus from Hearle et al., the S.D. (S_T) in F.O.S.M. is expressed as below.

$$S_T{}^2 = S_v{}^2 * \left(E_f cos^2\alpha - E_m\right)^2 + S_\alpha{}^2 * \left(-2cos\alpha sin\alpha E_f V_f\right)^2 \quad (19)$$

where S_v and S_α indicate S.D. of fiber volume fraction and surface fiber orientation angle, respectively. E_f and E_m are Young's modulus of fiber and matrix, respectively. α and V_f represent surface fiber orientation angle and fiber volume fraction, respectively.

The S.D. in F.O.S.M. approximate method uising Rao & Farris's equation is expressed as follows.

$$S_T{}^2 =$$

$$S_v{}^2 *$$

$$\left\{\frac{1}{2\tan^2\alpha}\left\{\ln\cos^4\alpha\left(\frac{\zeta^2\delta'-\delta 2\zeta\zeta'}{\zeta^4}\right)-\frac{2\tan^2\alpha\zeta'}{\zeta^2}-\left[\frac{(\delta'\zeta-2\delta\zeta')}{\zeta^3}\ln\left(\frac{\beta\cos^4\alpha+\delta\cos^2\alpha+\zeta}{\beta+\delta+\zeta}\right)+\frac{\delta}{\zeta^2}\left[\frac{\left(\beta'\cos^4\alpha+\delta'\cos^2\alpha+\zeta'\right)}{(\beta\cos^4\alpha+\delta\cos^2\alpha+\zeta)}-\frac{(\beta'+\delta'+\zeta')}{(\beta+\delta+\zeta)}\right]\right]\right.\right.$$

$$\left.\left.+\frac{\zeta^2\sqrt{\delta^2-4\beta\zeta}\left\{+\left(\delta^2-2\beta\zeta\right)\left\{\begin{matrix}\frac{2\beta+\delta+\sqrt{\delta^2-4\beta\zeta}}{2\beta+\delta-\sqrt{\delta^2-4\beta\zeta}}\left[-\frac{(2\beta+\delta)(2\delta\delta'-4\beta'\zeta-4\beta\zeta')}{\sqrt{\delta^2-4\beta\zeta}\left(2\beta+\delta+\sqrt{\delta^2-4\beta\zeta}\right)^2}+\frac{2(2\beta'+\delta')\sqrt{\delta^2-4\beta\zeta}}{\left(2\beta+\delta+\sqrt{\delta^2-4\beta\zeta}\right)^2}\right]\\ \frac{2\beta\cos^2\alpha+\delta+\sqrt{\delta^2-4\beta\zeta}}{2\beta\cos^2\alpha+\delta-\sqrt{\delta^2-4\beta\zeta}}\left[-\frac{(2\beta\cos^2\alpha+\delta)(2\delta\delta'-4\beta'\zeta-4\beta\zeta')}{\sqrt{\delta^2-4\beta\zeta}\left(2\beta\cos^2\alpha+\delta+\sqrt{\delta^2-4\beta\zeta}\right)^2}+\frac{2(2\beta'\cos^2\alpha+\delta')\sqrt{\delta^2-4\beta\zeta}}{\left(2\beta\cos^2\alpha+\delta+\sqrt{\delta^2-4\beta\zeta}\right)^2}\right]\end{matrix}\right\}\right.\right.$$

$$\left.\left.+\left(\delta^2-2\beta\zeta\right)\left[2\zeta\zeta'\sqrt{\delta^2-4\beta\zeta}+\frac{\zeta^2(2\delta\delta'-4\beta'\zeta-4\beta\zeta')}{2\sqrt{\delta^2-4\beta\zeta}}\right]\ln\frac{\left(2\beta\cos^2\alpha+\delta-\sqrt{\delta^2-4\beta\zeta}\right)\left(2\beta+\delta+\sqrt{\delta^2-4\beta\zeta}\right)}{\left(2\beta\cos^2\alpha+\delta+\sqrt{\delta^2-4\beta\zeta}\right)\left(2\beta+\delta-\sqrt{\delta^2-4\beta\zeta}\right)}\right\}\right.$$

$$\left.+\frac{}{\left(\zeta^2\sqrt{\delta^2-4\beta\zeta}\right)^2}\right\}\right\}^2$$

$$+S_\alpha{}^2 *\left\{-\frac{\delta}{2\zeta^2}\left\{2cot\alpha csc^2\alpha\left[\ln\cos^4\alpha-\ln\left(\frac{\beta\cos^4\alpha+\delta\cos^2\alpha+\zeta}{\beta+\delta+\zeta}\right)\right]+4\cot\alpha+\cot^2\alpha\left(\frac{-4\beta\cos^3\alpha\sin\alpha-2\delta\cos\alpha\sin\alpha}{\beta\cos^4\alpha+\delta\cos^2\alpha+\zeta}\right)\right\}+\right.$$

$$\left.\frac{\delta^2-2\beta\zeta}{2\zeta^2\sqrt{\delta^2-4\beta\zeta}}\frac{1}{\sin^3\alpha}\left[2cos\alpha\ln\frac{\left(2\beta\cos^2\alpha+\delta-\sqrt{\delta^2-4\beta\zeta}\right)\left(2\beta+\delta+\sqrt{\delta^2-4\beta\zeta}\right)}{\left(2\beta\cos^2\alpha+\delta+\sqrt{\delta^2-4\beta\zeta}\right)\left(2\beta+\delta-\sqrt{\delta^2-4\beta\zeta}\right)}+\frac{\cos^3\alpha\sin^2\alpha}{\left(2\beta\cos^2\alpha+\delta-\sqrt{\delta^2-4\beta\zeta}\right)}\frac{8\beta\sqrt{\delta^2-4\beta\zeta}}{\left(2\beta\cos^2\alpha+\delta+\sqrt{\delta^2-4\beta\zeta}\right)}\right]\right\}^2 \qquad 20$$

where $\beta=\frac{1}{\mathrm{E_p}}+\frac{1}{\mathrm{E_q}}-\frac{1}{G_{pq}}+\frac{2\nu_{pq}}{\mathrm{E_p}}$, $\delta=\frac{1}{G_{pq}}-\frac{2}{\mathrm{E_q}}-\frac{2\nu_{pq}}{\mathrm{E_p}}$, $\zeta=\frac{1}{\mathrm{E_q}}$, $\beta'=\frac{-E_f+E_m}{\left(E_fV_f+E_m-E_mV_f\right)^2}+\frac{E_m-E_f}{E_fE_m}+$

$\frac{-2\nu_{yz}(E_f-E_m)}{\left(E_fV_f+E_m-E_mV_f\right)^2}$, $\delta'=-\frac{2(E_m-E_f)}{E_fE_m}+\frac{2\nu_{yz}(E_f-E_m)}{(E_fV_f+E_m-E_mV_f)^2}$, and $\zeta'=\frac{E_m-E_f}{E_fE_m}$.

By using equation of elastic modulus from Thwaties, the S.D. in F.O.S.M. is expressed as follows.

$$S_T{}^2 =$$

$$S_v{}^2 *\left\{-2E_{33}{}' + 6\cot^2\alpha\, ln\sec\alpha\frac{(1+\upsilon_{12})[E_{33}{}'(\upsilon_{12}-2)+E_{33}\upsilon_{12}{}']-E_{33}(\upsilon_{12}-2)\upsilon_{12}{}'}{(1+\upsilon_{12})^2}+9E_{11}{}'\cot^2\alpha\, ln\sec\alpha-\right.$$

$$\left.9\frac{E_{11}{}'}{2}\cos^2\alpha+9\left[1-\frac{\sin^2\alpha}{2}\right]\frac{(1+\upsilon_{12})E_3{}'-E_3\upsilon_{12}{}'}{(1+\upsilon_{12})^2}\right\}+S_\alpha{}^2 *\left\{E_3\left\{\left[\frac{6(\upsilon_{12}-2)}{1+\upsilon_{12}}+\frac{18G}{E_3}\right]\left(\frac{-2cos\alpha ln\frac{1}{cos\alpha}}{\sin^3\alpha}+\frac{cos\alpha}{sin\alpha}\right)+\right.\right.$$

$$\left.\left.\frac{18G}{E_3}cos\alpha sin\alpha-\frac{9}{1+\upsilon_{12}}sin\alpha cos\alpha\right\}\right\}^2 \qquad 21$$

where $E_{33}{}'=E_f-E_m$, $\upsilon_{12}{}'=\frac{-E_{33}E_{11}{}'+E_{11}E_{33}{}'}{2E_{33}{}^2}$, $E_{11}{}'=\frac{-E_fE_m(E_m-E_f)}{(V_fE_m+E_f-V_fE_f)^2}$

In this study, mean and S.D. of fiber volume fraction on composite strands were 0.41 and 0.131, respectively. These values and mean and S.D. of surface fiber orientation angle were

Table 4.3 Experimental standard deviation of elastic modulus on composite strands and comparison with first order second moment (F.O.S.M.) approximate method. V_f of 0.41 was used to calculate F.O.S.M..

Experimental value [GPa]	F.O.S.M. [GPa]		
	Hearle et al.	Rao-Farris	Thwaites
3.30	4.53	2.55	3.20

substituted into eqs. (19), (20) and (21). Table 4.3 lists the results of S.D. of experimental value and F.O.S.M. approximate methods. It can be noted that any order of F.O.S.M. approximate method is closer to the experimental value, as compared with the single-variable-based F.O.S.M. Especially, that of Thwaites model shows a closer value than other theories.

4.4.3 Size effect on standard deviation in elastic modulus

In order to clarify the difference between statistical variations in elastic modulus of the composite strand and tape, in this subsection, F.O.S.M. approximate method is formulized to a reliability model including size effect. Figure 4.7 shows a schematic representation of a composite tape. In this figure, l_i (i=1, … , n) and w_j (j=1, … , m) indicate the element length and width, and n and m are the number of elements to longitudinal and transverse directions, respectively. In case of a composite tape consisting of n elements per strand and m strands, the elastic modulus E_T is expressed as below:

$$E_T = \frac{1}{m}\sum_{j=1}^{m} E^j = \frac{1}{m}\sum_{j=1}^{m} \frac{n}{\sum_{i=1}^{n}\left(\frac{1}{E_i{}^j}\right)} = \frac{n}{m}\sum_{j=1}^{m} \frac{1}{\sum_{i=1}^{n}\left(\frac{1}{E_i{}^j}\right)} \qquad 22$$

E^j is the elastic modulus of the strand j, and $E_i{}^j$ is the elastic modulus of the element j in the strand i. If each element modulus has the same elastic modulus E_0, then the mean value $\bar{E}$ is expressed as below:

$$\bar{E} = \frac{n}{m}\sum_{j=1}^{m} \frac{1}{\frac{n}{E_0}} = \frac{n}{m}\frac{m}{\frac{n}{E_0}} = E_0 \qquad 23$$

Variance in elastic modulus $Var\ [Z]$ by F.O.S.M. approximate method can be obtained as follows

$$Var[Z] = Var[E_i{}^j]\frac{1}{mn} \qquad 24$$

where, $Var\ [E_i{}^j]$ is the variance in elastic modus of each element.

In order to measure the S.D. in F.O.S.M. approximate method on composite tapes, 1 and 33 were given to n and m, respectively, following the actual numbers of spun yarns in the strand

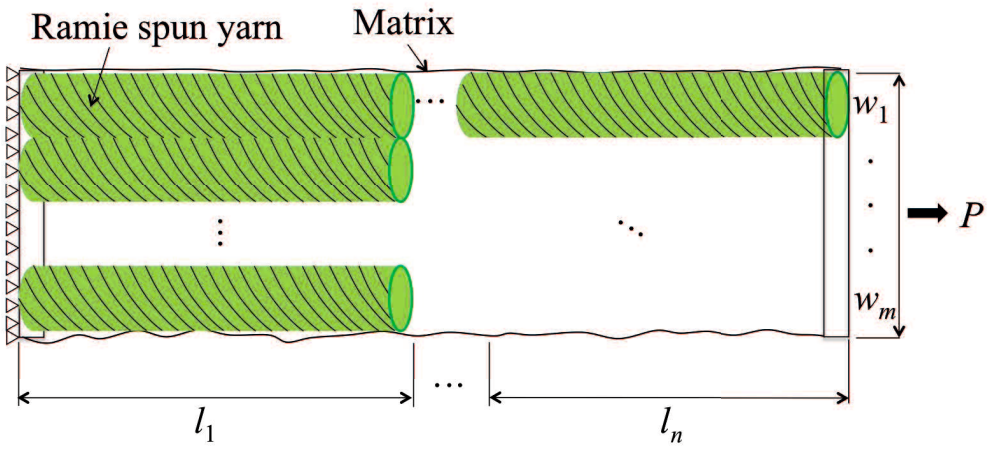

Figure 4.7 A schematic representation of a composite tape consisting of n elements per strand and m strands

and tape. These were substituted into eq. (24), and compared with the experimental results.

Figure 4.8 shows the comparison between S.D. of experimental values and F.O.S.M. approximate methods. Black closed circle indicates the S.D. of composite strands. Green and purple closed circles indicate the S.D. of Type I and Type II on composite tapes, respectively. Black, blue, and red lines represent the S.D. of Hearle et al., Rao-Farris, and Thwaites measured by F.O.S.M. approximate method, respectively. It can be observed that the S.D. of experimental values and results estimated by F.O.S.M decreased with increasing the product of *m* and *n*. And the F.O.S.M results are in a good agreement with the experimental S.D. Especially, the experimental values of the S.D. were relatively well fitted with the result obtained by Thwaites in F.O.S.M. method.

This trend indicates that fluctuation in elastic modulus on the composite tape using twisted yarns can be decreased when the composite materials are produced at larger size. In other words, relatively large size yarn composite materials can enhance the reliability in elastic modulus.

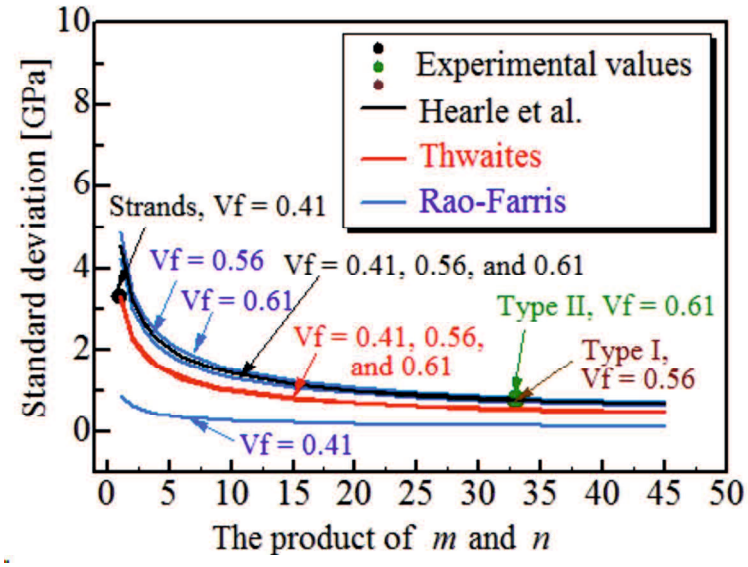

Figure 4.8 Standard deviation (S.D.) obtained by experimental values and first order second moment (F.O.S.M.) approximate method. Black closed circle indicates the S.D. of composite strands. Green and purple closed circles indicate the S.D. of Type I and Type II on composite tapes, respectively. Black, blue, and red lines represent the S.D. of Hearle et al., Rao-Farris, and Thwaites in F.O.S.M. approximate method, respectively.

4.5 Conclusion

Elastic modulus of a ramie spun yarn/PP composite strand obtained by M-PaRI process was discussed with conventional theoretical models, i.e., Hearle et al., Rao-Farris, and Thwaites. It was confirmed that Thwaites's model was relatively fitted with the experimental values. However, the theoretical models showed slightly lower values than the experimental values. It was also confirmed that the fluctuations of elastic modulus were caused by fiber orientation angles of a yarn as comparing to theoretical models. It means that fiber orientation angles have large fluctuations in the interior and exterior parts of a yarn. By comparison with first order second moment approximate methods, it was confirmed that fluctuation on composite materials using twisted yarn could be decreased when size of the composite materials becomes large. This means that reliable twisted yarn/PP composite materials can be produced by making it larger composite materials.

4.6 References

1) J. H. Sinclair and C. C. Chamis, Fracture modes in off-axis fiber composites, Polymer composites, Vol. 2, No. 1, 1981.

2) J. W. S. Hearle, P. Grosberg and S. Backer: John Wiley & Sons, Inc. NY. USA, 1969.

3) Rao Y, Farris RJ. A Modeling and Experimental Study of the Influence of Twist on the Mechanical Properties of High-Performance Fiber Yarns. J Appl Polym Sci, 77: 1938-1949, 2000.

4) J. J. Thwaites, THE ELASTIC DEFORMATION OF A ROD WITH HELICAL ANSIOTROPY, International Journal of Mechanical Sciences. 19, 161-168, 1977.

5) D. Hull and T.W. Clyne: An introduction to composite materials, Cambridge University Press, 1996.

6) B. Ren, J. Noda and K. Goda, Effects of Fiber Orientation Angles and Fluctuation on the stiffness and Strength of Sliver-Based Green Composites, Journal of the Society of Material Science, Japan, Vol. 59, No. 7, 567-574, 2010.

7) Manuel Chiachio, Juan Chiachio, Guillermo Rus, Reliability in Composites – A selective review and survey of current development, Composites: Part B, 2011.

8) M. Husnu Dirikolu, Alaattin Aktas, Statistical analysis of fracture strength of composite materials using weibull distribution, Turkish J. Eng. Env. Sci, 26, 45-48, 2002.

9) Thomas Y. Hou and Xaio-Hui Wu, A multiscale finite element method for elliptic problems in composite materials and porous media, Journal of computational physis, 134, 169-189, 1997.

10) A. Pegoretti, L. Fambri, G. Zappini, M. Bianchetti, Finite element analysis of a glass fire reinforced composite endodontic post, Biomaterials, 23, 2667-2682, 2002.

11) Masaru Zako, Yasutomo Uetsuji, Tetsusei Kurashiki, Finite element analysis of damaged woven fabric composite materials, Composites Science and Technology, 63, 507-516, 2003.

12) Cuthbert C. Hurd, A note on early monte carlo computations and scientific meetings, Annals of the history of computing, Vol 7, No. 2, 1985.

13) Koichi Goda, S. Leigh Phoenix, Reliability approach to the tensile strength of unidirectional CFRP composites by Monte-carlo simulation in a shear-lag model, Composites Science and Technology, 50, 457-468, 1994.

14) M. Ibnabdeljalil and W. A. Curtin, Strength and reliability of fiber-reinforced composites: Localized load-sharing and associated size effects, Int. J. Solids Structures, Vol. 34, No. 21, 2649-2668, 1997.

15) G. Cederbaum, I. Elishakoff, and L. Librescu, Reliability of laminated plates via the first-order second-moment method, Composite structures, 15, 161-167, 1990.

16) Alfredo H-S. Ang, Wilson H. Tang, Probability concepts in engineering, Emphasis on application to civil and environmental engineering, 2nd edition, JOHN WILEY & SONS, ING. 2007.

5. Conclusions and future researches.

5.1 Overall conclusions

The challenges for producing natural fiber composite materials are how to utilize the characters of natural fibers and thermoplastic polymers. Natural fibers are usually formed in a yarn during roving process. Therefore, it will be convenient to develop a technique by using a yarn as reinforcement. The technique can be applied to any natural fiber yarns. The critical point using a natural fiber yarns is that the yarn needs to be impregnated with thermoplastic polymers. It means that good impregnation of thermoplastic polymers between fibers is the key points to improving mechanical properties of short fiber composite materials. Furthermore, when the composite pellets were obtained by chopping yarn composite materials, it can be used as additive masterbatch for mass-production of interior parts in the field of transport industries such as automobile, railroad, and airplane.

In order to pursue the purposes of developing a production method by using natural fiber and thermoplastic polymer, a new method of producing a ramie yarn/PP composite strand was developed and the mechanical properties of short ramie/PP composite materials were also discussed for application to mass-production using the pellets of long ramie/PP composite strands in Chapter 2.

Tensile properties of a continuous ramie spun yarn/PP composite strand were discussed in different contents of MAPP using M-PaRI process in Chapter 3. Furthermore, by adding a die and a roller system after M-PaRI process, a ramie/PP composite tape was also produced. The aim of producing a composite tape is application to plain woven fabric reinforced composite materials like glass roving clothes.

The overall summaries are written in below.

1. Composite strands impregnated with matrices were obtainable by using M-PaRI process in a relatively simple way.
2. The optimal temperature of producing composite strands for injection molding was 195^{o}C.
3. Using the resultant composite strands, short composite materials were produced having fiber volume fraction of 10-50wt%. The optimal fiber volume fraction was around 40wt%.
4. Fiber lengths and distribution on the short fiber composite materials are critical parameters to improve mechanical properties such as tensile strength and Young's modulus. Using M-PaRI process, it was confirmed that fiber lengths longer than critical length were

obtainable.

5. The effects of MAPP contents on a single ramie spun yarn/PP composite materials were not significant. But, mechanical properties such as tensile strength and elastic modulus increased with increasing fiber volume fraction.
6. Fluctuations of elastic modulus were confirmed on composite yarns. It was also confirmed that fiber angles have a large variation even in the interior and exterior parts of the yarn. It is expected to decrease the fluctuation by controlling fiber orientation angles on a yarn.
7. Composite tapes were also obtainable using M-PaRI process. It was confirmed that tensile strength of composite tapes was lower than the values obtained by yarn composite materials since the sizing effects.
8. Making it bigger composite materials can also decrease fluctuation on composite materials using twisted yarn.

5.2 Future researches

Future researches are written as follows.

1. It has not been clear the interior parts of a yarn. Thus, it needs to be investigated the status of fibers of a yarn.
2. In this study, elastic modulus of a yarn was discussed. On the other hand, it is also necessary to discuss tensile strength of a yarn composite material since tensile strength is one of the most important factors.
3. Fracture mechanism of composite tapes needs to be investigated in different interfacial strengths.

APPENDIX A

1 Concerning tensile and transverse stresses

In the early 1960's, a yarn was enormously subjected of study in textile industry. One of prominent scientists was Hearle who dedicated his works to understand yarn geometry[1]. Tensile and transverse stresses were considered in his one of studies. Thus, it is worth to mention that mathematical formulae need to be reviewed in order to perceive geometric character of a yarn.

1.1 Yarn geometry

Yarn geometry is illustrated in Fig. 1.1. A ratio between external radical path and interior radical path is given as below

$$\zeta = \frac{\beta}{B} \rightarrow \beta = B\zeta \tag{1.1}$$

A trigonometric of cosine at the external layer can be expressed as follows

$$\cos\alpha = \frac{H}{B} \rightarrow H = B\cos\alpha \tag{1.2}$$

As illustrated in Fig. 1.1 (b) and (c), two diagonals can be expressed as blow

$$\beta^2 = 4\pi^2 r^2 + H^2 \rightarrow r^2 = \frac{\beta^2 - H^2}{4\pi^2} \tag{1.3}$$

$$B^2 = 4\pi^2 R^2 + H^2 \rightarrow R^2 = \frac{B^2 - H^2}{4\pi^2} \tag{1.4}$$

Equ. (1.3) and equ. (1.4) can be combined as

$$\rightarrow \left(\frac{r}{R}\right)^2 = \frac{\frac{\beta^2 - H^2}{4\pi^2}}{\frac{B^2 - H^2}{4\pi^2}} = \frac{\beta^2 - H^2}{B^2 - H^2} = \frac{(B\zeta)^2 - (B\cos\alpha)^2}{B^2 - (B\cos\alpha)^2} = \frac{\zeta^2 - \cos^2\alpha}{1 - \cos^2\alpha} \tag{1.5}$$

Trigonometric function as illustrated in Fig. 1.1 is determined by the expressions

$$\cos\theta = \frac{H}{\beta} = \frac{B\cos\alpha}{B\zeta} = \frac{\cos\alpha}{\zeta} \tag{1.6}$$

Using equ. (1.3) and equ. (1.4), the following formulae hold

$$\beta^2 = 4\pi^2 r^2 + H^2 \rightarrow 4\pi^2 r^2 = \beta^2 - H^2 \rightarrow \frac{4\pi^2 r^2}{\beta^2} = 1 - \left(\frac{H}{\beta}\right)^2$$

$$\rightarrow \left(\frac{r}{\beta}\right)^2 = \left[1 - \left(\frac{H}{\beta}\right)^2\right]\frac{1}{4\pi^2} \rightarrow \frac{r}{\beta} = \frac{1}{2\pi}\sqrt{1 - \left(\frac{H}{\beta}\right)^2} \tag{1.7}$$

The basic trigonometric function of sine can be written as

$$\sin\theta = \frac{2\pi r}{\kappa} \rightarrow \frac{r}{\beta} = \frac{\sin\theta}{2\pi} \tag{1.8}$$

Using equ. (1.7) and equ. (1.8), the following formulas can be obtained

$$\frac{\sin\theta}{2\pi} = \frac{1}{2\pi}\sqrt{1-\left(\frac{H}{\beta}\right)^2} \rightarrow \sin\theta = \sqrt{1-\left(\frac{H}{\beta}\right)^2} = \sqrt{1-\left(\frac{\cos\alpha}{\beta}\right)^2} \tag{1.9}$$

1.2 Variation of strain through the yarn

Let filament strain and yarn strain are defined by $(\varepsilon_f) = \frac{d\beta}{\beta}$ and $(\varepsilon_y) = \frac{dH}{H}$, respectively.

Derivative of equ. (1.3), then we have

$$\beta^2 = 4\pi^2 r^2 + H^2 \rightarrow 2\beta d\beta = 8\pi^2 r dr + 2HdH \rightarrow dr = \frac{\beta d\beta - HdH}{4\pi^2 r} \tag{1.10}$$

Let a yarn lateral contraction ratio be Ψ, which is defined as below

$$\Psi = -\frac{\frac{dR}{R}}{\frac{dH}{H}} \tag{1.11}$$

$$\Psi = -\frac{\frac{dr}{r}}{\frac{dH}{H}} \rightarrow \frac{dr}{r} = -\Psi\frac{dH}{H} \rightarrow dr = -\Psi\frac{dH}{H}r \tag{1.12}$$

Using equ. (1.10), then equ. (1.12) becomes

$$\frac{\beta d\beta - HdH}{4\pi^2 r} = -\Psi\frac{dH}{H}r \rightarrow \beta d\beta - HdH = -\Psi\frac{dH}{H}4\pi^2 r^2 \rightarrow \beta d\beta = HdH - \Psi\frac{dH}{H}4\pi^2 r^2 \rightarrow \frac{d\beta}{\beta} =$$

$$\frac{H}{\beta^2}dH - \Psi\frac{dH}{H}4\pi^2\frac{r^2}{\beta^2} \rightarrow \frac{d\beta}{\beta} = \left(\frac{H}{\beta}\right)^2\frac{dH}{H} - \Psi\frac{dH}{H}\left(\frac{2\pi r}{\beta}\right)^2 \tag{1.13}$$

Yarn strain can be written as the following by using equ. (1.6), and (1.13)

$$\varepsilon_f = \frac{d\beta}{\beta} = \cos^2\theta\,\varepsilon_y - \Psi\varepsilon_y\sin^2\theta = \varepsilon_y(\cos^2\theta - \Psi\sin^2\theta)$$

$$= \varepsilon_y\left[\left(\frac{\cos\alpha}{\zeta}\right)^2 - \Psi\left(1-\left(\frac{\cos\alpha}{\beta}\right)^2\right)\right] \tag{1.14}$$

1.3 Stress-strain relations

Fiber strain based on Hooke's law can be written in the form[(2)] as illustrated in Fig. 1.2.

$$\varepsilon_f = \frac{P}{E_f} - \frac{2\upsilon_2}{E_y}(-Q) \tag{1.15}$$

where E_f is Young's modulus of fiber, E_y is transverse modulus of fiber, υ_2 is Poison's ratio to transverse direction for a transverse stress, and Q is transverse stress.

When fiber is in symmetric condition, the following equation satisfies

$$\frac{\upsilon_2}{E_y} = \frac{\upsilon}{E_f} \tag{1.16}$$

Equ. (1.15) can be expressed as

$$\varepsilon_f = \frac{1}{E_f}(P + 2\upsilon Q) \tag{1.17}$$

where υ is Poison's ratio to the axial direction for a tensile stress.

Using eqs. (1.14) and (1.17), we have

$$\varepsilon_y \left[\left(\frac{\cos\alpha}{\zeta}\right)^2 - \Psi\left(1 - \left(\frac{\cos\alpha}{\beta}\right)^2\right)\right] = \frac{1}{E_f}(P + 2\upsilon Q) \tag{1.18}$$

Let us compute equ. (1.18)

$$P + 2\upsilon Q = \varepsilon_y E_f \left[\left(\frac{\cos\alpha}{\zeta}\right)^2 - \Psi\left(1 - \left(\frac{\cos\alpha}{\beta}\right)^2\right)\right] \tag{1.19}$$

$$P = \varepsilon_y E_f \left[\left(\frac{\cos\alpha}{\zeta}\right)^2 - \Psi\left(1 - \left(\frac{\cos\alpha}{\beta}\right)^2\right)\right] - 2\upsilon Q \tag{1.20}$$

Stress of p_s is defined as below which is in zero twist yarn.

$$p = \frac{P}{P_s},\ q = \frac{Q}{P_s} \tag{1.21}$$

Equ. (1.20) can be expressed as below

$$\frac{P}{P_s} = \left\{\varepsilon_y E_f \left[\left(\frac{\cos\alpha}{\zeta}\right)^2 - \Psi\left(1 - \left(\frac{\cos\alpha}{\beta}\right)^2\right)\right] - 2\upsilon Q\right\}\frac{1}{P_s}$$

$$= \left(\frac{\cos\alpha}{\zeta}\right)^2 - \Psi\left(1 - \left(\frac{\cos\alpha}{\beta}\right)^2\right) - 2\upsilon\frac{Q}{P_s} \tag{1.22}$$

We arrive at a complete form

$$p = \left(\frac{\cos\alpha}{\zeta}\right)^2 - \Psi\left(1 - \left(\frac{\cos\alpha}{\beta}\right)^2\right) - 2\upsilon q \tag{1.23}$$

1.4 Forces acting on six faces

Forces are defined as specific stress × area / specific volume.

1. Longitudinal force (ABCD and EFGF faces) as shown in Fig. 1.3 (a)

Trigonometric function of cosine illustrated in Fig. 1.4 (a) can be obtained as

$$\cos\theta = \frac{\mathrm{AB}}{\mathrm{AJ}} \rightarrow \mathrm{AB} = \mathrm{AJ}\cos\theta = \mathrm{rd}\phi\cos\theta \tag{1.24}$$

The following trigonometric function of cosine illustrated in Fig. 1.4 (b) can be also written as

$$\cos\theta = \frac{\mathrm{KE}}{\mathrm{AE}} \rightarrow \mathrm{AE} = \frac{\mathrm{KE}}{\cos\theta} = \frac{\mathrm{ds}}{\cos\theta} = \sec\theta\, ds \tag{1.25}$$

Thus, force acting on face of ABCD as shown in Fig. 1.3 (a) is given as

$$\text{specific stress} \times \mathrm{AB} \times \mathrm{AD} / \text{specific volume} = \mathrm{P}\times\mathrm{rd}\phi\cos\theta\times\mathrm{dr}\times\frac{1}{v_f} \tag{1.26}$$

2. Transverse forces acting on faces of ADHE and BCGF as shown in Fig. 1.3 (b) are expressed

$$\text{specific stress} \times \mathrm{AD} \times \mathrm{AE} / \text{specific volume} = \mathrm{Q}\times\mathrm{dr}\sec\theta\times ds\times\frac{1}{v_f} \tag{1.27}$$

3. Force acting on face of ABFE as shown in Fig. 1.3 (c) is as follows

$$\text{specific stress} \times \mathrm{AB} \times \mathrm{AE} / \text{specific volume} = \mathrm{Q}\times\mathrm{rd}\phi\cos\theta\times\frac{\mathrm{ds}}{\cos\theta}\times\frac{1}{v_f} = \mathrm{Q}\times\mathrm{rd}\phi\mathrm{ds}\times\frac{1}{v_f} \tag{1.28}$$

4. Force acting on face of DCGH as shown in Fig. 1.3 (d)

specific stress × area DCDH / specific volume

$$\mathrm{Qrd}\phi\mathrm{ds}\frac{1}{v_f} + \frac{1}{v_f}\frac{\partial}{\partial r}(\mathrm{Qr})\mathrm{d}\phi\mathrm{dsdr} = \frac{1}{v_f}\mathrm{Qrd}\phi\mathrm{ds} + \frac{1}{v_f}\left(\mathrm{Q} + \mathrm{r}\frac{dQ}{dr}\right)\mathrm{d}\phi\mathrm{dsdr} = \frac{1}{v_f}\left[\mathrm{Qrd}\phi\mathrm{ds} + \left(\mathrm{Q} + \mathrm{r}\frac{dQ}{dr}\right)\mathrm{d}\phi\mathrm{dsdr}\right] \tag{1.29}$$

As illustrated in Fig. 1.4 (b), a trigonometric function of tangent becomes

$$\tan\theta = \frac{AK}{KE} \rightarrow AK = \tan\theta\, KE = \tan\theta\, ds \tag{1.30}$$

Using equ. (1.30), angular displacement of $\widehat{KOA}$ has the form as shown in Fig. 1.5 (a)

$$\widehat{KOA} = \frac{AK}{r} \rightarrow \frac{\tan\theta ds}{r} \tag{1.31}$$

Angular displacement of $\widehat{AOL}$ can be expressed as below shown in Fig. 1.5 (b) by using a triangle of Fig. 1.4 (c)

$$\widehat{AOL} = \frac{AL}{r} = \frac{AB\cos\theta}{r} = \frac{\mathrm{rd}\phi\cos\theta\cos\theta}{r} = \mathrm{d}\phi\cos^2\theta \tag{1.32}$$

1.5 Equilibrium

1. Radial component of fiber tension

Using equ. (1.26) and equ. (1.31), force acting on face of ABCD can be calculated as

$$\left(\frac{P}{v_f}\right) r\cos\theta\, d\Phi dr\times\frac{\tan\theta ds}{r}\times\sin\theta = \left(\frac{P}{v_f}\right)\sin^2\theta\, d\Phi drds \tag{1.33}$$

2. Tangential transverse forces acting on face of ABFE and DCGH is given by

$$-\left(\frac{Q}{v_f}\right)\sec\theta\, drd\Phi\times ds\cos^2\theta\times\cos\theta = -\left(\frac{Q}{v_f}\right)\cos^2\theta\, d\Phi drds \tag{1.34}$$

3. Forces between ABFE and DCGH can be obtained as

$$\frac{1}{v_f}\left[\mathrm{Qrd\phi ds} + \left(\mathrm{Q} + \mathrm{r}\frac{dQ}{dr}\right)\mathrm{d\phi dsdr}\right] - \frac{Q}{v_f}\mathrm{rd\phi ds} = \left(\frac{1}{v_f}\right)\left(Q + \frac{rdQ}{dr}\right)d\Phi drds \quad (1.35)$$

4. By using eqs. (1.33), (1.34), and (1.35), net radial force (ABFE and DCGH) has the form as

$$\left(\frac{P}{v_f}\right)\sin^2\theta\, d\Phi drds - \left(\frac{Q}{v_f}\right)\cos^2\theta\, d\Phi drds + \left(\frac{1}{v_f}\right)\left(Q + \frac{rdQ}{dr}\right)d\Phi drds = 0 \quad (1.36)$$

Let us compute equ. (1.36)

$$P\sin^2\theta - Q\cos^2\theta + Q + \frac{rdQ}{dr} = 0 \quad (1.37)$$

$$\rightarrow \frac{rdQ}{dr} = -(P+Q)\sin^2\theta$$

(1.38)

Using a trigonometric function of sine

$$\sin\theta = \frac{2\pi r}{\beta} \quad (1.39)$$

Equ. (1.38) can be expressed as

$$\frac{rdQ}{dr} = -(P+Q)\sin^2\theta \quad (1.40)$$

$$\rightarrow \frac{rdQ}{dr} = -(P+Q)\left(\frac{2\pi r}{\beta}\right)^2$$

$$\rightarrow \frac{1}{r}\frac{dQ}{dr} = -(P+Q)4\frac{\pi^2}{\beta^2} \quad (1.41)$$

Recall equ. (1.3)

$$\beta^2 = 4\pi^2r^2 + H^2 \xrightarrow{Differenciation} 2\beta d\beta = 8\pi^2 rdr \rightarrow rdr = \frac{\beta d\beta}{4\pi^2} \quad (1.42)$$

Recall equ. (1.1)

$$\zeta = \frac{\beta}{B} \rightarrow \beta = B\zeta \xrightarrow{Differenciation} d\beta = Bd\zeta \quad (1.43)$$

Equ. (1.42) can be expressed as below

$$rdr = \frac{\beta d\beta}{4\pi^2} \rightarrow rdr = B\zeta\frac{Bd\zeta}{4\pi^2} \rightarrow rdr = B^2\zeta\frac{d\zeta}{4\pi^2} \rightarrow 4\pi^2 rdr = B^2\zeta d\zeta \rightarrow 4\pi^2 r = B^2\zeta\frac{d\zeta}{dr} \quad (1.44)$$

Using equ. (1.44), then equ. (1.41) becomes

$$\frac{1}{r}\frac{dQ}{dr} = -(P+Q)4\frac{\pi^2}{\beta^2} \rightarrow \frac{1}{r}\frac{dQ}{dr} = -(P+Q)\frac{1}{\beta^2}B^2\zeta\frac{d\zeta}{rdr} \rightarrow \frac{dQ}{dr} = -(P+Q)B^2\zeta\frac{d\zeta}{\beta^2 dr} \quad (1.45)$$

Equ. (1.45) becomes

$$\frac{dQ}{dr} = -(P+Q)\zeta\frac{d\zeta}{\zeta^2 dr} \quad (1.46)$$

$$\rightarrow \frac{dQ}{d\zeta} = -(P+Q)\frac{1}{\zeta} \tag{1.47}$$

Normalizing by division by P_s, we have

$$\frac{dq}{d\zeta} = -(p+q)\frac{1}{\zeta} \tag{1.48}$$

Using equation (1.23), equ. (1.48) becomes

$$p = \frac{\cos^2\alpha}{\zeta^2} - \Psi\left(1 - \frac{\cos^2\alpha}{\zeta^2}\right) - 2\upsilon q \tag{1.49}$$

$$\rightarrow \frac{dq}{d\zeta} = -\frac{\frac{\cos^2\alpha}{\zeta^2} - \Psi\left(1-\frac{\cos^2\alpha}{\zeta^2}\right) - 2\upsilon q + q}{\zeta} \tag{1.50}$$

$$\rightarrow \frac{dq}{d\zeta} - (2\upsilon - 1)\frac{q}{\zeta} = -(1+\Psi)\frac{\cos^2\alpha}{\zeta^3} + \frac{\Psi}{\zeta} \tag{1.51}$$

Equ. (1.51) can be solved as follows.

Let q=y, ζ=x, then

$$\frac{dy}{dx} - (2\upsilon - 1)\frac{y}{x} = -(1+\Psi)\frac{\cos^2\alpha}{x^3} + \frac{\Psi}{x} \tag{1.52}$$

$$\rightarrow y = x^{(2\upsilon-1)}\left\{(1+\Psi)\cos^2\alpha\frac{x^{(-2\upsilon-1)}}{2\upsilon+1} + \Psi\frac{x^{(-2\upsilon+1)}}{-2\upsilon+1} + c\right\} \tag{1.53}$$

$$\rightarrow y = \frac{(1+\Psi)\cos^2\alpha}{(2\upsilon+1)x^2} - \frac{\Psi}{2\upsilon-1} + cx^{(2\upsilon-1)} \tag{1.54}$$

Boundary conditions are prescribed as below

x=1, y=0 (1.55)

Constant *c* can be obtained as

$$c = -\frac{(1+\Psi)\cos^2\alpha}{(2\upsilon+1)} + \frac{\Psi}{2\upsilon-1} \tag{1.56}$$

Substituting equ. (1.56) into equ. (1.54), then we have

$$y = \frac{(1+\Psi)\cos^2\alpha}{(2\upsilon+1)x^2} - \frac{(1+\Psi)\cos^2\alpha}{(2\upsilon+1)x^2}x^{(2\upsilon-1)}x^2 + \frac{\Psi}{2\upsilon-1}x^{(2\upsilon-1)} - \frac{\Psi}{2\upsilon-1} \tag{1.57}$$

$$\rightarrow y = \frac{(1+\Psi)\cos^2\alpha}{(2\upsilon+1)x^2}\left(1 - x^{(2\upsilon+1)}\right) - \Psi\frac{1-x^{(2\upsilon-1)}}{2\upsilon-1} \tag{1.58}$$

Replace y and x to q and ζ, respectively, then we have

$$q = \frac{(1+\Psi)\cos^2\alpha}{(2\upsilon+1)\zeta^2}\left(1 - \zeta^{(2\upsilon+1)}\right) - \Psi\frac{1-\zeta^{(2\upsilon-1)}}{2\upsilon-1} \tag{1.60}$$

Putting equ. (1.60) into equ. (1.49), then let us compute

$$p = \left(\frac{\cos\alpha}{\zeta}\right)^2 - \Psi\left(1 - \left(\frac{\cos\alpha}{\kappa}\right)^2\right) - 2\upsilon\left[\frac{(1+\Psi)\cos^2\alpha}{(2\upsilon+1)\zeta^2}\left(1-\zeta^{(2\upsilon+1)}\right) - \Psi\frac{1-\zeta^{(2\upsilon-1)}}{2\upsilon-1}\right] \quad (1.61)$$

$$\rightarrow p = \frac{(1+\Psi)\cos^2\alpha(2\upsilon+1) - 2\upsilon(1+\Psi)\cos^2\alpha\left(1-\zeta^{(2\upsilon+1)}\right)}{\zeta^2(2\upsilon+1)} - \frac{\Psi(2\upsilon-1) - 2\upsilon\Psi\left[1-u^{(2\upsilon-1)}\right]}{2\upsilon-1} \quad (1.62)$$

$$\rightarrow p = \frac{(1+\Psi)\cos^2\alpha\left[1+2\upsilon\zeta^{(2\upsilon+1)}\right]}{\zeta^2(2\upsilon+1)} + \Psi\frac{\left[1-2\upsilon\zeta^{(2\upsilon-1)}\right]}{2\upsilon-1} \quad (1.63)$$

2.1.6 Tensile stress and transverse stress

Recall eqs. (1.5), equ. (1.2), and equ. (1.9)

$$\left(\frac{r}{R}\right)^2 = \frac{\zeta^2-\cos^2\alpha}{1-\cos^2\alpha} \rightarrow \frac{2rdr}{r^2} = \frac{1}{1-\cos^2\alpha}2\zeta d\zeta \rightarrow rdr = \frac{R^2}{1-\cos^2\alpha}\zeta d\zeta \ , \quad \cos\theta = \frac{H}{\beta} = \frac{\cos\alpha}{\zeta} \ , \quad \sin\theta = \frac{2\pi r}{\beta} = \sqrt{1-\frac{\cos^2\alpha}{\zeta^2}}$$

Tensile stress and transverse stress can be expressed as below

$$\frac{P}{v_f}(2\pi rdr\cos\theta)\cos\theta - \frac{Q}{v_f}(2\pi rdr\sin\theta)\sin\theta \quad (1.64)$$

Equ. (1.64) becomes

$$\frac{P}{v_f}\left(2\pi\frac{R^2}{1-\cos^2\alpha}\zeta d\zeta\cos\theta\right)\cos\theta - \frac{Q}{v_f}\left(2\pi\frac{R^2}{1-\cos^2\alpha}\zeta d\zeta\sin\theta\right)\sin\theta \quad (1.65)$$

$$\rightarrow \frac{1}{v_f}\frac{2\pi R^2}{1-\cos^2\alpha}\left[P\frac{\cos^2\alpha}{\zeta^2} - Q\left(1-\frac{\cos^2\alpha}{\zeta^2}\right)\right]\zeta d\zeta \quad (1.66)$$

Total yarn tension is expressed as below

$$\frac{1}{v_f}\frac{2\pi R^2}{1-\cos^2\alpha}\int_{\cos\alpha}^{1}\left[P\frac{\cos^2\alpha}{\zeta^2} - Q\left(1-\frac{\cos^2\alpha}{\zeta^2}\right)\right]\zeta d\zeta \quad (1.67)$$

$$\rightarrow \frac{yarn\ tension}{Ps\frac{\pi R^2}{v_f}} = \frac{2}{1-\cos^2\alpha}\int_{\cos\alpha}^{1}\left[p\frac{\cos^2\alpha}{\zeta^2} - q\left(1-\frac{\cos^2\alpha}{\zeta^2}\right)\right]\zeta d\zeta \quad (1.68)$$

$$\rightarrow \frac{2}{1-\cos^2\alpha}\int_{\cos\alpha}^{1}\left[p\frac{\cos^2\alpha}{\zeta^2} - q\left(1-\frac{\cos^2\alpha}{\zeta^2}\right)\right]\zeta d\zeta \quad (1.69)$$

$$\rightarrow \frac{2}{1-\cos^2\alpha}\int_{\cos\alpha}^{1}\left[(p+q)\frac{\cos^2\alpha}{\zeta^2} - q\right]\zeta d\zeta \quad (1.70)$$

Equ. (1.70) can be separated as below

$$\frac{2}{1-\cos^2\alpha}\int_{\cos\alpha}^{1}(p+q)\frac{\cos^2\alpha}{\zeta}d\zeta \tag{1.71}$$

$$-\frac{2}{1-\cos^2\alpha}\int_{\cos\alpha}^{1}q\zeta d\zeta \tag{1.72}$$

First, let us compute equ. (1.71) as follows

Using eqs. (1.60) and (1.63), then equ. (1.71) becomes

$$\frac{2}{1-\cos^2\alpha}\int_{\cos\alpha}^{1}\left\{\frac{(1+\Psi)\cos^2\alpha\left[1+2\upsilon\zeta^{(2\upsilon+1)}\right]}{\zeta^2(2\upsilon+1)}+\Psi\frac{\left[1-2\upsilon\zeta^{(2\upsilon-1)}\right]}{2\upsilon-1}+\frac{(1+\Psi)\cos^2\alpha}{(2\upsilon+1)\zeta^2}\left(1-\zeta^{(2\upsilon+1)}\right)-\right.$$

$$\left.\Psi\frac{1-\zeta^{(2\upsilon-1)}}{2\upsilon-1}\right\}\frac{\cos^2\alpha}{\zeta}d\zeta \tag{1.73}$$

$$\rightarrow\frac{2}{1-\cos^2\alpha}\int_{\cos\alpha}^{1}\left[\frac{(1+\Psi)\cos^2\alpha}{\zeta^2(2\upsilon+1)}\left[2+2\upsilon\zeta^{(2\upsilon+1)}-\zeta^{(2\upsilon+1)}\right]+\frac{\left[-2\Psi\upsilon\zeta^{(2\upsilon-1)}+\Psi\zeta^{(2\upsilon-1)}\right]}{2\upsilon-1}\right]\frac{\cos^2\alpha}{\zeta}d\zeta \tag{1.74}$$

Equ. (1.74) can be separated as follows

$$\frac{2}{1-\cos^2\alpha}\int_{\cos\alpha}^{1}\left[\frac{(1+\Psi)\cos^2\alpha}{\zeta^2(2\upsilon+1)}\left[2+2\upsilon\zeta^{(2\upsilon+1)}-\zeta^{(2\upsilon+1)}\right]\right]\frac{\cos^2\alpha}{\zeta}d\zeta \tag{1.75}$$

$$\frac{2}{1-\cos^2\alpha}\int_{\cos\alpha}^{1}\left[\frac{\left[-2\Psi\upsilon\zeta^{(2\upsilon-1)}+\Psi\zeta^{(2\upsilon-1)}\right]}{2\upsilon-1}\right]\frac{\cos^2\alpha}{\zeta}d\zeta \tag{1.76}$$

Let us compute equ. (1.75)

$$\frac{2}{1-\cos^2\alpha}\int_{\cos\alpha}^{1}\left[\frac{(1+\Psi)\cos^2\alpha}{\zeta^2(2\upsilon+1)}\left[2+2\upsilon\zeta^{(2\upsilon+1)}-\zeta^{(2\upsilon+1)}\right]\right]\frac{\cos^2\alpha}{\zeta}d\zeta \tag{1.77}$$

$$\rightarrow\frac{2}{1-\cos^2\alpha}\frac{(1+\Psi)\cos^4\alpha}{(2\upsilon+1)}\left[-1+\frac{1}{\cos^2\alpha}+(2\upsilon-1)\left(\frac{1-\cos^{(2\upsilon-1)}\alpha}{2\upsilon-1}\right)\right] \tag{1.78}$$

$$\rightarrow\frac{2}{1-\cos^2\alpha}\frac{(1+\Psi)\cos^2\alpha}{(2\upsilon+1)}\left[1-\cos^{(2\upsilon+1)}\alpha\right] \tag{1.79}$$

Let us compute equ. (1.76)

$$\frac{2}{1-\cos^2\alpha}\int_{\cos\alpha}^{1}\left[\frac{\left[-2\Psi\upsilon\zeta^{(2\upsilon-1)}+\Psi\zeta^{(2\upsilon-1)}\right]}{2\upsilon-1}\right]\frac{\cos^2\alpha}{\zeta}d\zeta \tag{1.80}$$

$$\rightarrow-\frac{2}{1-\cos^2\alpha}\frac{\Psi\cos^2\alpha}{2\upsilon-1}\left[1-\cos^{(2\upsilon-1)}\alpha\right] \tag{1.81}$$

Using equ (1.60), equ. (1.72) can be solved as

$$-\frac{2}{1-\cos^2\alpha}\int_{\cos\alpha}^{1}q\zeta d\zeta \tag{1.82}$$

$$\rightarrow-\frac{2}{1-\cos^2\alpha}\int_{\cos\alpha}^{1}\left[\frac{(1+\Psi)\cos^2\alpha}{(2\upsilon+1)\zeta}\left(1-\zeta^{(2\upsilon+1)}\right)-\Psi\frac{1-\zeta^{(2\upsilon-1)}}{2\upsilon-1}\zeta\right]d\zeta \tag{1.83}$$

Equ. (1.83) can be separated as follows

$$-\frac{2}{1-\cos^2\alpha}\int_{\cos\alpha}^{1}\left[\frac{(1+\Psi)\cos^2\alpha}{(2\upsilon+1)\zeta}\left(1-\zeta^{(2\upsilon+1)}\right)\right]d\zeta \tag{1.84}$$

$$\rightarrow \frac{2}{1-\cos^2\alpha}\int_{\cos\alpha}^{1}\left[\Psi\frac{1-\zeta^{(2\upsilon-1)}}{2\upsilon-1}\zeta\right]d\zeta \tag{1.85}$$

Let us compute equ. (1.84)

$$-\frac{2}{1-\cos^2\alpha}\int_{\cos\alpha}^{1}\left[\frac{(1+\Psi)\cos^2\alpha}{(2\upsilon+1)\zeta}\left(1-\zeta^{(2\upsilon+1)}\right)\right]d\zeta \tag{1.86}$$

$$\rightarrow \frac{2}{1-\cos^2\alpha}\frac{(1+\Psi)\cos^2\alpha}{(2\upsilon+1)}ln\cos\alpha+\frac{(1+\Psi)\cos^2\alpha}{(2\upsilon+1)}\left[\frac{1-\cos^{(2\upsilon+1)}\alpha}{2\upsilon+1}\right] \tag{1.87}$$

Equ. (1.85) can be solved as

$$\frac{2}{1-\cos^2\alpha}\int_{\cos\alpha}^{1}\left[\Psi\frac{1-\zeta^{(2\upsilon-1)}}{2\upsilon-1}\zeta\right]d\zeta \tag{1.88}$$

$$\rightarrow \frac{2}{1-\cos^2\alpha}\left[\frac{\Psi\left(1-\cos^2\alpha\right)}{2(2\upsilon-1)}-\frac{\Psi\left(1-\cos^{(2\upsilon+1)}\alpha\right)}{(2\upsilon-1)(2\upsilon+1)}\right] \tag{1.89}$$

Combining eqs. (1.79), (1.81), (1.87), and (1.89), then we have

$$\frac{2}{1-\cos^2\alpha}\left\{\frac{(1+\Psi)\cos^2\alpha}{(2\upsilon+1)}\left[1-\cos^{(2\upsilon+1)}\alpha\right]+\frac{(1+\Psi)\cos^2\alpha}{(2\upsilon+1)}\left[1-\cos^{(2\upsilon+1)}\alpha\right]+\right.$$

$$\left.\frac{(1+\Psi)\cos^2\alpha}{(2\upsilon+1)}\left[\frac{1-\cos^{(2\upsilon+1)}\alpha}{2\upsilon+1}\right]-\frac{\Psi\left(1-\cos^{(2\upsilon+1)}\alpha\right)}{(2\upsilon-1)(2\upsilon+1)}-\frac{\Psi\cos^2\alpha}{2\upsilon-1}\left[1-\cos^{(2\upsilon-1)}\alpha\right]+\frac{\Psi\left(1-\cos^2\alpha\right)}{2(2\upsilon-1)}\right\} \tag{1.90}$$

$$\rightarrow \frac{2}{1-\cos^2\alpha}\left\{\frac{(1+\Psi)\cos^2\alpha}{(2\upsilon+1)}ln\cos\alpha+2(\upsilon+1)\frac{(1+\Psi)\cos^2\alpha}{2\upsilon+1}\left[\frac{1-\cos^{(2\upsilon+1)}\alpha}{2\upsilon+1}\right]-\frac{\Psi\left(1-\cos^{(2\upsilon+1)}\alpha\right)}{(2\upsilon-1)(2\upsilon+1)}+\right.$$

$$\left.\frac{\Psi\cos^2\alpha}{2\upsilon-1}\cos^{(2\upsilon-1)}\alpha+\frac{\Psi}{2(2\upsilon-1)}-\frac{3\Psi\cos^2\alpha}{2(2\upsilon-1)}\right\} \tag{1.91}$$

$\rightarrow$

$$\frac{2}{1-\cos^2\alpha}\frac{\cos^2\alpha}{(2\upsilon+1)}\left\{(1+\Psi)\left[ln\cos\alpha+2(\upsilon+1)\left[\frac{1-\cos^{(2\upsilon+1)}\alpha}{2\upsilon+1}\right]\right]-\frac{\Psi}{2}\left[\frac{3(2\upsilon+1)}{2\upsilon-1}-\frac{4(\upsilon+1)\cos^{(2\upsilon-1)}\alpha}{2\upsilon-1}-\right.\right.$$

$$\left.\left.\frac{1}{\cos^2\alpha}\right]\right\} \tag{1.92}$$

$\rightarrow$

$$\frac{2}{(1-\cos^2\alpha)}\frac{\cos^2\alpha}{(2\upsilon+1)}\left\{(1+\Psi)\left[ln\cos\alpha+2(\upsilon+1)\left[\frac{1-\cos^{(2\upsilon+1)}\alpha}{2\upsilon+1}\right]\right]-\right.$$

$$\left.\frac{\Psi}{2}\left[\frac{3(2\upsilon+1)}{2\upsilon-1}-\frac{4(\upsilon+1)\cos^{(2\upsilon-1)}\alpha}{2\upsilon-1}-\frac{1}{\cos^2\alpha}\right]\right\} \quad (1.93)$$

In order to calculate equ. (1.93), two mathematical functions in equ. (1.93) should be considered as below

$$\frac{3(2\upsilon+1)}{2\upsilon-1} \quad (1.94)$$

$$-\frac{4(\upsilon+1)\cos^{(2\upsilon-1)}\alpha}{2\upsilon-1} \quad (1.95)$$

Let $2\upsilon-1$ to be denoted by x, then $\upsilon=\frac{x+1}{2}$. x approaches 0 as υ approaches 0.5 (i.e., $\upsilon\rightarrow 0.5$ then $x\rightarrow 0$)

Equ. (1.94) can be solved as blow

$$\frac{3(2\upsilon+1)}{(2\upsilon-1)}=\frac{3(x+1+1)}{(x+1-1)}=\frac{3x+6}{x}\rightarrow\lim_{x\rightarrow 0}\frac{3x+6}{x}=3 \quad (1.96)$$

Equ. (1.95) can be also solved as follows

$$-\frac{4(\upsilon_1+1)\cos^{(2\upsilon-1)}\alpha}{2\upsilon-1}=-\frac{4\cos^x\alpha\times\left(\frac{x+1}{2}+1\right)}{(x+1-1)}=-\frac{4\cos^x\alpha\times\left(\frac{x+3}{2}\right)}{x}=-\frac{2x\cos^x\alpha+6\cos^x\alpha}{x}=-\frac{2\,x\cos^x\alpha}{x}-$$

$$\frac{6\cos^x\alpha}{x} \quad (1.97)$$

then

$$=-\lim_{x\rightarrow 0}\frac{2\,x\cos^x\alpha}{x}-\lim_{x\rightarrow 0}\frac{6\cos^x\alpha}{x}=\left[-\lim_{x\rightarrow 0}\frac{2\,x\cos^x\alpha}{x}-\lim_{x\rightarrow 0}\frac{6\cos^x\alpha}{x}\right]'=-\lim_{x\rightarrow 0}(2\cos^x\alpha+$$

$$2x\cos^x\alpha\,ln\cos\alpha)-\lim_{x\rightarrow 0}(6\cos^x\alpha\,ln\cos\alpha)=-2-6ln\cos\alpha \quad (1.98)$$

Combining eqs. (1.96) and equ. (1.98), we have

$$3-2-6ln\cos\alpha=1-6ln\cos\alpha \quad (1.99)$$

Thus, eqs. (1.94) and (1.95) become

$$\frac{3(2\upsilon+1)}{2\upsilon-1}-\frac{4(\upsilon+1)\cos^{(2\upsilon-1)}\alpha}{2\upsilon-1}=1-6ln\cos\alpha \quad (1.100)$$

Put equ. (1.100) into equ. (1.93), then equ. (1.93) becomes

$$=\frac{2}{(1-\cos^2\alpha)}\frac{\cos^2\alpha}{(2\upsilon+1)}\left\{(1+\Psi)\left[ln\cos\alpha+2(\upsilon+1)\left[\frac{1-\cos^{(2\upsilon+1)}\alpha}{2\upsilon+1}\right]\right]-\frac{\Psi}{2}\left[1-6ln\cos\alpha-\frac{1}{\cos^2\alpha}\right]\right\}$$

(1.101)

In case of constant volume of yarn, i.e., $\Psi = 0.5, \upsilon = 0.5$

$$\rightarrow \frac{\cos^2\alpha}{1-\cos^2\alpha}\left[\frac{3}{2}\left(ln\cos\alpha + \frac{3\left(1-\cos^2\alpha\right)}{2}\right) - \frac{1}{4}\left(1 - 6ln\cos\alpha - \frac{1}{\cos^2\alpha}\right)\right] \quad (1.102)$$

$$\rightarrow \frac{3\cos^2\alpha}{1-\cos^2\alpha} ln\cos\alpha + \frac{9}{4}\cos^2\alpha + \frac{1}{4} \quad (1.103)$$

where α is surface fiber orientation angle of a twisted yarn.

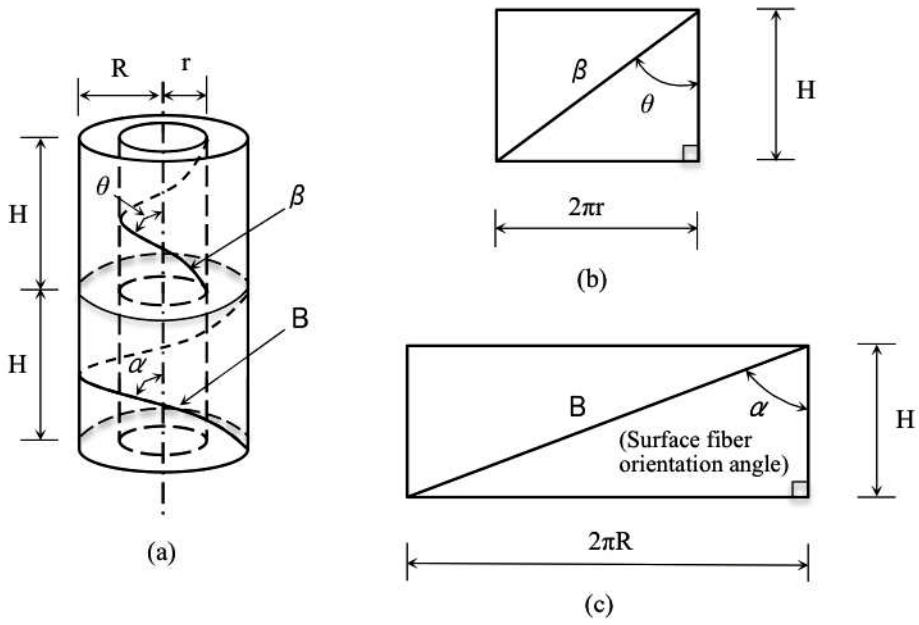

Fig. 1.1 A yarn geometric character. (a): Cylindrical figure, (b): Open-up figure at interior layer, (c): Open-up figure at external layer [1].

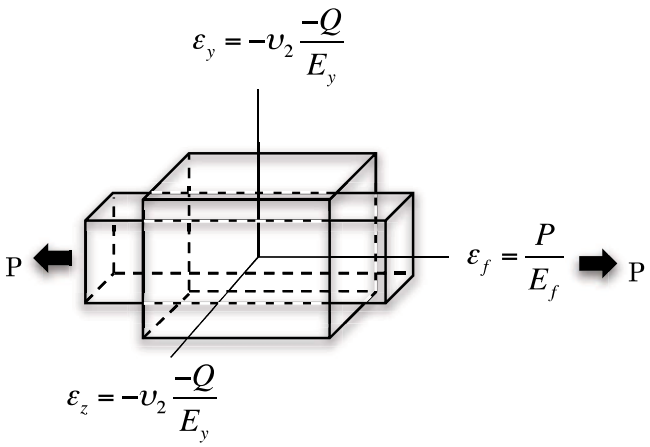

(a)

Fig. 1.2 An illustration subjected to a force along the axial direction.

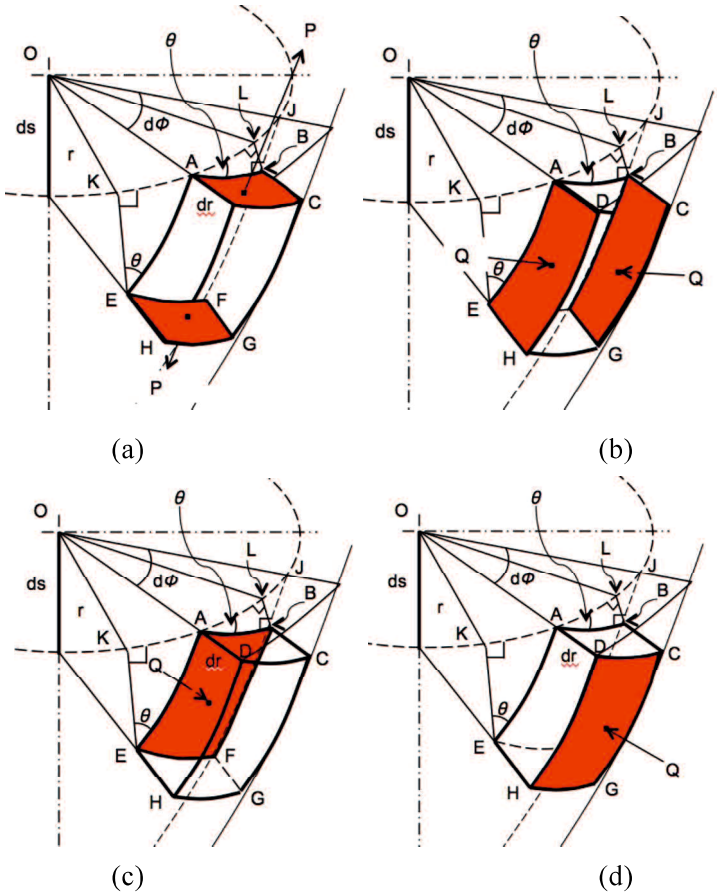

Fig. 1.3 Six forces acting on an element. P and Q are tensile and compression stresses, respectively.

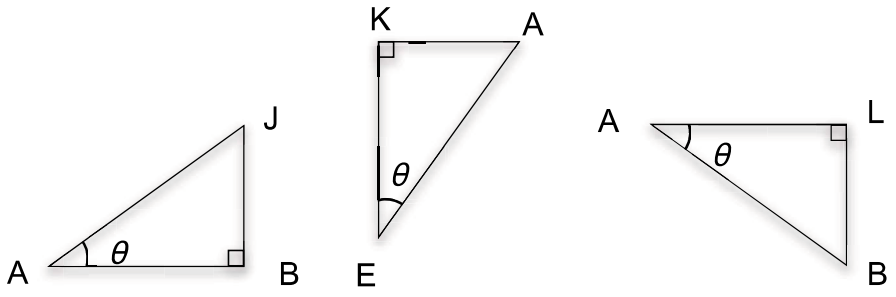

(a) (b) (c)

Fig. 1.4 Illustrations of triangles relating an element.

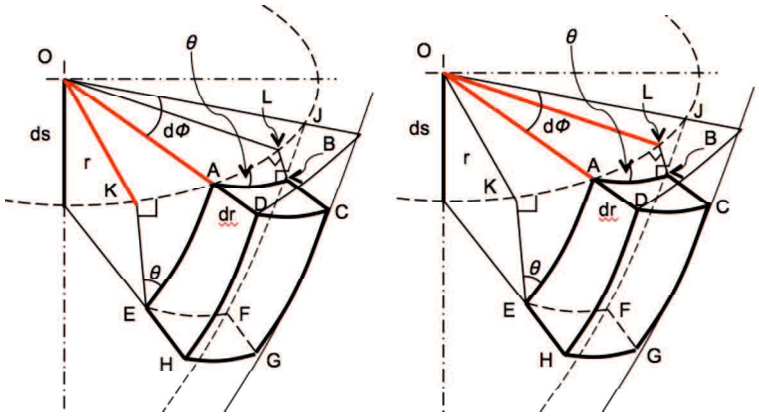

(a) (b)

Fig. 1.5 Illustrations of two angular displacements

APPENDIX B

2.2 Based on laminate theory

2.1 Stress-strain relations in a plane

Fig. 2.1 shows schematic representations of transformation of stress (a)[3] and three forces applying on the three faces[4]. Three forces can be obtained by considering equilibrium equations. Mathematical formulas are derived as follows

1. Stress σ_p

$$\sum F_p = 0 : \sigma_p \mathrm{A} - \sigma_x \mathrm{A}\cos\theta\cos\theta - \tau_{xy}\,\mathrm{A}\cos\theta\sin\theta - \sigma_y \mathrm{A}\sin\theta\sin\theta - \tau_{xy}\mathrm{A}\sin\theta\cos\theta = 0 \quad (2.1)$$

$$\rightarrow \sigma_p \mathrm{A} = \sigma_x \mathrm{A}\cos^2\theta + \tau_{xy}\mathrm{A}\cos\theta\sin\theta + \sigma_y \mathrm{A}\sin^2\theta + \tau_{xy}\mathrm{A}\sin\theta\cos\theta \quad (2.2)$$

$$\rightarrow \sigma_p = \sigma_x \cos^2\theta + \sigma_y \sin^2\theta + 2\tau_{xy}\sin\theta\cos\theta \quad (2.3)$$

2. Shear stress τ_{pq}

$$\sum F_q = 0 : \tau_{pq}\mathrm{A} + \sigma_x \mathrm{A}\cos\theta\sin\theta - \tau_{xy}\,\mathrm{A}\cos\theta\cos\theta - \sigma_y \mathrm{A}\sin\theta\cos\theta + \tau_{xy}\mathrm{A}\sin\theta\sin\theta = 0 \quad (2.4)$$

$$\rightarrow \tau_{pq}\mathrm{A} = -\sigma_x \mathrm{A}\cos\theta\sin\theta + \tau_{xy}\,\mathrm{A}\cos\theta\cos\theta + \sigma_y \mathrm{A}\sin\theta\cos\theta - \tau_{xy}\mathrm{A}\sin\theta\sin\theta \quad (2.5)$$

$$\rightarrow \tau_{pq} = -\sigma_x \cos\theta\sin\theta + \sigma_y \cos\theta\sin\theta + \tau_{xy}(\cos^2\theta - \sin^2\theta) \quad (2.6)$$

3. Stress σ_q

Stress (σ_q) can be obtained by substituting $(\theta + 90^0)$ for θ in equation (1.1). Because $\cos(2\theta + 180^0) = -\cos 2\theta$, $\sin(2\theta + 180^0) = -\sin 2\theta$, and by using trigonometric functions of $\sin 2\theta = 2\sin\theta\cos\theta$, $\cos 2\theta = \cos^2\theta - \sin^2\theta$, $\cos^2\theta = \frac{1+\cos 2\theta}{2}$, and $\sin^2\theta = \frac{1-\cos 2\theta}{2}$.

Stress (σ_p) written in equ. (2.3) can be modified as follows

$$\sigma_p = \sigma_x \cos^2\theta + \sigma_y \sin^2\theta + 2\tau_{xy}\sin\theta\cos\theta \quad (2.7)$$

$$\rightarrow \sigma_p = \sigma_x \frac{1+\cos 2\theta}{2} + \sigma_y \frac{1-\cos 2\theta}{2} + \tau_{xy}\sin 2\theta \quad (2.8)$$

$$\rightarrow \sigma_q = \sigma_x \frac{1+\cos(2\theta+180^0)}{2} + \sigma_y \frac{1-\cos(2\theta+180^0)}{2} + \tau_{xy}\sin(2\theta + 180^0) \quad (2.9)$$

$$\rightarrow \sigma_q = \sigma_x \frac{1-\cos 2\theta}{2} + \sigma_y \frac{1+\cos 2\theta}{2} - \tau_{xy}\sin 2\theta \quad (2.10)$$

$$\rightarrow \sigma_q = \sigma_x \sin^2\theta + \sigma_y \cos^2\theta - 2\tau_{xy}\sin\theta\cos\theta \quad (2.11)$$

Three stresses can be written in a matrix form from eqs. (2.3), (2.11), and (2.6) as below

$$\begin{bmatrix}\sigma_p\\ \sigma_q\\ \tau_{pq}\end{bmatrix}=\begin{bmatrix}\cos^2\theta & \sin^2\theta & 2\sin\theta\cos\theta\\ \sin^2\theta & \cos^2\theta & -2\sin\theta\cos\theta\\ -\cos\theta\sin\theta & \cos\theta\sin\theta & \cos^2\theta-\sin^2\theta\end{bmatrix}\begin{bmatrix}\sigma_x\\ \sigma_y\\ \tau_{xy}\end{bmatrix} \quad (2.12)$$

$$\rightarrow\begin{bmatrix}\sigma_p\\ \sigma_q\\ \tau_{pq}\end{bmatrix}=[\Phi]\begin{bmatrix}\sigma_x\\ \sigma_y\\ \tau_{xy}\end{bmatrix} \quad (2.13)$$

Trigonometric function is denoted by $[\Phi]$

$$[\Phi]=\begin{bmatrix}\cos^2\theta & \sin^2\theta & 2\sin\theta\cos\theta\\ \sin^2\theta & \cos^2\theta & -2\sin\theta\cos\theta\\ -\cos\theta\sin\theta & \cos\theta\sin\theta & \cos^2\theta-\sin^2\theta\end{bmatrix} \quad (2.14)$$

Strain transform can be written in a similar manner

$$\begin{bmatrix}\varepsilon_p\\ \varepsilon_q\\ \varepsilon_{pq}\end{bmatrix}=\begin{bmatrix}\cos^2\theta & \sin^2\theta & 2\sin\theta\cos\theta\\ \sin^2\theta & \cos^2\theta & -2\sin\theta\cos\theta\\ -\cos\theta\sin\theta & \cos\theta\sin\theta & \cos^2\theta-\sin^2\theta\end{bmatrix}\begin{bmatrix}\varepsilon_x\\ \varepsilon_y\\ \varepsilon_{xy}\end{bmatrix} \quad (2.15)$$

On the other hand, engineering shear strain (γ_{pq}) should be used for tensor shear strain (ε_{pq}) as

$$\varepsilon_{pq}=\frac{1}{2}\gamma_{pq} \quad (2.16)$$

Put engineering shear strain written in equ. (2.16) into equ. (2.15), we have

$$\begin{bmatrix}\varepsilon_p\\ \varepsilon_q\\ \frac{1}{2}\gamma_{pq}\end{bmatrix}=\begin{bmatrix}\cos^2\theta & \sin^2\theta & 2\sin\theta\cos\theta\\ \sin^2\theta & \cos^2\theta & -2\sin\theta\cos\theta\\ -\cos\theta\sin\theta & \cos\theta\sin\theta & \cos^2\theta-\sin^2\theta\end{bmatrix}\begin{bmatrix}\varepsilon_x\\ \varepsilon_y\\ \frac{1}{2}\gamma_{xy}\end{bmatrix} \quad (2.17)$$

$$\rightarrow\begin{bmatrix}\varepsilon_p\\ \varepsilon_q\\ \gamma_{pq}\end{bmatrix}=\begin{bmatrix}\cos^2\theta & \sin^2\theta & \sin\theta\cos\theta\\ \sin^2\theta & \cos^2\theta & -\sin\theta\cos\theta\\ -2\cos\theta\sin\theta & 2\cos\theta\sin\theta & \cos^2\theta-\sin^2\theta\end{bmatrix}\begin{bmatrix}\varepsilon_x\\ \varepsilon_y\\ \gamma_{xy}\end{bmatrix} \quad (2.18)$$

$$\rightarrow\begin{bmatrix}\varepsilon_p\\ \varepsilon_q\\ \gamma_{pq}\end{bmatrix}=[X]\begin{bmatrix}\varepsilon_x\\ \varepsilon_y\\ \gamma_{xy}\end{bmatrix} \quad (2.19)$$

where

$$[X]=\begin{bmatrix}\cos^2\theta & \sin^2\theta & \sin\theta\cos\theta\\ \sin^2\theta & \cos^2\theta & -\sin\theta\cos\theta\\ -2\cos\theta\sin\theta & 2\cos\theta\sin\theta & \cos^2\theta-\sin^2\theta\end{bmatrix} \quad (2.20)$$

Equ. (2.19) can be expressed as blow

$$\begin{bmatrix}\varepsilon_x\\ \varepsilon_y\\ \gamma_{xy}\end{bmatrix}=[X]^{-1}\begin{bmatrix}\varepsilon_p\\ \varepsilon_q\\ \gamma_{pq}\end{bmatrix} \quad (2.21)$$

2.2 Deriving transformed reduced compliances

Using engineering shear strains [3], the stress-strain relations in on-axis condition can be expressed the following reduced compliances.

$$\begin{bmatrix}\varepsilon_p\\ \varepsilon_q\\ \gamma_{pq}\end{bmatrix}=[\Psi]\begin{bmatrix}\sigma_p\\ \sigma_q\\ \tau_{pq}\end{bmatrix} \tag{2.22}$$

where

$$[\Psi]=\begin{bmatrix}S_{pp} & S_{pq} & 0\\ S_{pq} & S_{qq} & 0\\ 0 & 0 & S_{uu}\end{bmatrix}=\begin{bmatrix}\frac{1}{E_p} & \frac{-\upsilon_{pq}}{E_p} & 0\\ \frac{-\upsilon_{pq}}{E_p} & \frac{1}{E_q} & 0\\ 0 & 0 & \frac{1}{G_{pq}}\end{bmatrix} \tag{2.23}$$

Using equ. (2.22), equ.(2.21) becomes

$$\begin{bmatrix}\varepsilon_x\\ \varepsilon_y\\ \gamma_{xy}\end{bmatrix}=[X]^{-1}[\Psi]\begin{bmatrix}\sigma_p\\ \sigma_q\\ \tau_{pq}\end{bmatrix} \tag{2.24}$$

Using equ (2.13), then we have

$$\begin{bmatrix}\varepsilon_x\\ \varepsilon_y\\ \gamma_{xy}\end{bmatrix}=[X]^{-1}[\Psi][\Phi]\begin{bmatrix}\sigma_x\\ \sigma_y\\ \tau_{xy}\end{bmatrix} \tag{2.25}$$

Matrix form of $[X]^{-1}[\Psi][\Phi]$ is called transformed reduced compliances denoted by $[\Omega_{ij}]$

$$\begin{bmatrix}\varepsilon_x\\ \varepsilon_y\\ \gamma_{xy}\end{bmatrix}=[\Omega_{ij}]\begin{bmatrix}\sigma_x\\ \sigma_y\\ \tau_{xy}\end{bmatrix} \tag{2.26}$$

where

$$[\Omega_{ij}]=\begin{bmatrix}\Omega_{pp} & \Omega_{pq} & \Omega_{pu}\\ \Omega_{pq} & \Omega_{qq} & \Omega_{qu}\\ \Omega_{pu} & \Omega_{qu} & \Omega_{uu}\end{bmatrix} \tag{2.27}$$

The transformed reduced compliances in equ. (2.26) can be obtained by solving matrices as follows

2.2.1 Solution for inverse function of equ (2.21)

$$[X]=\begin{bmatrix}\cos^2\theta & \sin^2\theta & \sin\theta\cos\theta\\ \sin^2\theta & \cos^2\theta & -\sin\theta\cos\theta\\ -2\cos\theta\sin\theta & 2\cos\theta\sin\theta & \cos^2\theta-\sin^2\theta\end{bmatrix} \tag{2.28}$$

$detX=$

$$\cos^2\theta\cos^2\theta(\cos^2\theta-\sin^2\theta)+\sin^2\theta\,2\cos\theta\sin\theta\sin\theta\cos\theta+$$
$$\sin^2\theta\sin\theta\cos\theta\,2\cos\theta\sin\theta-$$
$$[-2\cos\theta\sin\theta\cos^2\theta\sin\theta\cos\theta-\cos^2\theta\sin\theta\cos\theta\,2\cos\theta\sin\theta+\sin^2\theta\sin^2\theta(\cos^2\theta-\sin^2\theta)] \tag{2.29}$$

$$=\cos^4\theta(\cos^2\theta-\sin^2\theta)+2\cos^2\theta\sin^4\theta+$$
$$2\cos^2\theta\sin^4\theta+2\cos^4\theta\sin^2\theta+2\cos^4\theta\sin^2\theta-\sin^4\theta(\cos^2\theta-\sin^2\theta) \tag{2.30}$$

$$= \cos^6\theta - \cos^4\sin^2\theta + 4\cos^2\theta\sin^4\theta + 4\cos^4\theta\sin^2\theta - \sin^4\theta\cos^2\theta + \sin^6\theta \quad (2.31)$$

$$= \cos^6\theta + \sin^6\theta - \sin^4\theta\cos^2\theta + 4\cos^2\theta\sin^4\theta + 4\cos^4\theta\sin^2\theta - \cos^4\sin^2\theta \quad (2.32)$$

$$= \cos^6\theta + \sin^6\theta + 3\cos^2\theta\sin^4\theta + 3\cos^4\theta\sin^2\theta \quad (2.33)$$

$$= (\cos^2\theta + \sin^2\theta)^3 = 1 \quad (2.34)$$

Thus,

$$[X]^{-1} = 1\times$$

$$\begin{bmatrix} \cos^2\theta(\cos^2\theta - \sin^2\theta) + 2\cos^2\theta\sin^2\theta & -\sin^2\theta(\cos^2\theta - \sin^2\theta) + 2\cos^2\theta\sin^2\theta & -\cos\theta\sin^3\theta - \cos^3\theta\sin\theta \\ -\sin^2\theta(\cos^2\theta - \sin^2\theta) + 2\cos^2\theta\sin^2\theta & \cos^2\theta(\cos^2\theta - \sin^2\theta) + 2\cos^2\theta\sin^2\theta & \cos\theta\sin^3\theta + \cos^3\theta\sin\theta \\ 2\cos\theta\sin^3\theta + 2\cos^3\theta\sin\theta & -2\cos\theta\sin^3\theta - 2\cos^3\theta\sin\theta & \cos^4\theta - \sin^4\theta \end{bmatrix} \quad (2.35)$$

2.2.2. Multiplying two matrices

$$\rightarrow [\Psi]\times[\Phi] = \begin{bmatrix} S_{pp} & S_{pq} & 0 \\ S_{pq} & S_{qq} & 0 \\ 0 & 0 & S_{uu} \end{bmatrix} \times \begin{bmatrix} \cos^2\theta & \sin^2\theta & 2\sin\theta\cos\theta \\ \sin^2\theta & \cos^2\theta & -2\sin\theta\cos\theta \\ -\cos\theta\sin\theta & \cos\theta\sin\theta & \cos^2\theta - \sin^2\theta \end{bmatrix} =$$

$$\begin{bmatrix} S_{pp}\cos^2\theta + S_{pq}\sin^2\theta & S_{pp}\sin^2\theta + S_{pq}\cos^2\theta & S_{pp}2\sin\theta\cos\theta - S_{pq}2\sin\theta\cos\theta \\ S_{pq}\cos^2\theta + S_{qq}\sin^2\theta & S_{pq}\sin^2\theta + S_{qq}\cos^2\theta & S_{pq}2\sin\theta\cos\theta - S_{qq}2\sin\theta\cos\theta \\ -S_{uu}\cos\theta\sin\theta & S_{uu}\cos\theta\sin\theta & S_{uu}(\cos^2\theta - \sin^2\theta) \end{bmatrix} \quad (2.36)$$

Equ. (2.27) can be obtained as below

$$[\Omega_{ij}] = \begin{bmatrix} \Omega_{pp} & \Omega_{pq} & \Omega_{pu} \\ \Omega_{pq} & \Omega_{qq} & \Omega_{qu} \\ \Omega_{pu} & \Omega_{qu} & \Omega_{uu} \end{bmatrix} = [X]^{-1}\times[\Psi]\times[\Phi] =$$

$$\begin{bmatrix} \cos^2\theta(\cos^2\theta - \sin^2\theta) + 2\cos^2\theta\sin^2\theta & -\sin^2\theta(\cos^2\theta - \sin^2\theta) + 2\cos^2\theta\sin^2\theta & -\cos\theta\sin^3\theta - \cos^3\theta\sin\theta \\ -\sin^2\theta(\cos^2\theta - \sin^2\theta) + 2\cos^2\theta\sin^2\theta & \cos^2\theta(\cos^2\theta - \sin^2\theta) + 2\cos^2\theta\sin^2\theta & \cos\theta\sin^3\theta + \cos^3\theta\sin\theta \\ 2\cos\theta\sin^3\theta + 2\cos^3\theta\sin\theta & -2\cos\theta\sin^3\theta - 2\cos^3\theta\sin\theta & \cos^4\theta - \sin^4\theta \end{bmatrix}$$

$$\times \begin{bmatrix} S_{pp}\cos^2\theta + S_{pq}\sin^2\theta & S_{pp}\sin^2\theta + S_{pq}\cos^2\theta & S_{pp}2\sin\theta\cos\theta - S_{pq}2\sin\theta\cos\theta \\ S_{pq}\cos^2\theta + S_{qq}\sin^2\theta & S_{pq}\sin^2\theta + S_{qq}\cos^2\theta & S_{pq}2\sin\theta\cos\theta - S_{qq}2\sin\theta\cos\theta \\ -S_{uu}\cos\theta\sin\theta & S_{uu}\cos\theta\sin\theta & S_{uu}(\cos^2\theta - \sin^2\theta) \end{bmatrix} \quad (2.37)$$

Ω_{pp} can be obtained as follows

$$\Omega_{pp} =$$

$$[\cos^2\theta(\cos^2\theta - \sin^2\theta) + 2\cos^2\theta\sin^2\theta]\left(S_{pp}\cos^2\theta + S_{pq}\sin^2\theta\right) + [-\sin^2\theta(\cos^2\theta - \sin^2\theta) + 2\cos^2\theta\sin^2\theta]\left(S_{pq}\cos^2\theta + S_{qq}\sin^2\theta\right) + (-\cos\theta\sin^3\theta - \cos^3\theta\sin\theta)(-S_{uu}\cos\theta\sin\theta) \quad (2.38)$$

$=$

$S_{pp}\cos^4\theta\,(\cos^2\theta-\sin^2\theta)+S_{pq}\sin^2\theta\cos^2\theta+S_{pp}2\cos^4\theta\sin^2\theta+S_{pq}\,2\cos^2\theta\sin^4\theta-$

$S_{pq}\cos^2\theta\sin^2\theta(\cos^2\theta-\sin^2\theta)-S_{qq}\sin^4\theta(\cos^2\theta-\sin^2\theta)+$

$S_{pq}\,2\cos^4\theta\sin^2\theta+S_{qq}2\cos^2\theta\sin^4\theta+S_{uu}\cos^2\theta\sin^4\theta+S_{uu}\cos^4\theta\sin^2\theta$ (2.39)

$=S_{pp}\cos^4\theta\,(\cos^2\theta-\sin^2\theta+2\sin^2\theta)+S_{pq}\sin^2\theta\cos^2\theta\,(2\sin^2\theta+2\cos^2\theta)+$

$S_{qq}\sin^4\theta(-\cos^2\theta+\sin^2\theta+2\cos^2\theta)+S_{uu}\cos^2\theta\sin^2\theta\,(\sin^2\theta+\cos^2\theta)$ (2.40)

$\rightarrow \Omega_{pp}=S_{pp}\cos^4\theta+S_{qq}\sin^4\theta+\left(2S_{pq}+S_{uu}\right)\cos^2\theta\sin^2\theta$ (2.41)

2.3 Elastic modulus of a twisted yarn

Schematic representations of ideal geometry of a twisted yarn as shown in Fig. 1.1 of Appendix A. Recall stress in off-axis condition written in equ (2.6)

$$\sigma_x=\frac{1}{\Omega_{pp}}\varepsilon_x \quad (2.42)$$

Ω_{pp} is given in equation (2.41)

$\Omega_{pp}=S_{pp}\cos^4\theta+S_{qq}\sin^4\theta+\left(2S_{pq}+S_{uu}\right)\cos^2\theta\sin^2\theta$

where

$$S_{pp}=\frac{1}{E_p},S_{pq}=\frac{-\nu_{pq}}{E_p},S_{qq}=\frac{1}{E_q},S_{uu}=\frac{1}{G_{pq}}\ ^{3)} \quad (2.43)$$

$$E_p=\left(1-V_f\right)E_m+V_fE_m\ ^{5)} \quad (2.44)$$

$$E_q=\frac{E_fE_m}{(1-V_f)E_m+V_fE_m}\ ^{5)} \quad (2.45)$$

in which V_f: Volume fraction of fiber, E_f: Young's modulus of fiber, E_m: Young's modulus of matrix, ν_{pq}: Poison's ratio, and G_{pq}: Shear modulus.

Using equation (2.43), equation (2.41) can be transformed as follows

$\Omega_{pp}=S_{pp}\cos^4\theta+S_{qq}\sin^4\theta+\left(2S_{pq}+S_{uu}\right)\cos^2\theta\sin^2\theta$

$=\cos^4\theta\frac{1}{\mathrm{E_p}}+\left\{\frac{1}{8}-\cos^2\theta+\cos^4\theta-\cos^2\theta+\frac{1}{2}+\frac{3}{8}\right\}\frac{1}{\mathrm{E_q}}+\cos^2\theta\left\{-\cos^2\theta+\frac{1}{2}+\frac{1}{2}\right\}\frac{1}{G_{pq}}+$

$2\cos^2\theta\left\{-\cos^2\theta+\frac{1}{2}+\frac{1}{2}\right\}\left(-\frac{\nu_{pq}}{\mathrm{E_p}}\right)$ (2.46)

$=\frac{1}{\mathrm{E_q}}+\left(\frac{1}{G_{pq}}-\frac{2}{\mathrm{E_q}}-\frac{2\nu_{pq}}{\mathrm{E_p}}\right)\cos^2\theta+\left(\frac{1}{\mathrm{E_p}}+\frac{1}{\mathrm{E_q}}-\frac{1}{G_{pq}}+\frac{2\nu_{pq}}{\mathrm{E_p}}\right)\cos^4\theta$ (2.47)

The axial force in a twisted yarn is expressed as follows by assuming no slippage between layers because of the integrity of a twisted yarn[6].

$$F = \int \sigma_x dA = \int_0^R \sigma_x \, 2\pi r dr \tag{2.48}$$

Axial force can be expressed as the following equation, if the yarn is treated as one body.

$$F = E_{cy} \varepsilon_x A \tag{2.49}$$

where A is the cross sectional area of a yarn.

The ideal twist geometries as illustrated Fig. 1 are expressed as

$$\tan\theta = \frac{2\pi r}{H} \quad \text{and} \quad \tan\alpha = \frac{2\pi R}{H} \tag{2.50}$$

Using equation (2.50), we have

$$\rightarrow h = \frac{2\pi r}{\tan\theta} \text{ and } h = \frac{2\pi R}{\tan\alpha} \rightarrow \frac{2\pi r}{\tan\theta} = \frac{2\pi R}{\tan\alpha} \rightarrow r = \frac{\tan\theta}{\tan\alpha} R \tag{2.51}$$

where α is surface fiber orientation angle of a twisted yarn.

Taking the derivative of equation (2.51), then we have

$$dr = \frac{R}{\tan\alpha} \frac{1}{\cos^2\theta} d\theta \tag{2.52}$$

We write elastic modulus (E_{cy}) of a twisted yarn from equ (2.49) using eqs. (2.48), (2.51), and (2.52), then we have

$$E_{cy} = \frac{F}{\pi R^2 \varepsilon_x} = \frac{1}{\pi R^2 \varepsilon_x} \int_0^R \sigma_x \, 2\pi r dr = \frac{2}{R^2 \varepsilon_x} \int_0^R \sigma_x \, r dr \tag{2.53}$$

$$= \frac{2}{\tan^2\alpha \varepsilon_x} \int_0^\alpha \sigma_x \tan\theta \frac{1}{\cos^2\theta} d\theta \tag{2.54}$$

$$= \frac{2}{\tan^2\alpha} \int_0^\alpha \frac{1}{\Omega_{pp}} \tan\theta \sec^2\theta \, d\theta \tag{2.55}$$

Using equ (2.47), we have

$$E_{cy} = \frac{2}{\tan^2\alpha} \int_0^\alpha \frac{1}{\left\{\frac{1}{E_q} + \left(\frac{1}{G_{pq}} - \frac{2}{E_q} - \frac{2\nu_{pq}}{E_p}\right)\cos^2\theta + \left(\frac{1}{E_p} + \frac{1}{E_q} - \frac{1}{G_{pq}} + \frac{2\nu_{pq}}{E_p}\right)\cos^4\theta\right\}} \tan\theta \sec^2\theta \, d\theta \tag{2.56}$$

let

$$\cos^2\theta = \lambda \tag{2.57}$$

$$\beta = \frac{1}{E_p} + \frac{1}{E_q} - \frac{1}{G_{pq}} + \frac{2\nu_{pq}}{E_p} \tag{2.58}$$

$$\delta = \frac{1}{G_{pq}} - \frac{2}{E_q} - \frac{2\nu_{pq}}{E_p} \tag{2.59}$$

$$\zeta = \frac{1}{E_q} \tag{2.60}$$

Taking the derivative of equation (2.57), then we have

$$-2\cos\theta \sin\theta d\theta = d\Lambda \rightarrow \sin\theta d\theta = -\frac{1}{2\cos\theta} d\Lambda \tag{2.61}$$

Using eqs. from (2.57) to (2.60), elastic modulus of a twisted yarn written in equ (2.56) is expressed as below

$$E_{cy} = \frac{2}{\tan^2\alpha}\int_1^{\cos^2\alpha}\frac{1}{(\beta\Lambda^2+\delta\Lambda+\zeta)}\tan\theta\sec^2\theta\,d\theta \tag{2.62}$$

$$= \frac{2}{\tan^2\alpha}\int_1^{\cos^2\alpha}\frac{1}{(\beta\Lambda^2+\delta\Lambda+\zeta)}\frac{-d\Lambda}{2\cos^2\theta}\frac{1}{\cos^2\theta} \tag{2.63}$$

$$= -\frac{1}{\tan^2\alpha}\int_1^{\cos^2\alpha}\frac{1}{(\beta\Lambda^2+\delta\Lambda+\zeta)}\frac{1}{\Lambda^2}d\Lambda \tag{2.64}$$

To solve equ. (2.64), we modify it as the follows

$$\frac{1}{(\beta\Lambda^2+\delta\Lambda+\zeta)}\frac{1}{\Lambda^2} = \frac{-\frac{\delta}{\zeta^2}}{\Lambda} + \frac{\frac{1}{\zeta}}{\Lambda^2} + \frac{\frac{\beta\delta}{\zeta^2}\Lambda+\left(\frac{\delta^2}{\zeta^2}-\frac{\beta}{\zeta}\right)}{(a\Lambda^2+b\Lambda+c)} \tag{2.65}$$

Using equation (2.65), equ (2.64) is expressed as below

$$E_{cy} = -\frac{1}{\tan^2\alpha}\int_1^{\cos^2\alpha}\frac{1}{(\beta\Lambda^2+\delta\Lambda+\zeta)}\frac{1}{\Lambda^2}d\Lambda \tag{2.66}$$

$$= -\frac{1}{\tan^2\alpha}\int_1^{\cos^2\alpha}\frac{-\frac{\delta}{\zeta^2}}{\Lambda} + \frac{\frac{1}{\zeta}}{\Lambda^2} + \frac{\frac{\beta\delta}{\zeta^2}\Lambda+\left(\frac{\delta^2}{\zeta^2}-\frac{\beta}{\zeta}\right)}{(a\Lambda^2+b\Lambda+c)}d\Lambda \tag{2.67}$$

Equation (2.67) can be separated as below

$$-\frac{1}{\tan^2\alpha}\int_1^{\cos^2\alpha}\frac{-\frac{\delta}{\zeta^2}}{\Lambda}d\Lambda \tag{2.68}$$

$$-\frac{1}{\tan^2\alpha}\int_1^{\cos^2\alpha}\frac{\frac{1}{\zeta}}{\Lambda^2}d\Lambda \tag{2.69}$$

$$-\frac{1}{\tan^2\alpha}\int_1^{\cos^2\alpha}\frac{\frac{\beta\delta}{\zeta^2}\Lambda+\left(\frac{\delta^2}{\zeta^2}-\frac{\beta}{\zeta}\right)}{(\beta\Lambda^2+\delta\Lambda+\zeta)}d\Lambda \tag{2.70}$$

The solution of equ. (2.2.68) is

$$-\frac{1}{\tan^2\alpha}\int_1^{\cos^2\alpha}\frac{-\frac{\delta}{\zeta^2}}{\Lambda}d\Lambda \tag{2.2.71}$$

$$= \left(-\frac{1}{\tan^2\alpha}\right)\left(-\frac{\delta}{2\zeta^2}\right)\ln\cos^4\alpha \tag{2.2.72}$$

The solution of equ. (2.69) is

$$-\frac{1}{\tan^2\alpha}\int_0^{\cos^2\alpha}\frac{\frac{1}{\zeta}}{\Lambda^2}d\Lambda \tag{2.73}$$

$$= -\frac{1}{\tan^2\alpha}\frac{(\cos^2\alpha-1)}{\zeta\cos^2\alpha} \tag{2.74}$$

The solution of equ. (2.70) is

$$-\frac{1}{\tan^2\alpha}\int_1^{\cos^2\alpha}\frac{\frac{\beta\delta}{\zeta^2}\Lambda+\left(\frac{\delta^2}{\zeta^2}-\frac{\beta}{\zeta}\right)}{(\beta\Lambda^2+\delta\Lambda+\zeta)}\,d\Lambda \tag{2.75}$$

$$=-\frac{1}{\tan^2\alpha}\int_1^{\cos^2\alpha}\frac{\frac{\delta}{2\zeta^2}\left(2\Lambda+\frac{\delta}{\beta}\right)+\left(\frac{\delta^2}{2\beta\zeta^2}-\frac{1}{\zeta}\right)}{\{(\beta\Lambda^2+\delta\Lambda+\zeta)\}\times\frac{1}{\beta}}\,d\Lambda \tag{2.76}$$

Equ. (2.76) can be separated as below

$$-\frac{1}{\tan^2\alpha}\int_1^{\cos^2\alpha}\frac{\frac{\delta}{2\zeta^2}\left(2\Lambda+\frac{\delta}{\beta}\right)}{\{(\beta\Lambda^2+\delta\Lambda+\zeta)\}\times\frac{1}{\beta}}\,d\Lambda \tag{2.77}$$

$$-\frac{1}{\tan^2\alpha}\int_1^{\cos^2\alpha}\frac{\left(\frac{\delta^2}{2\beta\zeta^2}-\frac{1}{\zeta}\right)}{\{(\beta\Lambda^2+\delta\Lambda+\zeta)\}\times\frac{1}{\beta}}\,d\Lambda \tag{2.78}$$

The solution of equ. (2.77) is

$$-\frac{1}{\tan^2\alpha}\int_1^{\cos^2\alpha}\frac{\frac{\delta}{2\zeta^2}\left(2\Lambda+\frac{\delta}{\beta}\right)}{\{(\beta\Lambda^2+\delta\Lambda+\zeta)\}\times\frac{1}{\beta}}\,d\Lambda \tag{2.79}$$

$$=-\frac{1}{\tan^2\alpha}\frac{\delta}{2\zeta^2}\ln\left(\frac{\beta\cos^4\alpha+\delta\cos^2\alpha+\zeta}{\beta+\delta+\zeta}\right) \tag{2.80}$$

The solution of equ. (2.78) is

$$-\frac{1}{\tan^2\alpha}\int_1^{\cos^2\alpha}\frac{\left(\frac{\delta^2}{2\beta\zeta^2}-\frac{1}{\zeta}\right)}{\{(\beta\Lambda^2+\delta\Lambda+\zeta)\}\times\frac{1}{\beta}}\,d\Lambda \tag{2.81}$$

$$=-\frac{1}{\tan^2\alpha}\frac{(\delta^2-2\beta\zeta)}{2\zeta^2}\int_1^{\cos^2\alpha}\frac{1}{\beta\Lambda^2+\delta\Lambda+\zeta}\,d\Lambda \tag{2.82}$$

Equ. (2.82) can be modified as below

$$\beta\Lambda^2+\delta\Lambda+\zeta=\beta\left(\Lambda+\frac{\delta}{2\beta}\right)^2-\frac{\delta}{4\beta}+\zeta \tag{2.83}$$

$$=\beta\left[\left(\Lambda+\frac{\delta}{2\beta}\right)^2-\left(\frac{\sqrt{\delta^2-4\delta\zeta}}{2\beta}\right)^2\right] \tag{2.84}$$

Using equ. (2.84), equ. (2.82) becomes

$$-\frac{1}{\tan^2\alpha}\frac{(\delta^2-2\beta\zeta)}{2\zeta^2}\int_1^{\cos^2\alpha}\frac{1}{\beta\left[\left(\Lambda+\frac{\delta}{2\beta}\right)^2-\left(\frac{\sqrt{\delta^2-4\delta\zeta}}{2\beta}\right)^2\right]}\,d\Lambda \tag{2.85}$$

$$=-\frac{1}{\tan^2\alpha}\frac{(\delta^2-2\beta\zeta)}{2\beta\zeta^2}\left(\frac{1}{2\frac{\sqrt{\delta^2-4\delta\zeta}}{2\beta}}\ln\left|\frac{\cos^2\alpha+\frac{\delta}{2\beta}-\frac{\sqrt{\delta^2-4\delta\zeta}}{2\beta}}{\cos^2\alpha+\frac{\delta}{2\beta}+\frac{\sqrt{\delta^2-4\delta\zeta}}{2\beta}}\right|-\frac{1}{2\frac{\sqrt{\delta^2-4\delta\zeta}}{2\beta}}\ln\left|\frac{1+\frac{\delta}{2\beta}-\frac{\sqrt{\delta^2-4\delta\zeta}}{2\beta}}{1+\frac{\delta}{2\beta}+\frac{\sqrt{\delta^2-4\delta\zeta}}{2\beta}}\right|\right) \tag{2.86}$$

$$= -\frac{1}{\tan^2\alpha}\frac{\delta^2-2\beta\zeta}{2\zeta^2\sqrt{\delta^2-4\beta\zeta}}\ln\frac{\left(2\beta\cos^2\alpha+\delta-\sqrt{\delta^2-4\beta\zeta}\right)}{\left(2\beta\cos^2\alpha+\delta+\sqrt{\delta^2-4\beta\zeta}\right)}+\frac{1}{\tan^2\alpha}\frac{\delta^2-2\beta\zeta}{2\zeta^2\sqrt{\delta^2-4\beta\zeta}}\ln\frac{\left(2\beta+\delta-\sqrt{\delta^2-4\beta\zeta}\right)}{\left(2\beta+\delta+\sqrt{\delta^2-4\beta\zeta}\right)} \quad (2.87)$$

Using eqs. (2.72), (2.74), (2.80), and (2.87), elastic modulus (E_{cy}) of a twisted yarn can be expressed as follows

$$E_{cy} = -\frac{1}{\tan^2\alpha}\int_0^{\alpha}\frac{1}{(\beta\Lambda^2+\delta\Lambda+\zeta)}\frac{1}{\Lambda^2}\,d\Lambda$$

$$=$$

$$-\frac{1}{\tan^2\alpha}\left[-\frac{\delta}{2\zeta^2}\ln\cos^4\alpha+\frac{\cos^2\alpha-1}{\zeta\cos^2\alpha}+\frac{\delta}{2\zeta^2}\ln\left(\frac{\beta\cos^4\alpha+\delta\cos^2\alpha+\zeta}{\beta+\delta+\zeta}\right)+\right.$$

$$\left.\frac{\delta^2-2\beta\zeta}{2\zeta^2\sqrt{\delta^2-4\beta\zeta}}\ln\frac{\left(2\beta\cos^2\alpha+\delta-\sqrt{\delta^2-4\beta\zeta}\right)}{\left(2\beta\cos^2\alpha+\delta+\sqrt{\delta^2-4\beta\zeta}\right)}-\frac{\delta^2-2\beta\zeta}{2\zeta^2\sqrt{\delta^2-4\beta\zeta}}\ln\frac{\left(2\beta+\delta-\sqrt{\delta^2-4\beta\zeta}\right)}{\left(2\beta+\delta+\sqrt{\delta^2-4\beta\zeta}\right)}\right] \quad (2.88)$$

$$= \frac{1}{\tan^2\alpha}\left[\frac{\delta}{2\zeta^2}\ln\frac{(\beta+\delta+\zeta)\cos^2\alpha}{\beta\cos^4\alpha+\delta\cos^2\alpha+\zeta}-\frac{\cos^2\alpha-1}{\zeta\cos^2\alpha}+\frac{\delta^2-2\beta\zeta}{2\zeta^2\sqrt{\delta^2-4\beta\zeta}}\ln\frac{\frac{\left(2\beta+\delta-\sqrt{\delta^2-4\beta\zeta}\right)}{\left(2\beta+\delta+\sqrt{\delta^2-4\beta\zeta}\right)}}{\frac{\left(2\beta\cos^2\alpha+\delta-\sqrt{\delta^2-4\beta\zeta}\right)}{\left(2\beta\cos^2\alpha+\delta+\sqrt{\delta^2-4\beta\zeta}\right)}}\right] \quad (2.89)$$

$$=$$

$$\frac{1}{\tan^2\alpha}\left[\frac{\delta}{2\zeta^2}\ln\frac{(\beta+\delta+\zeta)\cos^4\alpha}{\beta\cos^4\alpha+\delta\cos^2\alpha+\zeta}-\frac{\cos^2\alpha-1}{\zeta\cos^2\alpha}+\frac{\delta^2-2\beta\zeta}{2\zeta^2\sqrt{\delta^2-4\beta\zeta}}\ln\frac{\left(2\beta+\delta-\sqrt{\delta^2-4\beta\zeta}\right)\left(2\beta\cos^2\alpha+\delta+\sqrt{\delta^2-4\beta\zeta}\right)}{\left(2\beta\cos^2\alpha+\delta-\sqrt{\delta^2-4\beta\zeta}\right)\left(2\beta+\delta+\sqrt{\delta^2-4\beta\zeta}\right)}\right] \quad (2.90)$$

where

$$\beta = \frac{1}{E_p}+\frac{1}{E_q}-\frac{1}{G_{pq}}+\frac{2\nu_{pq}}{E_p}\ ,\ \delta = \frac{1}{G_{pq}}-\frac{2}{E_q}-\frac{2\nu_{pq}}{E_p},\ \text{and}\ \ \zeta = \frac{1}{E_q} \quad (2.91)$$

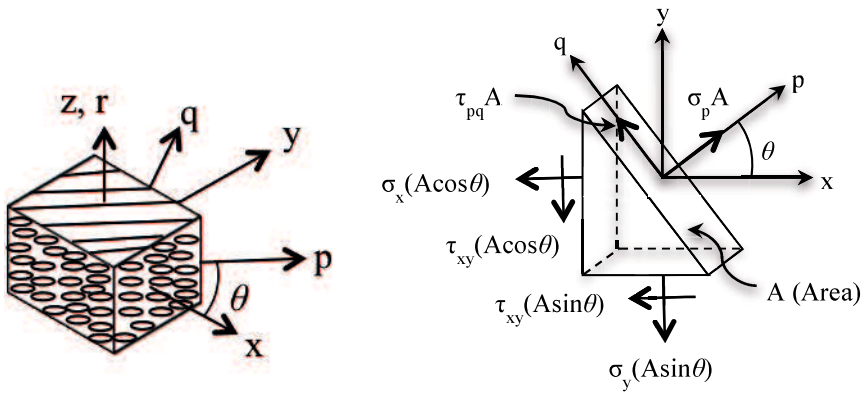

(a) Element of x-y-z and p-q-r system (b) Three forces

Fig. 2.1 (a) Cartesian coordinate system (Off-axis): x-y-z global and p-q-r principle material system [3], (b) Three forces on a plane [4].

APPENDIX C

3 Dealing with shear stresses

Hearle et al. did not consider shear stresses as explained in Appendix A. Further theoretical method was studied by Thwaites[7] who introduced the effect of shear stresses.

A schematic representation of a filament yarn is presented in Fig. 3.1. The components of strain in the case of cylindrical coordinates (i.e., r, ϕ, and z) are given as[2),7)]

$$\varepsilon_{rr} = \frac{\partial u}{\partial r}, \varepsilon_{\phi\phi} = \frac{1}{r}\frac{\partial u}{\partial \phi} + \frac{u}{r}, \varepsilon_{zz} = \frac{\partial u}{\partial z} \tag{3.1}$$

$$\gamma_{\phi z} = \frac{1}{r}\frac{\partial u}{\partial \phi} + \frac{\partial u}{\partial z}, \gamma_{zr} = \frac{\partial u}{\partial z} + \frac{\partial u}{\partial r}, \gamma_{r\phi} = \frac{\partial u}{\partial r} - \frac{u}{r} + \frac{1}{r}\frac{\partial u}{\partial \phi} \tag{3.2}$$

Eqs. (3.1) and (3.2) can be reduced to the following equation in the axial symmetry condition.

$$\varepsilon_{rr} = \frac{\partial u}{\partial r}, \varepsilon_{\phi\phi} = \frac{u}{r}, \varepsilon_{zz} = \frac{\partial u}{\partial z} = \varepsilon \tag{3.3}$$

$$\gamma_{\phi z} = \beta r, \gamma_{zr} = 0, \gamma_{r\phi} = 0 \tag{3.4}$$

where β is axial twist per unit length.

Using transformation of plane strain[8)], the following equation can be obtained

$$\varepsilon_{11} = \frac{\partial u}{\partial r} \tag{3.5}$$

$$\varepsilon_{22} = \varepsilon \sin^2\theta + \frac{u}{r}\cos^2\theta - \gamma \sin^2\theta \tag{3.6}$$

$$\varepsilon_{33} = \varepsilon \cos^2\theta + \frac{u}{r}\sin^2\theta + \gamma \sin^2\theta \tag{3.7}$$

$$\gamma_{23} = 2\left(\frac{u}{r} - \varepsilon\right)\sin\theta\cos\theta + \gamma\tan\theta\,(\cos^2\theta - \sin^2\theta) \tag{3.8}$$

in which $\gamma = \frac{\beta r}{\tan\theta}$ (3.9)

When a solid is strained symmetrically by forces applied at its surface, the stress-equations of equilibrium in cylindrical coordinates and r, ϕ, and z is expressed as below[2)]

$$\frac{\partial \widehat{rr}}{\partial r} + \frac{\widehat{rr} - \widehat{\theta\theta}}{r} = 0 \tag{3.10}$$

As illustrated in Fig. 3.1, $\widehat{rr}$ and $\widehat{\theta\theta}$ are identical with σ_{11} and $\sigma_{\phi\phi}$, respectively. Thus, equ. (3.10) can be written as

$$\frac{\partial \sigma_{11}}{\partial r} + \frac{\sigma_{11} - \sigma_{\phi\phi}}{r} = 0 \tag{3.11}$$

The stresses are independent of z and ϕ. Thus, the partial differential equilibrium equation becomes ordinary differential equations in r only as follows

$$r\frac{d\sigma_{11}}{dr} + \sigma_{11} - \sigma_{\phi\phi} = 0 \tag{3.12}$$

In case of the helical coordinate of ideal twisted geometry $(\sigma_{11} = \sigma_{rr})$, as illustrated in Fig. 3.1.

$$\mathrm{R}\tan\theta = r\tan\alpha \rightarrow r = R\frac{\tan\theta}{\tan\alpha} \tag{3.13}$$

$$\xrightarrow{Differentiation} dr = \frac{Rd\theta}{\cos^2\theta\tan\alpha} \tag{3.14}$$

$$\rightarrow \frac{1}{dr} = \frac{\tan\alpha\cos^2\theta}{Rd\theta} \tag{3.15}$$

Putting eqs. (3.13) and (3.14) into equ. (3.12), then we have

$$R\frac{\tan\theta}{\tan\alpha}\frac{\tan\alpha\cos^2\theta d\sigma_{11}}{Rd\theta}d\sigma_{11} + \sigma_{11} - \sigma_{\phi\phi} = 0 \tag{3.16}$$

$$\rightarrow \frac{\sin\theta}{\cos\theta}\frac{\cos^2\theta d\sigma_{11}}{d\theta}d\sigma_{11} + \sigma_{11} - \sigma_{\phi\phi} = 0 \tag{3.17}$$

$$\rightarrow \sin\theta\cos\theta\frac{d\sigma_{11}}{d\theta} + \sigma_{11} - \sigma_{\phi\phi} = 0 \tag{3.18}$$

and $\tau_{r\phi} = \tau_{zr} = 0$ (3.19)

When all tensile stresses are loaded at the same time, the strain in any one direction is a combination of all effects[3]. In addition to this, when strains to the direction 11 and 22 are identical as shown in Fig. 3.1, the following equation can be obtained.

$$\begin{Bmatrix} E_1\varepsilon_{11} \\ E_1\varepsilon_{22} \\ E_1\varepsilon_{33} \end{Bmatrix} = \begin{bmatrix} 1 & -\upsilon_{12} & -\upsilon_{13} \\ -\upsilon_{12} & 1 & -\upsilon_{13} \\ -\upsilon_{13} & -\upsilon_{13} & \frac{E_1}{E_3} \end{bmatrix} \begin{Bmatrix} \sigma_{11} \\ \sigma_{22} \\ \sigma_{33} \end{Bmatrix} \tag{3.20}$$

$$\tau_{23} = G\gamma_{23} \tag{3.21}$$

In order to have simple solution, one assumption was adopted that the sum of direct components must be zero.

$$\varepsilon_{11} + \varepsilon_{22} + \varepsilon_{33} = 0 \tag{3.22}$$

Using eqs. (3.5), (3.6), and (3.7), we have

$$\frac{\partial u}{\partial r} + \varepsilon\sin^2\theta + \frac{u}{r}\cos^2\theta - \gamma\sin^2\theta + \varepsilon\cos^2\theta + \frac{u}{r}\sin^2\theta + \gamma\sin^2\theta = 0 \tag{3.23}$$

$$\rightarrow \frac{\partial u}{\partial r} + \frac{u}{r}\cos^2\theta + \frac{u}{r}\sin^2\theta + \varepsilon\sin^2\theta + \varepsilon\cos^2\theta = 0 \tag{3.24}$$

$$\rightarrow \frac{\partial u}{\partial r} + \frac{u}{r} + \varepsilon = 0 \tag{3.25}$$

$$\rightarrow u = -\frac{1}{r}\left(\frac{1}{2}r^2\varepsilon\right) \tag{3.26}$$

$$\rightarrow u = -\frac{1}{2}r\varepsilon \tag{3.27}$$

σ_{11}, σ_{22}, and σ_{33} must independently add to zero. From equ. (3.20), we have

$$E_1(\varepsilon_{11} + \varepsilon_{22} + \varepsilon_{33}) = (1 - \upsilon_{12} - \upsilon_{13})\sigma_{11} + (-\upsilon_{12} + 1 - \upsilon_{13})\sigma_{22} + \left(-\upsilon_{13} - \upsilon_{13} + \frac{E_1}{E_3}\right)\sigma_{33} \tag{3.28}$$

$$\rightarrow \upsilon_{13} = 1 - \upsilon_{12} = \frac{E_1}{2E_3} \tag{3.29}$$

From equ. (3.20), we have

$$E_1\varepsilon_{22} = -\upsilon_{12}\sigma_{11} + \sigma_{22} - \upsilon_{13}\sigma_{33} \tag{3.30}$$

$$E_1\varepsilon_{11} = \sigma_{11} - \upsilon_{12}\sigma_{22} - \upsilon_{13}\sigma_{33} \tag{3.31}$$

Using eqs. (3.30) and (3.31), the following equation is obtainable.

$$E_1(\varepsilon_{22} - \varepsilon_{11}) = -(\upsilon_{12} + 1)\sigma_{11} + (1 + \upsilon_{12})\sigma_{22} \tag{3.32}$$

$$\rightarrow E_1(\varepsilon_{22} - \varepsilon_{11}) = (\upsilon_{12} + 1)(\sigma_{22} - \sigma_{11}) \tag{3.33}$$

$$\rightarrow \sigma_{22} - \sigma_{11} = \frac{E_1(\varepsilon_{22} - \varepsilon_{11})}{1 + \upsilon_{12}} \tag{3.34}$$

Using equ. (3.29), we have

$$\upsilon_{13} = 1 - \upsilon_{12} = \frac{E_1}{2E_3} \rightarrow E_1 = 2E_3(1 - \upsilon_{12}) \tag{3.35}$$

Putting equ. (3.35) into (3.34), then we have

$$\sigma_{22} - \sigma_{11} = \frac{2E_3(1 - \upsilon_{12})(\varepsilon_{22} - \varepsilon_{11})}{1 + \upsilon_{12}} \tag{3.36}$$

Using eqs. (3.6) and (3.27)

$$\varepsilon_{11} = \frac{\partial u}{\partial r} = -\frac{\varepsilon}{2} \tag{3.37}$$

Equ. (3.36) becomes

$$\sigma_{22} - \sigma_{11} = \frac{2E_3(1 - \upsilon_{12})\left(\varepsilon \sin^2\theta - \frac{\varepsilon}{2}\cos^2\theta - \gamma \sin^2\theta + \frac{\varepsilon}{2}\right)}{1 + \upsilon_{12}} \tag{3.38}$$

$$\rightarrow \sigma_{22} - \sigma_{11} = \frac{E_3(1 - \upsilon_{12}) \sin^2\theta (3\varepsilon - 2\gamma)}{1 + \upsilon_{12}} \tag{3.39}$$

Equ. (3.29) can be modified as below

$$\blacksquare \upsilon_{13} = \frac{E_1}{2E_3} \rightarrow \frac{E_1}{E_3} = 2\upsilon_{13} \tag{3.40}$$

From equ. (3.20)

$$E_1\varepsilon_{33} = -\upsilon_{13}\sigma_{11} - \upsilon_{13}\sigma_{22} + 2\upsilon_{13}\sigma_{33} \tag{3.41}$$

$$E_1\varepsilon_{22} = -\upsilon_{12}\sigma_{11} + \sigma_{22} - \upsilon_{13}\sigma_{33} \quad (\times \upsilon_{13}) \tag{3.42}$$

$$\rightarrow \upsilon_{13}E_1\varepsilon_{22} = -\upsilon_{13}\upsilon_{12}\sigma_{11} + \upsilon_{13}\sigma_{22} - \upsilon_{13}\upsilon_{13}\sigma_{33} \tag{3.43}$$

$$\rightarrow \upsilon_{13}E_1\varepsilon_{22} = -\upsilon_{13}\upsilon_{12}\sigma_{11} + \upsilon_{13}\sigma_{22} - \upsilon_{13}\upsilon_{13}\sigma_{33} \tag{3.44}$$

$$(E_1\varepsilon_{33} = -\upsilon_{13}\sigma_{11} - \upsilon_{13}\sigma_{22} + 2\upsilon_{13}\sigma_{33}) + (\upsilon_{13}E_1\varepsilon_{22} = -\upsilon_{13}\upsilon_{12}\sigma_{11} + \upsilon_{13}\sigma_{22} - \upsilon_{13}\upsilon_{13}\sigma_{33}) \tag{3.45}$$

$$\rightarrow E_1\varepsilon_{33} + \upsilon_{13}E_1\varepsilon_{22} = -\upsilon_{13}\sigma_{11} - \upsilon_{13}\sigma_{22} + 2\upsilon_{13}\sigma_{33} - \upsilon_{13}\upsilon_{12}\sigma_{11} + \upsilon_{13}\sigma_{22} - \upsilon_{13}\upsilon_{13}\sigma_{33}$$

$$\left(\times\frac{1}{\upsilon_{13}}\right) \tag{3.46}$$

$$\rightarrow \frac{E_1\varepsilon_{33}}{\upsilon_{13}} + E_1\varepsilon_{22} = -\sigma_{11} - \sigma_{22} + 2\sigma_{33} - \upsilon_{12}\sigma_{11} + \sigma_{22} - \upsilon_{13}\sigma_{33} \tag{3.47}$$

$$\rightarrow E_1\left(\frac{\varepsilon_{33}}{\upsilon_{13}} + \varepsilon_{22}\right) = -\sigma_{11} - \upsilon_{12}\sigma_{11} + 2\sigma_{33} - \upsilon_{13}\sigma_{33} \tag{3.48}$$

$$\rightarrow E_1\left(\frac{\varepsilon_{33}}{\upsilon_{13}} + \varepsilon_{22}\right) = -(1 + \upsilon_{12})\sigma_{11} + (2 - \upsilon_{13})\sigma_{33} \tag{3.49}$$

$$\rightarrow E_1\left(\frac{\varepsilon_{33}}{1-\upsilon_{12}} + \varepsilon_{22}\right) = -(1 + \upsilon_{12})\sigma_{11} + (2 - 1 + \upsilon_{12})\sigma_{33} \tag{3.50}$$

$$\rightarrow E_1\left(\frac{\varepsilon_{33}}{1-\upsilon_{12}} + \varepsilon_{22}\right) = (1 + \upsilon_{12})(\sigma_{33} - \sigma_{11}) \tag{3.51}$$

From equ. (3.20), the following equation can be obtained

$$\sigma_{33} - \sigma_{11} = \frac{E_1\left(\frac{\varepsilon_{33}}{1-\upsilon_{12}} + \varepsilon_{22}\right)}{1+\upsilon_{12}} \tag{3.52}$$

$$\rightarrow \sigma_{33} - \sigma_{11} = \frac{2E_3[(1-\upsilon_{12})\varepsilon_{22} + \varepsilon_{33}]}{1+\upsilon_{12}} \tag{3.53}$$

Eqs. (3.6) and (3.7) are modified as below

$$\varepsilon_{22} = \varepsilon\sin^2\theta + \frac{u}{r}\cos^2\theta - \gamma\sin^2\theta = \varepsilon\sin^2\theta - \frac{\varepsilon}{2}\cos^2\theta - \gamma\sin^2\theta \tag{3.54}$$

$$\varepsilon_{33} = \varepsilon\cos^2\theta + \frac{u}{r}\sin^2\theta + \gamma\sin^2\theta = \varepsilon\cos^2\theta - \frac{\varepsilon}{2}\sin^2\theta + \gamma\sin^2\theta \tag{3.55}$$

Equ. (3.53) becomes

$$\rightarrow \sigma_{33} - \sigma_{11} = \frac{2E_3\left[(1-\upsilon_{12})\left(\varepsilon\sin^2\theta - \frac{\varepsilon}{2}\cos^2\theta - \gamma\sin^2\theta\right) + \varepsilon\cos^2\theta - \frac{\varepsilon}{2}\sin^2\theta + \gamma\sin^2\theta\right]}{1+\upsilon_{12}} \tag{3.56}$$

$$\rightarrow \sigma_{33} - \sigma_{11} = \frac{2E_3}{1+\upsilon_{12}}\left[\frac{1}{2}\varepsilon(\sin^2\theta + \cos^2\theta) - \upsilon_{12}\varepsilon\sin^2\theta + \frac{1}{2}\upsilon_{12}\varepsilon(1 - \sin^2\theta) + \gamma\upsilon_{12}\sin^2\theta\right] \tag{3.57}$$

$$\rightarrow \sigma_{33} - \sigma_{11} = E_3\left[\varepsilon\left(1 - \frac{3\upsilon_{12}\sin^2\theta}{1+\upsilon_{12}}\right) + \frac{2\gamma\upsilon_{12}\sin^2\theta}{1+\upsilon_{12}}\right] \tag{3.58}$$

Equ. (3.8) can also modified as the follows

$$\gamma_{23} = 2\left(\frac{u}{r} - \varepsilon\right)\sin\theta\cos\theta + \gamma\tan\theta\,(\cos^2\theta - \sin^2\theta) \tag{3.59}$$

$$= 2\left(\frac{-\frac{\varepsilon r}{2}}{r} - \varepsilon\right)\sin\theta\cos\theta + \gamma\tan\theta\,(\cos^2\theta - \sin^2\theta) \tag{3.60}$$

$$= -3\varepsilon \sin\theta \cos\theta + \gamma \tan\theta \,(\cos^2\theta - \sin^2\theta) \tag{3.61}$$

Thus, τ_{23} becomes

$$\tau_{23} = G\gamma_{23} = G\left[-3\varepsilon \sin\theta \cos\theta + \gamma\left(\sin\theta \cos\theta - \sin\theta \cos\theta \frac{\sin^2\theta}{\cos^2\theta}\right)\right] \tag{3.62}$$

$$\rightarrow \tau_{23} = G\gamma_{23} = G \sin\theta \cos\theta \,[-3\varepsilon + \gamma(1 - \tan^2\theta)] \tag{3.63}$$

Recall equ. (2.12) in Appendix B. Using stress $(\sigma_{\phi\phi})$, equ. (3.19) can be expressed as below

$$\sin\theta \cos\theta \frac{d\sigma_{11}}{d\theta} + \sigma_{11} - \sigma_{22}\cos^2\theta - \sigma_{33}\sin^2\theta - 2\tau_{23}\sin\theta\cos\theta = 0 \tag{3.64}$$

Using eqs. (3.39), (3.58), and (3.63), equ. (3.64) can be modified as follows

$$\sin\theta \cos\theta \frac{d\sigma_{11}}{d\theta} + \sigma_{11} - \sigma_{11}\cos^2\theta - \frac{E_3(1-\upsilon_{12})\sin^2\theta\cos^2\theta(3\varepsilon-2\gamma)}{1+\upsilon_{12}} - \sigma_{11}\sin^2\theta -$$

$$E_3 \sin^2\theta\left[\varepsilon\left(1 - \frac{3\upsilon_{12}\sin^2\theta}{1+\upsilon_{12}}\right) + \frac{2\gamma\upsilon_{12}\sin^2\theta}{1+\upsilon_{12}}\right] - 2\sin\theta\cos\theta\, G \sin\theta\cos\theta\,[-3\varepsilon + \gamma(1 -$$

$$\tan^2\theta)] = 0 \tag{3.65}$$

$$\rightarrow \frac{\cot\theta}{E_3}\frac{d\sigma_{11}}{d\theta} =$$

$$\left[\frac{3(1+\cos^2\theta)}{1+\upsilon_{12}} - \frac{2(1+\upsilon_{12})}{1+\upsilon_{12}} - 6\frac{G}{E_3}\cos^2\theta\right]\varepsilon + \left[-\frac{2(1+\cos^2\theta)}{1+\upsilon_{12}} + \frac{2(1+\upsilon_{12})}{1+\upsilon_{12}} + 2\frac{G}{E_3}(\cos^2\theta - \sin^2\theta)\right]\gamma \tag{3.66}$$

$$\rightarrow \frac{1}{E_3}\frac{d\sigma_{11}}{d\theta} = \frac{3\varepsilon}{1+\upsilon_{12}}\frac{\sin\theta}{\cos\theta} + \frac{3\varepsilon\cos\theta\sin\theta}{1+\upsilon_{12}} - 2\varepsilon\frac{\sin\theta}{\cos\theta} - 3\frac{2G}{E_3}\varepsilon\cos\theta\sin\theta + 2\gamma\frac{\sin\theta}{\cos\theta} - \frac{2\gamma}{1+\upsilon_{12}}\frac{\sin\theta}{\cos\theta} -$$

$$\frac{2\gamma\cos\theta\sin\theta}{1+\upsilon_{12}} + 2\frac{2G}{E_3}\gamma\cos\theta\sin\theta - \frac{2G}{E_3}\gamma\frac{\sin\theta}{\cos\theta} \tag{3.67}$$

Now, equ. (3.67) can be integrated as below

$$\int \frac{1}{E_3}\frac{d\sigma_{11}}{d\theta} = \int\left(\frac{3\varepsilon}{1+\upsilon_{12}}\frac{\sin\theta}{\cos\theta} + \frac{3\varepsilon\cos\theta\sin\theta}{1+\upsilon_{12}} - 2\varepsilon\frac{\sin\theta}{\cos\theta} - 3\frac{2G}{E_3}\varepsilon\cos\theta\sin\theta + 2\gamma\frac{\sin\theta}{\cos\theta} - \frac{2\gamma}{1+\upsilon_{12}}\frac{\sin\theta}{\cos\theta} -\right.$$

$$\left.\frac{2\gamma\cos\theta\sin\theta}{1+\upsilon_{12}} + 2\frac{2G}{E_3}\gamma\cos\theta\sin\theta - \gamma\frac{2G}{E_3}\frac{\sin\theta}{\cos\theta}\right) \tag{3.68}$$

Equ. (3.68) can be separated and integrated as below

1

$$\int \frac{3\varepsilon}{1+\upsilon_{12}}\frac{\sin\theta}{\cos\theta}d\theta \tag{3.69}$$

$$\rightarrow -\frac{3\varepsilon}{1+\upsilon_{12}} lncos\theta + C \quad (3.70)$$

2

$$\int \frac{3\varepsilon \cos\theta \sin\theta}{1+\upsilon_{12}} d\theta \quad (3.71)$$

$$\rightarrow \frac{3\varepsilon}{1+\upsilon_{12}} \times \left(-\frac{1}{4}\right) \cos 2\theta + C \quad (3.72)$$

3

$$\int -2\varepsilon \frac{\sin\theta}{\cos\theta}\, d\theta \quad (3.73)$$

$$\rightarrow 2\varepsilon lncos\theta + C \quad (3.74)$$

4

$$\int -3\frac{2G}{E_3} \varepsilon \cos\theta \sin\theta\, d\theta \quad (3.75)$$

$$\rightarrow \frac{3}{4}\frac{2G}{E_3} \varepsilon \cos 2\theta + C \quad (3.76)$$

5

$$\int 2\gamma \frac{\sin\theta}{\cos\theta} d\theta \quad (3.77)$$

$$\rightarrow -2\gamma lncos\theta + C \quad (3.78)$$

6

$$\int -\frac{2\gamma}{1+\upsilon_{12}} \frac{\sin\theta}{\cos\theta} d\theta \quad (3.79)$$

$$\rightarrow \frac{2\gamma}{1+\upsilon_{12}} lncos\theta + C \quad (3.80)$$

7

$$\int -\frac{2\gamma \cos\theta \sin\theta}{1+\upsilon_{12}} d\theta \quad (3.81)$$

$$\rightarrow \frac{\gamma}{1+\upsilon_{12}} \times \left(\frac{1}{2}\right) \cos 2\theta + C \quad (3.82)$$

8

$$\int 2\frac{2G}{E_3} \gamma \cos\theta \sin\theta\, d\theta \quad (3.83)$$

$$\rightarrow \left(-\frac{1}{2}\right)\frac{2G}{E_3} \gamma \cos 2\theta + C \quad (3.84)$$

9

$$\rightarrow \int -\frac{2G}{E_3}\gamma \frac{\sin\theta}{\cos\theta}\, d\theta \tag{3.85}$$

$$\rightarrow \frac{2G}{E_3}\gamma lncos\theta + C \tag{3.86}$$

Sum from equ. (3.70) to equ. (3.86), then equ. (3.68) becomes

$$\frac{\sigma_{11}}{E_3} = -\frac{3\varepsilon}{1+\upsilon_{12}} lncos\theta + \frac{3\varepsilon}{1+\upsilon_{12}} \times \left(-\frac{1}{4}\right)\cos 2\theta + 2\varepsilon lncos\theta + \frac{3}{4}\frac{2G}{E_3}\varepsilon \cos 2\theta - 2\gamma lncos\theta +$$

$$\frac{2\gamma}{1+\upsilon_{12}} lncos\theta + \frac{1}{2} \times \frac{\gamma}{1+\upsilon_{12}} \cos 2\theta - \frac{1}{2}\frac{2G}{E_3}\gamma \cos 2\theta + \frac{2G}{E_3}\gamma lncos\theta + f(x) \tag{3.87}$$

where *f(x)* is constant.

Boundary condition is considered that the radical stress must be zero at the cylinder surface, $\sigma_{11} = 0$ when $\theta = \alpha$.

Thus equ. (3.87) becomes 0. Then we have

$$f(x) = \frac{3\varepsilon}{1+\upsilon_{12}} lncos\alpha + \frac{3\varepsilon}{1+\upsilon_{12}} \times \left(\frac{1}{4}\right)\cos 2\alpha - 2\varepsilon lncos\alpha - \frac{3}{4}\frac{2G}{E_3}\varepsilon \cos 2\alpha + 2\gamma lncos\alpha -$$

$$\frac{2\gamma}{1+\upsilon_{12}} lncos\alpha - \frac{1}{2} \times \frac{\gamma}{1+\upsilon_{12}} \cos 2\alpha + \frac{1}{2}\frac{2G}{E_3}\gamma \cos 2\alpha - \frac{2G}{E_3}\gamma lncos\alpha \tag{3.88}$$

Putting equ. (3.88) into equ. (3.87). Then we have

$$\frac{\sigma_{11}}{E_3} = -\frac{3\varepsilon}{1+\upsilon_{12}} lncos\theta + \frac{3\varepsilon}{1+\upsilon_{12}} \times \left(-\frac{1}{4}\right)\cos 2\theta + 2\varepsilon lncos\theta + \frac{3}{4}\frac{2G}{E_3}\varepsilon \cos 2\theta - 2\gamma lncos\theta +$$

$$\frac{2\gamma}{1+\upsilon_{12}} lncos\theta + \frac{1}{2} \times \frac{\gamma}{1+\upsilon_{12}} \cos 2\theta - \frac{1}{2}\frac{2G}{E_3}\gamma \cos 2\theta + \frac{2G}{E_3}\gamma lncos\theta + \frac{3\varepsilon}{1+\upsilon_{12}} lncos\alpha + \frac{3\varepsilon}{1+\upsilon_{12}} \times$$

$$\left(\frac{1}{4}\right)\cos 2\alpha - 2\varepsilon lncos\alpha - \frac{3}{4}\frac{2G}{E_3}\varepsilon \cos 2\alpha + 2\gamma lncos\alpha - \frac{2\gamma}{1+\upsilon_{12}} lncos\alpha - \frac{1}{2} \times \frac{\gamma}{1+\upsilon_{12}} \cos 2\alpha +$$

$$\frac{1}{2}\frac{2G}{E_3}\gamma \cos 2\alpha - \frac{2G}{E_3}\gamma lncos\alpha \tag{3.89}$$

Equ. (3.89) can be rearranged as follows

$$\frac{\sigma_{11}}{E_3} = -\left(\frac{3\varepsilon}{1+\upsilon_{12}} - 2\varepsilon\right) ln cos\theta + \left(\frac{3\varepsilon}{1+\upsilon_{12}} - 2\varepsilon\right) ln cos\alpha - \left(\frac{1}{4}\frac{3\varepsilon}{1+\upsilon_{12}} - \frac{3}{4}\frac{2G}{E_3}\varepsilon\right)\cos 2\theta + \left(\frac{1}{4}\frac{3\varepsilon}{1+\upsilon_{12}} -$$

$$\frac{3}{4}\frac{2G}{E_3}\varepsilon\right)\cos 2\alpha + \left(\frac{2\gamma}{1+\upsilon_{12}} - 2\gamma + \frac{2G}{E_3}\gamma\right) ln cos\theta - \left(\frac{2\gamma}{1+\upsilon_{12}} - 2\gamma + \frac{2G}{E_3}\gamma\right) ln cos\alpha + \left(\frac{1}{2}\frac{\gamma}{1+\upsilon_{12}} -$$

$$\frac{1}{2}\frac{2G}{E_3}\gamma\right)\cos 2\theta - \left(\frac{1}{2}\frac{\gamma}{1+\upsilon_{12}} - \frac{1}{2}\frac{2G}{E_3}\gamma\right)\cos 2\alpha \tag{3.90}$$

$$\rightarrow \frac{\sigma_{11}}{E_3} =$$

$$\varepsilon\left[\left(\frac{3}{1+\upsilon_{12}} - 2\right) ln\frac{\sec\theta}{\sec\alpha} - \frac{3}{2}\left(\frac{1}{1+\upsilon_{12}} - \frac{2G}{E_3}\right)(\cos^2\theta - \cos^2\alpha)\right] + \gamma\left[\left(\frac{2\upsilon_{12}}{1+\upsilon_{12}} - \frac{2G}{E_3}\right) ln\frac{\sec\theta}{\sec\alpha} +\right.$$

$$\left.\left(\frac{1}{1+\upsilon_{12}} - \frac{2G}{E_3}\right)(\cos^2\theta - \cos^2\alpha)\right] \tag{3.91}$$

Thus we have

$$\sigma_{11} =$$

$$E_3\left\{\varepsilon\left[\left(\frac{3}{1+\upsilon_{12}} - 2\right) ln\frac{\sec\theta}{\sec\alpha} - \frac{3}{2}\left(\frac{1}{1+\upsilon_{12}} - \frac{2G}{E_3}\right)(\cos^2\theta - \cos^2\alpha)\right] + \gamma\left[\left(\frac{2\upsilon_{12}}{1+\upsilon_{12}} - \frac{2G}{E_3}\right) ln\frac{\sec\theta}{\sec\alpha} +\right.\right.$$

$$\left.\left.\left(\frac{1}{1+\upsilon_{12}} - \frac{2G}{E_3}\right)(\cos^2\theta - \cos^2\alpha)\right]\right\} \tag{3.92}$$

Using equ. (3.92), we have

$$\sigma_{22} = E_3\left\{\varepsilon\left[\left(\frac{3}{1+\upsilon_{12}} - 2\right) ln\frac{\sec\theta}{\sec\alpha} - \frac{3}{2}\left(\frac{1}{1+\upsilon_{12}} - \frac{2G}{E_3}\right)(\cos^2\theta - \cos^2\alpha) + \frac{3(1-\upsilon_{12})\sin^2\theta}{1+\upsilon_{12}}\right] +\right.$$

$$\left.\gamma\left[\left(\frac{2\upsilon_{12}}{1+\upsilon_{12}} - \frac{2G}{E_3}\right) ln\frac{\sec\theta}{\sec\alpha} + \left(\frac{1}{1+\upsilon_{12}} - \frac{2G}{E_3}\right)(\cos^2\theta - \cos^2\alpha) - \frac{2(1-\upsilon_{12})\sin^2\theta}{1+\upsilon_{12}}\right]\right\} \tag{3.93}$$

From equ. (3.58), we also have

$$\sigma_{33} = E_3\left\{\varepsilon\left[\left(\frac{3}{1+\upsilon_{12}} - 2\right) ln\frac{\sec\theta}{\sec\alpha} - \frac{3}{2}\left(\frac{1}{1+\upsilon_{12}} - \frac{2G}{E_3}\right)(\cos^2\theta - \cos^2\alpha) + 1 - \frac{3\upsilon_{12}\sin^2\theta}{1+\upsilon_{12}}\right] +\right.$$

$$\left.\gamma\left[\left(\frac{2\upsilon_{12}}{1+\upsilon_{12}} - \frac{2G}{E_3}\right) ln\frac{\sec\theta}{\sec\alpha} + \left(\frac{1}{1+\upsilon_{12}} - \frac{2G}{E_3}\right)(\cos^2\theta - \cos^2\alpha) + \frac{2\upsilon_{12}\sin^2\theta}{1+\upsilon_{12}}\right]\right\} \tag{3.94}$$

Equ. (3.63) can be expressed as below

$$\tau_{23} = E_3\left[-\varepsilon\frac{3}{2}\frac{2G}{E_3}\sin\theta\cos\theta + \gamma(1-\tan^2\theta)\frac{1}{2}\frac{2G}{E_3}\sin\theta\cos\theta\right] \tag{3.95}$$

Using equ. (2.12) and (2.53) in Appendix B, we have elastic modulus of a yarn in tension as below.

$$\frac{T}{\pi R^2} = \frac{1}{\tan^2\alpha}\int_0^{\alpha}(\sigma_{22}\sin^2\theta + \sigma_{33}\cos^2\theta - 2\tau_{23}\sin\theta\cos\theta)2\tan\theta\sec^2\theta\, d\theta \quad (3.96)$$

Substituting from eqs. (3.92) to equ. (3.95) into equ. (3.96), then we have the following equation for tension.

$$\frac{T}{\pi R^2 E_3} =$$

$$\frac{1}{\tan^2\alpha}\int_0^{\alpha}\left\{\varepsilon\left[\left(\frac{3}{1+\upsilon_{12}}-2\right)ln\frac{\sec\theta}{\sec\alpha}-\frac{3}{2}\left(\frac{1}{1+\upsilon_{12}}-\frac{2G}{E_3}\right)(\cos^2\theta-\cos^2\alpha)+\frac{3(1-\upsilon_{12})\sin^2\theta}{1+\upsilon_{12}}\right]\sin^2\theta+\right.$$

$$\varepsilon\left[\left(\frac{3}{1+\upsilon_{12}}-2\right)ln\frac{\sec\theta}{\sec\alpha}-\frac{3}{2}\left(\frac{1}{1+\upsilon_{12}}-\frac{2G}{E_3}\right)(\cos^2\theta-\cos^2\alpha)+1-\frac{3\upsilon_{12}\sin^2\theta}{1+\upsilon_{12}}\right]\cos^2\theta+$$

$$\left.\varepsilon 3\frac{2G}{E_3}\sin^2\theta\cos^2\theta\right\}2\tan\theta\sec^2\theta\, d\theta \quad (3.97)$$

Equ. (3.97) can be integrated as follows

$$\frac{T}{\pi R^2 E_3} =$$

$$\frac{1}{\tan^2\alpha}\int_0^{\alpha}\left\{\varepsilon\left[\left(\frac{3}{1+\upsilon_{12}}-2\right)ln\frac{\sec\theta}{\sec\alpha}-\frac{3}{2}\left(\frac{1}{1+\upsilon_{12}}-\frac{2G}{E_3}\right)(\cos^2\theta-\cos^2\alpha)+\frac{3(1-\upsilon_{12})\sin^2\theta}{1+\upsilon_{12}}\right]\sin^2\theta+\right.$$

$$\varepsilon\left[\left(\frac{3}{1+\upsilon_{12}}-2\right)ln\frac{\sec\theta}{\sec\alpha}-\frac{3}{2}\left(\frac{1}{1+\upsilon_{12}}-\frac{2G}{E_3}\right)(\cos^2\theta-\cos^2\alpha)+1-\frac{3\upsilon_{12}\sin^2\theta}{1+\upsilon_{12}}\right]\cos^2\theta+$$

$$\left.\varepsilon 3\frac{2G}{E_3}\sin^2\theta\cos^2\theta\right\}2\tan\theta\sec^2\theta\, d\theta \quad (3.97)$$

$$\rightarrow \frac{T}{\pi R^2 E_3} = \varepsilon\frac{1}{\tan^2\alpha}\int_0^{\alpha}\left(\left(\frac{3}{1+\upsilon_{12}}-2\right)ln\frac{\sec\theta}{\sec\alpha}\sin^2\theta-\frac{3}{2}\left(\frac{1}{1+\upsilon_{12}}-\frac{2G}{E_3}\right)(\cos^2\theta-\cos^2\alpha)\sin^2\theta+\right.$$

$$\left(\frac{3}{1+\upsilon_{12}}-2\right)ln\frac{\sec\theta}{\sec\alpha}\cos^2\theta-\frac{3}{2}\left(\frac{1}{1+\upsilon_{12}}-\frac{2G}{E_3}\right)(\cos^2\theta-\cos^2\alpha)\cos^2\theta+\frac{3(1-\upsilon_{12})\sin^2\theta\sin^2\theta}{1+\upsilon_{12}}-$$

$$\left.\frac{3\upsilon_{12}\sin^2\theta\cos^2\theta}{1+\upsilon_{12}}+\cos^2\theta+3\frac{2G}{E_3}\sin^2\theta\cos^2\theta\right)2\tan\theta\sec^2\theta\, d\theta \quad (3.98)$$

$$\rightarrow \frac{T}{\pi R^2 E_3} = \varepsilon\frac{1}{\tan^2\alpha}\int_0^{\alpha}\left(\frac{3}{1+\upsilon_{12}}-2\right)ln\frac{\sec\theta}{\sec\alpha}\frac{2\sin\theta}{\cos^3\theta}-3\left(\frac{1}{1+\upsilon_{12}}-\frac{2G}{E_3}\right)(\cos^2\theta-\cos^2\alpha)\frac{\sin\theta}{\cos^3\theta}+$$

$$\frac{6(1-\upsilon_{12})}{1+\upsilon_{12}}\frac{\sin^5\theta}{\cos^3\theta}-\frac{6\upsilon_{12}}{1+\upsilon_{12}}\frac{\sin^3\theta}{\cos\theta}+\frac{2\sin\theta}{\cos\theta}+6\frac{2G}{E_3}\frac{\sin^3\theta}{\cos\theta}d\theta \quad (3.99)$$

Equ. (3.99) can be separated as follows

1

$$\frac{1}{\tan^2\alpha}\int_0^{\alpha}\left(\frac{3}{1+\upsilon_{12}}-2\right)ln\frac{\sec\theta}{\sec\alpha}\frac{2\sin\theta}{\cos^3\theta}d\theta \tag{3.100}$$

$$\rightarrow \frac{1}{\tan^2\alpha}\left(\frac{3}{1+\upsilon_{12}}-2\right)\left[\left(2\int_0^{\alpha} ln\sec\theta\frac{\sin\theta}{\cos^3\theta}d\theta\right)-\left(2ln\sec\alpha\int_0^{\alpha}\frac{\sin\theta}{\cos^3\theta}d\theta\right)\right] \tag{3.101}$$

Let $\cos\theta$ is x, and integrate it, then we have $-\sin\theta\, d\theta = dx$. Thus

$$\frac{1}{\tan^2\alpha}\left(\frac{3}{1+\upsilon_{12}}-2\right)\left[\left(-2\int_1^{\cos\alpha} ln\frac{1}{x}\frac{1}{x^3}dx\right)+\left(2ln\sec\alpha\int_1^{\cos\alpha}\frac{1}{x^3}dx\right)\right] \tag{3.102}$$

$$\rightarrow \frac{3}{1+\upsilon_{12}}\cot^2\alpha\, ln\sec\alpha-\frac{3}{1+\upsilon_{12}}\frac{1}{2}-2\cot^2\alpha\, ln\sec\alpha+1 \tag{3.103}$$

2

$$-\frac{1}{\tan^2\alpha}\int_0^{\alpha}3\left(\frac{1}{1+\upsilon_{12}}-\frac{2G}{E_3}\right)(\cos^2\theta-\cos^2\alpha)\frac{\sin\theta}{\cos^3\theta}d\theta \tag{3.104}$$

$$\rightarrow \frac{-3}{1+\upsilon_{12}}\cot^2\alpha\, ln\sec\alpha+\frac{3}{2}\cos^2\alpha\frac{1}{1+\upsilon_{12}}+3\frac{2G}{E_3}\cot^2\alpha\, ln\sec\alpha-\frac{3}{2}\frac{2G}{E_3}\cos^2\alpha \tag{3.105}$$

3

$$\frac{1}{\tan^2\alpha}\int_0^{\alpha}\frac{6(1-\upsilon_{12})}{1+\upsilon_{12}}\frac{\sin^5\theta}{\cos^3\theta}d\theta \tag{3.106}$$

$$\rightarrow \frac{1}{2}(1+\cos^2\alpha)\frac{6(1-\upsilon_{12})}{1+\upsilon_{12}}-2\frac{6(1-\upsilon_{12})}{1+\upsilon_{12}}\cot^2\alpha\, ln\sec\alpha \tag{3.107}$$

4

$$-\frac{1}{\tan^2\alpha}\int_0^{\alpha}\frac{6\upsilon_{12}}{1+\upsilon_{12}}\frac{\sin^3\theta}{\cos\theta}d\theta \tag{3.108}$$

$$\rightarrow \frac{6\upsilon_{12}}{1+\upsilon_{12}}\cot^2\alpha\, ln\cos\alpha+\frac{1}{2}\frac{6\upsilon_{12}}{1+\upsilon_{12}}\cos^2\alpha \tag{3.109}$$

5

$$\frac{1}{\tan^2\alpha}\int_0^{\alpha}\frac{2\sin\theta}{\cos\theta}d\theta \tag{3.110}$$

$$\rightarrow 2\cot^2\alpha\, ln\sec\alpha \tag{3.111}$$

6

$$\frac{1}{\tan^2\alpha}\int_0^{\alpha}6\frac{2G}{E_3}\frac{\sin^3\theta}{\cos\theta}d\theta \tag{3.112}$$

$$\rightarrow 6\frac{2G}{E_3}\cot^2\alpha\, ln\sec\alpha-\frac{6}{2}\frac{2G}{E_3}\cos^2\alpha \tag{3.113}$$

Let sum from eqs. (3.101) to (3.113), then equ. (3.99) becomes

$$\varepsilon\left[\frac{3}{1+\upsilon_{12}}\cot^2\alpha\, ln\sec\alpha-\frac{3}{1+\upsilon_{12}}\frac{1}{2}-2\cot^2\alpha\, ln\sec\alpha+1+\frac{-3}{1+\upsilon_{12}}\cot^2\alpha\, ln\sec\alpha+\right.$$

$$\frac{3}{2}\cos^2\alpha\frac{1}{1+\upsilon_{12}}+3\frac{2G}{E_3}\cot^2\alpha\, ln\sec\alpha-\frac{3}{2}\frac{2G}{E_3}\cos^2\alpha+\frac{1}{2}(1+\cos^2\alpha)\frac{6(1-\upsilon_{12})}{1+\upsilon_{12}}-$$

$$2\frac{6(1-\upsilon_{12})}{1+\upsilon_{12}}\cot^2\alpha\, ln\sec\alpha+\frac{6\upsilon_{12}}{1+\upsilon_{12}}\cot^2\alpha\, ln\cos\alpha+\frac{1}{2}\frac{6\upsilon_{12}}{1+\upsilon_{12}}\cos^2\alpha+2\cot^2\alpha\, ln\sec\alpha+$$

$$\left.6\frac{2G}{E_3}\cot^2\alpha\, ln\sec\alpha-\frac{6}{2}\frac{2G}{E_3}\cos^2\alpha\right] \tag{3.114}$$

$$\rightarrow\varepsilon\left\{-2+\left[\frac{6(\upsilon_{12}-2)}{1+\upsilon_{12}}+\frac{18G}{E_3}\right]\cot^2\alpha\, ln\sec\alpha-\frac{9G}{E_3}\cos^2\alpha+\left(1-\frac{\sin^2\alpha}{2}\right)\frac{9}{1+\upsilon_{12}}\right\} \tag{3.115}$$

Elastic modulus is expressed as

$$E_3\left\{-2+\left[\frac{6(\upsilon_{12}-2)}{1+\upsilon_{12}}+\frac{18G}{E_3}\right]\cot^2\alpha\, ln\sec\alpha-\frac{9G}{E_3}\cos^2\alpha+\left(1-\frac{\sin^2\alpha}{2}\right)\frac{9}{1+\upsilon_{12}}\right\} \tag{3.116}$$

in case of $G = 0$ or $E_1 = 0$ (constant volume fraction: $\upsilon_{12}=1$). Because $(1-\upsilon_{12}=\frac{E_1}{2E_3}=0\rightarrow \upsilon_{12}=1)$. Equ. (3.116) is expressed as follows

$$E_3\left\{-2+\left[\frac{6(\upsilon_{12}-2)}{1+\upsilon_{12}}+\frac{18G}{E_3}\right]\cot^2\alpha\, ln\sec\alpha-\frac{9G}{E_3}\cos^2\alpha+\left(1-\frac{1}{2}\sin^2\alpha\right)\frac{9}{1+\upsilon_{12}}\right\} \tag{3.117}$$

$$\rightarrow E_3\left[-2-3\cot^2\alpha\, ln\sec\alpha+\left(1-\frac{1}{2}\sin^2\alpha\right)\frac{9}{2}\right] \tag{3.118}$$

$$\rightarrow E_3\left(-2-3\cot^2\alpha\, ln\sec\alpha+\frac{9}{2}-\frac{9}{4}\sin^2\alpha\right) \tag{3.119}$$

$$\rightarrow E_3\left(\frac{5}{2}-3\cot^2\alpha\, ln\sec\alpha-\frac{9}{4}\sin^2\alpha\right) \tag{3.120}$$

where E_3 is identical with equ. (2.44) of Appendix B.

The value written in parenthesis of equ. (3.120) is the same value listed in equ. (1.103) of Appendix A.

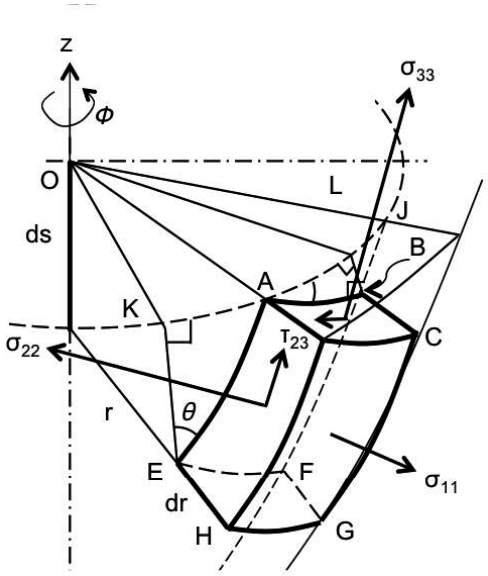

Fig. 3.1 A schematic representation of three stresses and shear stresses [7].

References

1) J. W. S. Hearle, P. Grosberg and S. Backer: John Wiley & Suns, Inc. NY. USA, 1969.
2) A. E. H. LOVE, M.A., D.Sc., F.R.S., A TREATISE ON THE MATHEMATICAL THEORY OF ELASTICITY, 4th edition, NEW YOUR DOVER PUBLICATIONS, 274, 1944.
3) Hyer MW. Stress Analysis of Fiber-Reinforced Composite Materials, Updated edition. DEStech Publications, Inc., 2009.
4) Beer FP, Johnston ERJr, Dewolf JT, Mazurek DF. Mechanics of Materials, 6th ed. McGraw-Hill Science/Engineering/Math, 2011.
5) Hull D, Clyne TW. AN INTRODUCTION TO COMPOSITE MATERIALS, 2nd ed. Cambridge university press, 1996.
6) Rao Y, Farris RJ. A Modeling and Experimental Study of the Influence of Twist on the Mechanical Properties of High-Performance Fiber Yarns. J Appl Polym Sci, 77: 1938-1949, 2000.
7) J. J. Thwaites, THE ELASTIC DEFORMATION OF A ROD WITH HELICAL ANSIOTROPY, International Journal of Mechanical Sciences. 19, 161-168, 1977.
8) Ferdinand P. Beer, E. Russell Johnston, Jr., John T. Dewolf, David F. Mazurek, MECHANICS OF MATERIALS, 6th edition, The MaGraw Hill Componies, 2012.

Acknowledgements

This study was conducted in materials reliability engineering laboratory of Yamaguchi University during the years of 2011.10 - 2015.03

First of all, I would like to express my deepest appreciation to my supervisor, Professor Koichi Goda, who has tirelessly assisted me with his insightful knowledge, energy, inexhaustible support, advice, and direction when I struggled to overcome so many problems. Without having his supports such as discussions until late at night and day off works, this work would not have been possible.

I also equally wish to give my thanks to Associate Professor 野田淳二, 喜多村竜太、新田悠二、Taweesak Piyatuchsananon, Azmi nordin,今津弘太、杉田朋洋、伊達雄人、花表孝亮、山崎恵理、ヌル　フルカン、長澤昌也、古賀恭平、伊達宝子、中島航希、坂本瞳、権藤純平、清水貴大、本田宗靖、槙野裕太、佐藤優斗、and 山口雄大 for their kindnesses.

I am especially grateful to Professor Tae-jin Chung, Professor Seung-Kee Koh, Professor Sin-Young Lee and Professor Hui-Chan Gang, Kunsan National University, for recommending me to study in Prof. Goda's laboratory and their encouragement, advice and support from the beginning of my study in Japan.

I would like to express my thanks to Professor Donghwan Cho, Kumoh National Institute of Technology, Polymer/Bio-Composites Research Lab, Department of Polymer Science and Engineering, and Professor Jungil Song, Changwon National University, School of Mechanics Department of Mechanical Engineering for their useful advices.

I also would like to express thanks to Kayaku Akzo Corporation for their kindness.

Finally, I would like to express thanks to my loving family members for their endless support and encouragement throughout the entire my life.